Behavior of the Diamond Difference and Low-Order Nodal Numerical Transport Methods in the Thick Diffusion Limit for Slab Geometry

DF Gill

The Pennsylvania State University

The Graduate School

BEHAVIOR OF THE DIAMOND DIFFERENCE AND

LOW-ORDER NODAL NUMERICAL TRANSPORT METHODS IN

THE THICK DIFFUSION LIMIT FOR SLAB GEOMETRY

A Thesis in

Nuclear Engineering

by

Daniel Fury Gill

Submitted in Partial Fulfillment

of the Requirements

for the Degree of

Master of Science

May 2007

The thesis of Daniel Fury Gill was reviewed and approved* by the following:

Yousry Y. Azmy
Professor of Nuclear Engineering
Thesis Advisor

Kostadin Ivanov
Professor of Nuclear Engineering

Jack Brenizer
Professor of Nuclear and Mechanical Engineering
Chair of Nuclear Engineering

Robert Grove
KAPL Nuclear Design Methods
Naval Nuclear Propulsion Graduate Fellowship Laboratory Advisor
Special Signatory

*Signatures are on file in the Graduate School.

Abstract

The objective of this work is to investigate the thick diffusion limit of various spatial discretizations of the one-dimensional, steady-state, monoenergetic, discrete-ordinates neutron transport equation. This work specifically addresses the two lowest order nodal methods, AHOT-N0 and AHOT-N1, as well as reconsiders the asymptotic limit of the Diamond Difference method.

The asymptotic analyses of the AHOT-N0 and AHOT-N1 nodal methods show that AHOT-N0 does not possess the thick diffusion limit for cell edge or cell average fluxes except under very limiting conditions, which is to be expected considering the AHOT-N0 method limits to the Step method in the thick diffusion limit. The AHOT-N1 method, which uses a linear in-cell representation of the flux, was shown to possess the thick diffusion limit for both cell average and cell edge fluxes. The thick diffusion limit of the DD method, including the boundary conditions, was derived entirely in terms of cell average scalar fluxes. It was shown that, for vacuum boundaries, only when σ_t, h, and Q are constant and $\sigma_a = 0$ is the asymptotic limit of the DD method close to the finite-differenced diffusion equation in the system interior, and that the boundary conditions between the systems will only agree in the absence of an external source. For a homogeneous medium an effective diffusion coefficient was shown to be present, which was responsible for causing numeric diffusion in certain cases. A technique was presented to correct the numeric diffusion in the interior by altering certain problem parameters. Numerical errors introduced by the boundary conditions and material interfaces were also explored for a two-region problem using the Diamond Difference method. A discrete diffusion solution which exactly solves the one-dimensional diffusion equation in a homogeneous region with constant cross sections and a uniform external source was also developed and shown to be equal to the finite-differenced diffusion discretization for $c = 1$ in the system interior, where again the boundary conditions again only agree in the absence of an external source. It was also shown that

for $c < 1$ the exact discrete diffusion solution is written in terms of hyperbolic functions, with expressions which limit to the exact solution for the $c = 1$ case as $c \to 1$. Finally, a transport discretization is developed which reproduces the exact S_2 solution for the case of a purely scattering homogeneous region with vacuum boundary conditions, and an extension to the discretization for the case of $c < 1$ is found by considering a Taylor series expansion of the exact answer centered at $c = 0$.

TABLE OF CONTENTS

Chapter 4

Asymptotic Analysis of the Diamond Difference Method   **65**

Chapter 5

Discrete S$_N$ Transport Solution   **98**

Chapter 6

Conclusions   **107**

Appendix A

c=1 Mathematica Notebook   **111**

Appendix B

c < 1 Mathematica Notebook   **113**

Bibliography   **116**

LIST OF FIGURES

LIST OF TABLES

Acknowledgments

I would also like to take this opportunity to express my deep gratitude to the National Nuclear Security Administration and the United States Department of Energy for providing the funding that made this research possible and for their continuing support through the NNP Fellowship Program.

Introduction

It has been said that the central problem of nuclear reactor theory is the determination of the distribution of neutrons in the reactor, for it is this distribution which determines the rate at which nuclear reactions occur. From detailed knowledge of this distribution it is also possible to determine the stability of the nuclear chain reaction. The process by which neutrons interact, be it through scattering off other nuclei, being absorbed by other nuclei, or leaking out of system, is known as neutron transport.

In a broad sense there are two approaches to the neutron transport problem, stochastic and deterministic methods. The stochastic approach or Monte Carlo method, is based on using pseudorandom numbers and nuclear interaction data to simulate the life of a large number of neutrons on a digital computer and then statistics are used to determine the behavior of the average particle. Deterministic methods on the other hand generally deal with a mathematical relationship possessing a solution which describes the expected neutron distribution with the two major deterministic approaches being diffusion theory and transport theory. Diffusion theory treats neutrons in the reactor much like gas molecules in air, with the process being driven by the movement of neutrons from an area of high concentration to an area of low concentration. This theory can be inaccurate in cases where neutrons travel a relatively large distance between successive interactions, and in this case it is desirable to use the neutron transport equation.

The neutron transport equation is often called the linear Boltzmann equation because of its resemblance to the Boltzmann equation which describes the kinetic theory of gas mixtures. The neutron transport equation is a more accurate description of the transport process, but unfortunately it is very difficult to solve for almost all practical problems. For this reason a multitude of numerical methods have been developed so that the transport equation can be solved on a computer. The numerical methods used to solve the transport equation are a very active area of research and are at the heart of this work.

Specifically we will examine a number of spatial discretizations of the transport equation for the simplified case of one-dimensional, monoenergetic, steady-state transport. The spatial discretizations we will consider include the Diamond Difference, Step, AHOT-N0, and AHOT-N1 methods. We are interested to see whether these spatial discretizations, for a so-called diffusive problem, asymptotically limit to the spatially discretized diffusion equation. We know that if an ultra-fine spatial mesh is used that all of the transport discretizations considered will result in "good" solutions. However this type of analysis asks whether they will still result in "good" solutions if the spatial cells used in the problem are optically thick. This asymptotic analysis allows us to gauge the accuracy of these numerical methods for certain types of problems and also sheds lights on the limitations of the methods. It is important to know as much as possible about any numerical method so that the numerical results generated by the computer can be trusted by the engineers who rely on them.

In this work we will present a brief literature review which covers the general areas of neutron transport, the diffusion limit analysis, and the class of nodal methods. Some mathematical background on transport and diffusion theories will be given and previous developed results of interest will be rederived and presented. In Chapter 3 we will analyze the nodal methods while in Chapter 4 we will consider the asymptotic analysis of the Diamond Difference method and also an analytically exact discretization of the diffusion equation. Finally in Chapter 5 we will present preliminary results from an attempt to develop a transport discretization which is based on the exact solution to the discrete-ordinates transport equation with the S_2 quadrature set.

1.1 Literature Review

This work is primarily focused on analyzing the behavior of the one-dimensional, monoenergetic, neutron transport equation in so-called diffusive regimes using an asymptotic expansion of the neutron flux. The neutron transport equation analyzed as well as being one-dimensional and monoenergetic is time-independent and discretized in angle and space. Angular discretization is achieved through the use of discrete-ordinates, commonly known as the S_N method. The spatial discretization schemes considered include the well known Diamond Difference (DD) and Step methods as well as the zeroth and first order nodal methods, AHOT-N0 and AHOT-N1. Although this work at its core deals with the neutron transport equation, the asymptotic limits of interest have strong ties to the diffusion approximation, sometimes referred to as the P_1 approximation. Therefore the accuracy and behavior of the diffusion approximation as a mathematical representation of radiation transport phenomena is also a topic of interest.

In an attempt to briefly review the relevant work fundamental to this thesis there are a number of topics which will be discussed. First classic works detailing the foundations of neutron transport theory will be examined, followed by a discussion on the development of asymptotic solutions to transport problems in diffusive regimes. The extension of asymptotic methods to angularly and spatially discretized one-speed problems will then be covered in detail before attention is shifted to the development of nodal discretization methods for the neutron transport equation.

1.1.1 Neutron Transport Theory

The neutron transport equation, also known as the linear Boltzmann equation, has been studied extensively due to describing phenomena ranging from the theory of sound propagation to radiative transfer in the atmosphere, although in this work we will only be considering the linear Boltzmann equation as a way to describe the transport of neutrons through a medium. The conceptual framework for applying the linear Boltzmann equation to neutral particle transport has been described in depth in a number of books and solutions under many limiting conditions have also been developed. The works by Davison and Sykes [1], Case and Zweifel [2], and Bell

and Glasstone [3] stand out as thorough and detailed studies on the formulation of neutron transport theory and its general properties. These manuscripts also discuss various approximations to the transport equation and describe analytic solutions of classic problems which are still of interest today. Bell and Glasstone also contains two particularly useful chapters regarding the Discrete-Ordinates Method and the P_1 Approximation.

However, with the advent of digital computing numerical solutions to the transport equation have become the primary tool of nuclear reactor designers and shielding analysts, thus making computational methods for the solution of the transport equation an important focus of the transport community. Much of the conceptual foundation for computational transport methods has been compiled and systematically described in the text by Lewis and Miller [4]. This is a detailed work which begins from the basics with the formulation of the transport equation and methodically leads to derivations and analyses of a broad range of numerical techniques. The sections pertaining to the Diamond Difference and Step spatial discretizations of the S_N method are especially relevant to this work.

1.1.2 Asymptotic Solutions of Neutron Transport Problems

Work on asymptotic solutions to the neutron transport equation for diffusive problems was started in the early 1970's. One of the earliest articles published on the topic was in 1974 by Larsen and Keller [5], who considered an asymptotic solution of the multi-dimensional, time and energy dependent transport equation. The solution was separated into an interior part, a boundary layer part, an initial part, and an initial boundary part. They employed an asymptotic expansion of the interior neutron flux about a small dimensionless parameter, ε, which is the ratio of a typical mean free path to a typical problem dimension. The other solution components were also analyzed using relationships in ε. The results obtained from the generalized analysis were then applied to one-speed transport theory and it was shown to leading order that for a near critical reactor the steady-state asymptotic expansion of the interior neutron flux satisfies the well-known diffusion equation. The relationship developed between transport and diffusion theory through this

analysis was very significant. For the class of problems considered diffusion theory emerged not as the result of a set of approximations but rather as a rigorous asymptotic limit of the full transport equation.

Habetler and Matkowksy [6] closely followed this work with an article which reiterated the details of deriving diffusion theory as an asymptotic limit of transport theory on a system's interior, for problem configurations whose characteristic dimensions are large compared to the medium's mean free path. Boundary layer analyses were performed for a general inhomogeneous medium using matched asymptotic expansions which resulted in a uniform asymptotic expansion of the solution. The resulting boundary conditions are written in terms of incident angular flux and the X function [2, 7], which repeatedly appears in asymptotic analyses of the transport equation. The extrapolation distance derived from the resulting asymptotic boundary condition is compared to the extrapolation distance of other commonly used diffusion boundary conditions (Mark, Marshak and Variational), for the Milne problem. It is seen that the extrapolation distance resulting from the matched asymptotic expansions is equivalent to the exact value obtained analytically for the Milne problem, while the Marshak and Mark extrapolation distances are not equivalent, at least up to the P_5 angular approximation.

Much subsequent work was done on diffusion theory as an asymptotic limit to transport theory for nearly critical systems with small mean free paths. The results are presented by Larsen [8] in an excellent review article which summarizes all of the previous work on the topic. He first describes the premise of the analysis and then outlines the entire development of asymptotic theories for both homogeneous and heterogeneous media. The review also covers open questions by discussing the theoretical gaps which exist in the asymptotic theories outlined. This article is valuable because it condenses many preexisting analyses and ideas into a concise and very manageable work.

1.1.3 Asymptotic Diffusion Limit of Discretized Transport Problems

The body of work dealing with asymptotic solutions of transport problems had to this point only been concerned with the continuum transport equation, but in

1983 Larsen published an article [9] which analyzed certain spatial differencing schemes in the same asymptotic limit as the continuum analyses. These analyses showed that with vacuum boundary conditions the DD, Linear Characteristic, Linear Discontinuous, Linear Moments, Exponential, and Alcouffe schemes converge in this limit to the correct transport or diffusion result while Weighted Diamond Difference schemes do not. This article proved to be only a starting point for a much more detailed analysis of spatially discretized transport equations in slab geometry.

In 1987 Larsen, Morel, and Miller [10] wrote their seminal paper considering asymptotic solutions to transport problems discretized in space and angle. The diffusive regime considered is equivalent to that considered by the works summarized in [8]: an optically thick, scattering dominated medium. The regime could now be characterized as either thick or intermediate depending on the optical thickness of the cells relative to ε. The asymptotic limit of the spatially discretized transport equation was then shown to be dependent upon both the optical thickness regime and the spatial discretization method. Furthermore the discretized system of equations could either be formulated in terms of cell edge or cell average fluxes. For either a cell edge or cell center formulation and a given optical thickness regime any spatial discretization which asymptotically limits to a legitimate diffusion discretization is said to have the thick or intermediate diffusion limit, respectively (a discretization is said to be legitimate if analytic diffusion theory results from the discretized equations for an infinitely fine spatial mesh.

Asymptotic analyses were then carried out for a handful of spatial discretization methods so that each method could be characterized as possessing or lacking the diffusion limit for the specified optical thickness regime and cell or edge based quantity. Five numerical problems were then chosen to test the theoretical predictions. These numerical results confirmed the predictions generated from the asymptotic analyses. Among other results, it was shown that the Diamond Difference method possesses the intermediate diffusion limit for both cell edge and cell average fluxes and that it has the thick diffusion limit for cell average fluxes and conditionally for cell edge fluxes. It was also shown that the Step method has the thick and intermediate diffusion limits for both the cell edge and cell average fluxes only under *very* limiting conditions. Unlike the work done for the continuum

transport problem, this work did not consider any type of boundary layer analysis, which was the motivation for the complimentary work done by Larsen and Morel [11].

The analyses carried out in [10] were only applicable in the problem interior and assumed any boundary layers had been sufficiently resolved by the spatial mesh. In the 1989 article by Larsen and Morel [11] these analyses were extended to predict the behavior of spatial discretization schemes in the presence of numerically unresolved boundary layers. Before determining the accuracy of the boundary conditions resulting from the asymptotic analysis it was first necessary to determine the appropriate boundary conditions for the continuum diffusion system and then discretize them. The resulting discretized boundary condition is written in terms of the Case W-function [2], which can also be approximated as a polynomial in the "directional" variable μ. This condition then provides a basis for comparing the asymptotic conditions derived in the work. The asymptotic analysis used is identical to that used in [10], however, angularly discretized transport boundary conditions are now included and only the thick diffusion limit is considered. By comparing the resulting asymptotic boundary conditions to the discretized transport conditions the authors are able to predict whether or not a given spatial discretization scheme will be accurate in the thick diffusion limit.

Two numerical problems were chosen to test the predictions and indeed the results of these numerical tests support the predictions made. For the Diamond Difference method it is shown that for the cell average fluxes to be accurate the prescribed incident fluxes must satisfy a certain condition derived by Larsen and Morel, which is satisfied, for instance, if the prescribed incident fluxes are isotropic, in which case the cell edge fluxes will also be accurate. Should the prescribed incident fluxes be anisotropic not only can both the cell edge and cell center fluxes be inaccurate, but the inaccuracy will be dependent on whether the total number of cells used in the problem is even or odd. These results show that only under rather restrictive conditions for the prescribed incident flux on the boundary will the Diamond Difference method produce accurate solutions in the thick diffusion limit. Another method of interest analyzed in this work was the Linear Moments method. This method is of interest due to its equivalence with the first order nodal method, AHOT-N1. The authors show for this method that the cell edge fluxes

are accurate throughout the problem domain and that the cell average fluxes are accurate in all cells with the possible exception of those in unresolved boundary layers. The analytic methods developed in [10] and [11] spawned a large amount of work in the transport methods community.

Asymptotic analyses have been carried out for a wide range of spatial discretizations and for multiple geometric configurations. Discretizations analyzed include, but are not limited to, the multiple balance S_N differencing [12], discontinuous finite element schemes [13] [14] [15], and characteristic methods [16]. Attention has also been devoted to even-parity finite element transport solutions in the thick diffusion limit [17] [18], while some analyses done have considered spherical geometry [19] and others have worked with two-dimensional Cartesian space [15]. In 1992 Larsen published an article [20] which describes the underlying ideas behind the asymptotic analysis, reviews the main results, and discusses some of the open questions at the time. This article has an excellent section containing the derivation of the continuum diffusion equation as an asymptotic limit of the spatially and angularly continuous one-dimensional transport equation. Larsen presents a new analysis which considers a general Weighted Diamond Difference discretization and he also includes a discussion on the potential applications of the asymptotic results to diffusion synthetic acceleration (DSA) algorithms.

1.1.4   Nodal Transport Methods

Though asymptotic analyses have been carried out for a multitude of discretization schemes, as mentioned previously, the class of nodal transport methods has not been explicitly addressed. Nodal methods have the advantage of producing results with accuracy comparable to conventional, finite difference methods, only on much coarser meshes. By employing higher order nodal methods both solution accuracy and computational efficiency can be enhanced.

The first generation of nodal discrete ordinates methods were developed in the late 1970's and early 1980's. The methods included in this generation were unique from other contemporary nodal methods in the fact that they converge to the exact discrete ordinates equations as the spatial mesh becomes infinitely fine. This class of methods includes the Discrete Nodal Transport Method (DNTM), the

TWOTRAN nodal method, and an exponential expansion method. The DNTM method was developed by Lawrence and Dorning [21] [22] [23], TWOTRAN came about through the efforts of Walters [24] [25] [26] [27], and the exponential expansion method was the product of Pevey [28] [29] at Oak Ridge. A review article by Lawrence describes each of these methods and provides a historical overview of the development of nodal transport methods up to 1986 [30].

At their core, all nodal methods are based on expanding the in-cell and surface angular fluxes in locally defined truncated series. The early nodal transport methods differed in the order of the truncation and the relationships derived between the expansion coefficients for the in-cell and surface fluxes. Initial work was carried out in slab geometry but was soon extended to two-dimensional geometry. Each of the methods developed were derived for a truncation order and dimensionality which were decided beforehand so that any results were specific to that particular case. If a method for higher orders or dimensionality was required then the derivation would have to be repeated. However, Azmy was able to generalize the entire class of nodal transport methods in terms of dimensionality and truncation order and cast them in a Weighted Diamond Difference form in his 1988 work [31]. (For a much more comprehensive review of the development of higher order nodal methods see Azmy's 1992 work regarding the derivation of Arbitrarily High Order Characteristic methods (AHOT-C) [32].)

The generalized nodal framework developed by Azmy [31] was able to compactly yet completely yield a closed system of equations in a general-dimension Cartesian geometry with an arbitrary truncation order of the in-cell and surface angular fluxes. The methods developed from this framework have come to be known as Arbitrarily High Order Transport Nodal methods (AHOT-N), where AHOT-N1 for example indicates the nodal scheme using a linear spatial representation of the in-cell and surface fluxes. The AHOT-N schemes are also general in the sense that previously developed nodal methods can be shown to be specialized instances of AHOT-N, under certain simplifying assumptions. The AHOT-N framework also allows for the spatial nodal moments of the flux to be written in terms of the transverse flux moments evaluated at node surfaces as a generalized weighted difference relation. That is, even with the complexity introduced by the generality of the derivation the final form of the equations can still be cast in a

simple Weighted Diamond Difference form. The AHOT-N schemes also have the advantage of being characterized, for a given spatial expansion order, by one spatial weight per dimension per direction per discrete-ordinate for all flux moments whereas previous methods included multiple coefficients.

Many numerical experiments have been carried out to test not only the accuracy of the high order nodal methods but the computational efficiency as well. Azmy [33] compared the AHOT-N1 scheme in two-dimensions to two previously developed linear nodal methods (the LN and LL methods) for three sample problems. Of the three methods considered AHOT-N1 retains the most analyticity while the LN method retains the least. Numerical results show that the solutions produced by the varying methods are all similar, especially on fine meshes. The largest variations were seen in locations with low flux levels. While this set of experiments was focused on comparing a fixed order AHOT-N scheme to previously developed methods, numerical experiments have also been carried out which demonstrate the capabilities of the higher order AHOT-N schemes.

Azmy [31] used a two-dimensional, four quadrant sample problem, known now as the Azmy benchmark, with orders from 0–9 to demonstrate the accuracy of the AHOT-N methods. It was shown that for very high order methods (AHOT-N6 and greater) solutions are extremely accurate with only one node per quadrant while AHOT-N0 requires a very fine mesh to produce accurate results. In fact, results show that AHOT-N5 requires less storage and computational time to compute a solution with the same accuracy.

Azmy [32] also compared numerical results produced by AHOT-N and AHOT-C methods of varying spatial approximation orders on two two-dimensional test problems. It was shown that reference solutions produced by the nodal and characteristic methods were in agreement with one another. It was also found that in general nodal methods are advantageous for computing integrated quantities, such as the scalar flux, while the characteristic methods excel at computing deep penetration quantities, such as leakage. Azmy notes that in the quadrant containing the fixed source in the first test problem as the scattering ratio, c, increases for a given order and mesh the accuracy will deteriorate because the contribution from the scattering source (approximated) increases relative to the contribution from the fixed source (exact).

We have outlined the development of many topics which are fundamental to the work being presented in this thesis: neutron transport theory, numerical solutions of transport problems, asymptotic solutions to transport problems in the continuum, asymptotic solutions to discretized transport problems, and the the class of nodal methods. It will also be of great value to present here the most relevant aspects of these topics from a mathematical and not a developmental perspective.

Introduction to Transport and Diffusion Theories and their Asymptotic Equivalence

As mentioned previously, this work is primarily concerned with the analysis of the one-dimensional, monoenergetic, neutron transport equation. The specific transport equation of interest is also time-independent and discretized in angle and space. To angularly discretize the problem, the well-known discrete-ordinates (S_N) method is employed. The spatial discretization schemes specifically considered are the DD, Step, AHOT-N0, and AHOT-N1 methods. The discretized equations will be analyzed using an asymptotic expansion of the angular flux. The cross sections and external source will also be scaled in such a way that the analysis applies to diffusive regimes. Although this will be explained in more detail later, it presently suffices to say that in a diffusive regime the solution of the continuum diffusion equation is a good representation of the solution of the spatially continuous S_N equations. For this reason we are also interested in time-independent, one-dimensional, monoenergetic diffusion solutions.

This chapter will present the general neutral particle transport problem and reduce it to the specialized case considered. The generalized diffusion approximation will also be presented and subsequently reduced to the form used throughout

this work. Both the transport and diffusion equations will next be spatially discretized and then the premise and mechanics of the continuum asymptotic analysis in diffusive regimes will be presented. Finally results of interest from asymptotic analyses of spatially discretized transport problems will be explained.

2.1 The Neutron Transport Equation

The general form of the time-independent neutron transport equation in a non-multiplying medium is given by

$$\left[\hat{\Omega} \cdot \vec{\nabla} + \sigma_t(\vec{r}, E)\right] \psi(\vec{r}, \hat{\Omega}, E) =$$
$$Q(\vec{r}, \hat{\Omega}, E) + \int dE' \int d\Omega' \sigma_s(\vec{r}, E' \to E, \hat{\Omega}' \cdot \hat{\Omega}) \psi(\vec{r}, \hat{\Omega}', E'), \quad (2.1)$$

where these quantities represent,

- $\vec{r} \equiv$ Position vector ,

- $\hat{\Omega} \equiv$ Unit vector along the direction of neutron travel ,

- $E \equiv$ Neutron energy ,

- $\psi(\vec{r}, \hat{\Omega}, E) \equiv$ Angular neutron flux ,

- $\sigma_t \equiv$ Total interaction macroscopic cross section ,

- $\sigma_s \equiv$ Double-differential scattering macroscopic cross section ,

- $Q \equiv$ External source .

For the case of one-dimensional, monoenergetic, isotropic-scattering neutron transport, Eq. (2.1) simplifies to

$$\left[\mu \frac{\partial}{\partial x} + \sigma_t(x)\right] \psi(x, \mu) = \frac{\sigma_s(x)}{2} \int_{-1}^{1} \psi(x, \mu') d\mu' + Q(x). \quad (2.2)$$

The variable μ in this equation represents the direction cosine that the direction of neutron travel makes with the x-axis, in the sense that $\mu = \cos\theta$ and θ is the

angle between the flight path of the neutron and the x-axis. In Eq. (2.2) the angular variable, μ, is continuous and varies in $[-1, 1]$. The S_N approximation consists of requiring that Eq. (2.2) hold only in certain angular directions, μ_n, such that

$$\left[\mu_n \frac{\partial}{\partial x} + \sigma_t(x) \right] \psi_n(x) = \frac{\sigma_s(x)}{2} \int_{-1}^{1} \psi(x, \mu') d\mu' + Q(x), \quad n = 1, \ldots, N.$$

A numerical quadrature rule is then used to introduce an approximation to the true value of the integral term.

$$\int_{-1}^{1} \psi(x, \mu') d\mu' \approx \sum_{n=1}^{N} w_n \psi_n(x), \quad n = 1, \ldots, N$$

Here N refers to the total number of "directions" or discrete-ordinates to be used. As with any numerical quadrature rule, the accuracy of the solution increases with N. It is strongly preferred that the quadrature set chosen meets the following three conditions:

1. The quadrature set is even-ordered and symmetric about $\mu = 0$.

2. The rule integrates up to cubic polynomials exactly.

3. The weights are normalized to unity.

These three assumptions result in the properties of the quadrature set given by

$$\sum_{n=1}^{N} \mu_n w_n = 0, \tag{2.3a}$$

$$\sum_{n=1}^{N} \mu_n^2 w_n = \frac{1}{3}, \tag{2.3b}$$

$$\sum_{n=1}^{N} w_n = 1. \tag{2.3c}$$

The most commonly used quadrature set which meets these conditions is the Gauss-Legendre quadrature with appropriately normalized weights, which pos-

sesses a high degree of precision, given by $2N - 1$. Thus even when $N = 2$ this quadrature rule can integrate up to cubic polynomials exactly. The Gauss-Legendre quadrature set is readily available from a multitude of published sources, e.g. for N up to 12 they are given in [4], although in that specific listing the weights are normalized to 2. Still other quadrature sets may be used, and in some special cases will yield more accurate results. The general S_N approximation in slab geometry can now be written as

$$\left[\mu_n \frac{d}{dx} + \sigma_t(x)\right]\psi_n(x) = \sigma_s(x)\sum_{m=1}^{N} w_m \psi_m(x) + Q(x), \quad n = 1, \ldots, N \qquad (2.4)$$

comprising a set of N first-order coupled ordinary differential equations. Due to the weight normalization chosen in Eq. (2.3) the factor of $1/2$ can be removed from the scattering source term. This form of the transport equation has now been discretized in both angle and energy with only the spatial variable still continuous. To derive an approximation to the transport solution that can be solved numerically it is now necessary to discretize the spatial variable, x.

This discretization is achieved by first considering a spatial grid of I intervals, as in Fig. 2.1. Each cell, i, covers the domain $[x_{i-1/2}, x_{i+1/2}]$ and the midpoint value, x_i is taken to be the arithmetic average of the edge points, denoted by the half-integer subscripts $i - 1/2$ and $i + 1/2$. The discretization process also assumes that all cross section values are constant throughout a spatial cell.
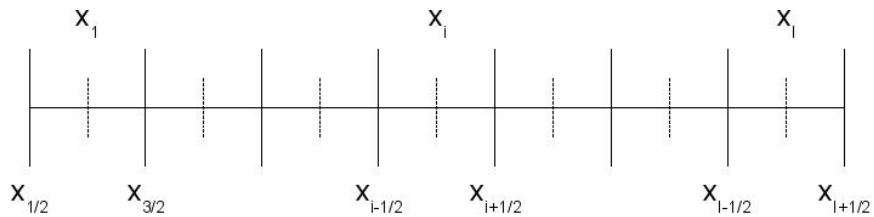
Figure 2.1. Slab-Geometry Spatial Discretization into I Intervals

Using the angularly constant cross section assumption, integrating Eq. (2.4) for a single discrete-ordinate, n, over the cell domain, $[x_{i-1/2}, x_{i+1/2}]$, yields

$$\frac{\mu_n}{h_i} \left(\psi_{n,i+1/2} - \psi_{n,i-1/2} \right) + \sigma_{t,i} \psi_{n,i} = \sigma_{s,i} \sum_{m=1}^{N} w_m \psi_{m,i} + Q_i, \quad n = 1, \ldots, N. \quad (2.5)$$

Equation (2.5) is the set of one-dimensional discretized balance equations, it is a mathematical expression which describes the conservation of neutrons over each cell in the slab. In Eq. (2.5) we have defined

$$h_i \equiv x_{i+1/2} - x_{i-1/2}, \quad (2.6)$$

$$\psi_{n,i\pm1/2} \equiv \psi_n(x_{i\pm1/2}), \quad (2.7)$$

$$\psi_{n,i} \equiv \frac{1}{h_i} \int_{x_{i-1/2}}^{x_{i+1/2}} \psi_n(x) dx, \quad (2.8)$$

$$Q_i \equiv \frac{1}{h_i} \int_{x_{i-1/2}}^{x_{i+1/2}} Q(x) dx. \quad (2.9)$$

Equation (2.5) describes the spatially discretized flux in terms of the edge quantities, $\psi_{n,i\pm1/2}$, and the averaged quantities, $\psi_{n,i}$. However Eq. (2.5) presents I relations among $2I+1$ unknown quantities per discrete-ordinate. To solve for these quantities it is necessary to introduce an approximation via the so-called auxiliary relationship. A very simple and common auxiliary relationship is the Diamond Difference approximation stated as

$$\psi_{n,i} = \frac{1}{2} \left(\psi_{n,i+1/2} + \psi_{n,i-1/2} \right). \quad (2.10)$$

The DD relation will be referred to extensively throughout this work; Chapter 4 deals exclusively with the asymptotic analysis of the DD approximation. The DD relation is a second-order accurate method. That is, the error introduced is $O(h^2)$ as $h \to 0$. The DD section in [4] also explains the positivity problems experienced by the DD method, that is for h sufficiently large it is possible for the DD method to produce unphysical, negative flux values. Moreover, as the number of discrete-ordinates used increases, the mesh sizing, h, must decrease in order for the solution to remain positive. For this reason another commonly used auxiliary

scheme is the Step, or Upwind scheme, that has the advantage of always producing positive results. The Step method is defined by

$$\psi_{n,i\pm1/2} = \psi_{n,i}, \quad \mu_n \gtrless 0. \tag{2.11}$$

Upwind is an appropriate name for this scheme. It can be seen that the number of neutrons on the cell edge which is "upwind" of the direction of neutron flight is simply set equal to the average number of neutrons in this cell. Although this scheme has both the advantages of simplicity and positivity it is also fairly inaccurate. The order of the error for the Step scheme is only $O(h)$. The comparative accuracy of the DD and Step discretization schemes is displayed quite clearly in Figure 3-5 of [4]. A solution algorithm which iterates on the scattering source is also explained fully in [4]. The same algorithm is used for both of the discretization schemes mentioned. It is important to note that the error estimates provided in [4] and cited above are in the limit $h \to 0$, in contrast to the thick diffusion limit that is the primary focus of this work where $h \to \infty$.

Both the DD and Step methods are specialized cases of a larger class of schemes termed Weighted Diamond-Difference (WDD) schemes. The generalized WDD scheme is defined via the terms $\alpha_{n,i}$, known as spatial weights. The auxiliary relation for the general WDD scheme thus is given by

$$\psi_{n,i} = \left(\frac{1 + \alpha_{n,i}}{2}\right)\psi_{n,i+1/2} + \left(\frac{1 - \alpha_{n,i}}{2}\right)\psi_{n,i-1/2}. \tag{2.12}$$

It is then apparent that $\alpha_{n,i} = 0$ corresponds to the DD scheme and $\alpha_{n,i} = \mu_n/|\mu_n|$ corresponds to the Step scheme.

The two previously described discretization schemes are indeed simple but also have well-known disadvantages. More advanced methods have also been used to spatially discretize the discrete-ordinates equations with one class of advanced methods of interest being the nodal methods. Some prominent work in the area of nodal methods has been covered in 1.1. The two nodal schemes of particular interest to this work are the zeroth and first order spatial expansion nodal approximations, AHOT-N0 and AHOT-N1 respectively.

Nodal methods are based on expanding the in-cell angular fluxes and surface angular fluxes in locally defined truncated series. In multi-dimensional problems

it is necessary to transverse average the flux over each spatial dimension, but this step, as well as the expansion of the surface fluxes in a truncated series, is not necessary in slab geometry. Thus, for one-dimensional problems using nodal transport methods the only approximation made is the expansion of the scattering and external sources as polynomials. However, the analyses in this work will only consider external sources which are constant throughout a cell such that the *only* approximation made is the spatial expansion of the scattering source in a truncated series.

The AHOT-N0 method approximates the scattering source as constant in space for each cell and like all AHOT-N schemes, the method can be written in a WDD form which utilizes one spatial weight per cell per discrete ordinate. The AHOT-N0 scheme is written similarly to the DD and Step schemes as a balance equation and an auxiliary WDD relation, Eqs. (2.5) and (2.12), with the spatial weights given by

$$\alpha_{n,i} = \coth\left(\delta_{n,i}\right) - \left(\frac{1}{\delta_{n,i}}\right), \tag{2.13}$$

where the parameter $\delta_{n,i}$, which is used in the AHOT-N0 spatial weights, represents half the cell optical width measured in mean free paths, and is defined by

$$\delta_{n,i} = \frac{\sigma_{t,i} h_i}{2\mu_n}. \tag{2.14}$$

This system of equations can be solved using the same iterative sweeping algorithm used for DD and Step schemes. This scheme has the advantage of being analytically exact aside from the approximation of the scattering source. To raise the accuracy of the AHOT-N0 method a logical extension is to treat the scattering source in each cell as a linear function. This is exactly what is achieved in the AHOT-N1 method. To achieve this increase in accuracy, the AHOT-N1 scheme requires storage of an extra flux variable, the first flux moment, in each computational cell. Thus in addition to the balance and auxiliary relations for the zeroth spatial moments of the flux, Eqs. (2.5) and (2.12), which have been used in the previous methods, an extra equation balancing the first flux moment is also necessary. The balance equation for the first order moment is given by

$$\frac{3\mu_n}{h_i}\left(\psi_{n,i+1/2} - 2\psi_{n,i} + \psi_{n,i-1/2}\right) + \sigma_{t,i}\hat{\psi}_{n,i} = \frac{\sigma_{s,i}}{2}\sum_{m=1}^{M} w_m\hat{\psi}_{m,i}, \qquad (2.15)$$

while the auxiliary relation for AHOT-N1 generalizes Eq. (2.12) to

$$\left(\frac{1+\alpha_{n,i}}{2}\right)\psi_{n,i+1/2} + \left(\frac{1-\alpha_{n,i}}{2}\right)\psi_{n,i-1/2} = \psi_{n,i} + \alpha_{n,i}\hat{\psi}_{n,i}, \qquad (2.16)$$

where the spatial weights for AHOT-N1 are given by

$$\alpha_{n,i} = \frac{\left[\coth\left(\delta_{n,i}\right) - \frac{1}{\delta_{n,i}}\right]}{\left[1 - \frac{3}{\delta_{n,i}}\left(\coth\left(\delta_{n,i}\right) - \frac{1}{\delta_{n,i}}\right)\right]}. \qquad (2.17)$$

In this set of equations the zeroth flux moment is equivalent to the cell-averaged flux calculated by AHOT-N0, DD, and Step and is represented by $\psi_{n,i}$. The first moment of the flux is present due to the linear representation of the flux and is denoted by $\hat{\psi}_{n,i}$. The parameter $\delta_{n,i}$ is defined as in Eq. (2.14) for the AHOT-N0 equations.

To form a closed system of equations, i.e. the same number of equations as unknowns solved for, it is necessary to include boundary conditions for all of the aforementioned systems of equations. The vacuum boundary condition is used throughout much of this work for the sake of simplicity. The vacuum boundary condition imposes the condition that there is no incident neutron flux on the external boundaries of the problem domain and it is independent of the discretization scheme used. Hence, when using the discrete-ordinates angular discretization method, the vacuum boundary conditions amounts to

$$\psi_{n,1/2} = 0, \quad \mu_n > 0 \qquad (2.18\text{a})$$

$$\psi_{n,I+1/2} = 0, \quad \mu_n < 0. \qquad (2.18\text{b})$$

All of the numerical schemes described to this point are discretizations of the one-dimensional discrete-ordinates equations. However, the neutron scalar flux is also frequently approximated using neutron diffusion theory. In fact, in large systems with little neutron absorption, diffusion theory yields sufficiently accurate

solutions at a lower computational cost.

2.2 The Neutron Diffusion Equation

The one-speed, time-independent diffusion equation can be derived directly from the one-speed transport equation given the appropriate assumptions are made. By assuming that the angular flux has a linearly anisotropic angular dependence it is possible to arrive at the P_1 transport approximation. The P_1 approximation can be solved to find the distribution of neutrons in the spatial domain, but this can be simplified further by assuming an isotropic external source. In the diffusion approximation the neutron current is proportional to the spatial gradient of the flux. This relationship is referred to as *Fick's Law*,

$$\mathbf{J}(\vec{r}) = -D(\vec{r})\nabla\phi(\vec{r}), \tag{2.19}$$

where the proportionality constant, $D(\hat{r})$, is termed the diffusion coefficient.

The diffusion equation resulting from these approximations has no explicit angular dependence and is written purely in terms of the scalar flux. The one-speed, time-independent, neutron diffusion equation is given by

$$-\nabla \cdot D(\vec{r})\nabla\phi(\vec{r}) + \sigma_a(\vec{r})\phi(\vec{r}) = Q(\vec{r}). \tag{2.20}$$

The absorption macroscopic cross section, σ_a, is related to the total and scattering macroscopic cross sections by the relation, $\sigma_a = \sigma_t - \sigma_s$. The diffusion coefficient, D, for the case of isotropic-scattering is given by

$$D(\vec{r}) = \frac{1}{3\sigma_t(\vec{r})}. \tag{2.21}$$

If Eqs. (2.20) and (2.21) are written for the specialized case of slab geometry they yield

$$-\frac{d}{dx}D(x)\frac{d}{dx}\phi(x) + \sigma_a(x)\phi(x) = Q(x), \tag{2.22}$$

$$D(x) = \frac{1}{3\sigma_t(x)}. \tag{2.23}$$

Spatial discretization is achieved by again considering a spatial grid of I intervals, as in Fig. 2.1. Each cell, i, covers the domain $[x_{i-1/2}, x_{i+1/2}]$ and the midpoint value, x_i is taken to the be the arithmetic average of the edge points, denoted by the half-integer subscripts $i-1/2$ and $i+1/2$. If it is assumed that all cross sections are constant within a computational cell, Eq. (2.22) can be integrated over the interval $[x_{i-1/2}, x_{i+1/2}]$, resulting in

$$-D_i \left.\frac{d}{dx}\phi(x)\right|_{x_{i-1/2}}^{x_{i+1/2}} + \sigma_{a,i}\phi_i = Q_i. \tag{2.24}$$

In accordance with previous notation, in this equation D_i refers to the value of the diffusion coefficient in cell i with the same notation used for $\sigma_{a,i}$. The cell average value of the scalar flux has been approximated by the midpoint value, $\phi(x_i) \approx \phi_i$ and similarly the cell average value of the external source, if not constant, has been approximated by the midpoint value, $Q(x_i) \approx Q_i$.

The derivative term in Eq. (2.24) is then evaluated by using forward/backward finite differencing and imposing continuity of the neutron current at a cell interface, e.g. $x_{i+1/2}$, using Fick's Law.

$$-D_i \frac{\phi_{i+1/2} - \phi_i}{h_i/2} = -D_{i+1} \frac{\phi_{i+1} - \phi_{i+1/2}}{h_{i+1}/2} \tag{2.25}$$

The notation used for the edge valued scalar flux in Eq. (2.25) is analogous to that used for the cell edge angular fluxes in Eq. (2.7). The edge value $\phi_{i+1/2}$ can be explicitly solved for in terms of cell average fluxes, approximated by their cell-center values, using this condition. An analogous condition can be written for the interface at $x_{i-1/2}$ so that $\phi_{i-1/2}$ can also be found in terms of cell average scalar flux values. The final step to finding a discretized diffusion system is evaluating the derivative term in Eq. (2.24) and again using forward/backward finite differencing. The edge values found from the continuity condition can then be substituted and a relation involving three adjacent cell centered scalar flux values is found, resulting in the standard three-point diffusion stencil

$$-\left(a_{i,i-1}\right)\phi_{i-1} + \left(a_{i,i-1} + a_{i,i+1}\right)\phi_i - \left(a_{i,i+1}\right)\phi_{i+1} + \sigma_{a,i}\phi_i = Q_i, \quad i = 2, \ldots, I-1,$$
$$\tag{2.26}$$

where the a coefficients are given by

$$a_{i,i\pm 1} = \frac{2/h_i}{h_{i\pm 1}/D_{i\pm 1} + h_i/D_i}. \tag{2.27}$$

All that remains to be done so that the diffusion equation may solved numerically is to account for the boundary conditions. Eq. (2.26) comprises $I - 2$ equations in I unknowns, the cell centered, or approximately the cell-averaged scalar fluxes. The most commonly used boundary conditions are the vacuum and reflective boundary. This work primarily concerns itself with the vacuum boundary, which in the case of diffusion theory and ignoring the extrapolation length is the same as saying that $\phi_{1/2} = \phi_{I+1/2} = 0$. Integrating Eq. (2.22) in cells $i = 1$ and $i = I$ and imposing the vacuum boundary condition at the system edges yields

$$\left(a_{1,2} + \frac{2D_1}{h_1^2} + \sigma_{a,1} \right) \phi_1 - (a_{1,2}) \phi_2 = Q_1, \tag{2.28a}$$

$$- (a_{I,I-1}) \phi_{I-1} + \left(a_{I,I-1} + \frac{2D_I}{h_I^2} + \sigma_{a,I} \right) \phi_I = Q_I. \tag{2.28b}$$

With these equations the system is now closed, i.e. I equations in I unknowns, and it is possible to solve for all the ϕ_i unknowns explicitly. In fact, it is possible to write this system in the simple tridiagonal matrix form

$$\mathbf{A}\vec{\phi} = \vec{Q}, \tag{2.29}$$

where the elements of the tridiagonal matrix $\mathbf{A}$ are given by the coefficients of the ϕ_i unknowns in Eqs. (2.26), (2.28a), and (2.28b), while element i of $\vec{\phi}$ and $\vec{Q}$ are given by ϕ_i and Q_i respectively.

Equation (2.29) can then be solved using any standard linear algebra technique such as LU Decomposition or a stationary iterative method. Both the boundary equations, Eqs. (2.28a) and (2.28b), and the balance equation, Eq. (2.26), simplify considerably in a homogeneous medium with uniform cell spacing and external source. The simplified equations are worth writing out since they will be referred to explicitly in Chapter 4. The homogeneous medium, uniform mesh analog to Eqs. (2.26) and (2.28) are

$$-D\left(\frac{\phi_{i-1} - 2\phi_i + \phi_{i+1}}{h^2}\right) + \sigma_a\phi_i = Q, \tag{2.30}$$

$$\left(\frac{3D}{h^2} + \sigma_a\right)\phi_1 - \left(\frac{D}{h^2}\right)\phi_2 = Q, \tag{2.31a}$$

$$-\left(\frac{D}{h^2}\right)\phi_{I-1} + \left(\frac{3D}{h^2} + \sigma_a\right)\phi_I = Q. \tag{2.31b}$$

This simplified system can also be written in matrix form, only the elements in matrix **A** will differ. While finding the diffusion theory solution is obviously a simpler problem than finding the transport theory solution it should be emphasized that diffusion theory is only applicable for large systems with little absorption. Diffusion theory is also known to be inaccurate near material interfaces and at system boundaries. Essentially diffusion theory fails where the flux becomes strongly anisotropic in its angular dependence.

Now that the foundations of both transport and diffusion theories, and the numerical methods for their discretization, have been reviewed and with all dependent and independent variables discretized so that a numerical solution can be sought, an asymptotic analysis of the transport equation in the so-called diffusion limit will be presented.

2.3 The Asymptotic Diffusion Limit

Analyses of the asymptotic limit of the neutron transport equation in the continuum for diffusive regimes were performed by Larsen and Keller [5], Habetler and Matkowsky [6], and Larsen [8] between 1974 and 1980. These analyses showed that in diffusive regimes diffusion theory constitutes an asymptotic limit of transport theory. Diffusive systems are loosely defined as those with large total cross sections, σ_t, and small absorption cross sections and external sources, σ_a and Q, respectively, effectively allowing the neutrons to experience many collisions and survive many such collisions.

In this section the asymptotic analysis of the one-speed, isotopic scattering, one-dimensional, discrete-ordinates transport equation, published by Larsen, Morel, and Miller [10], will be reviewed. The one-dimensional discrete-ordinates transport

equation is given by Eq. (2.4), but here the cross sections and external source are denoted using tildes (e.g., $\sigma_t \to \tilde{\sigma}_t$), and the scattering cross section, σ_s, has been rewritten as the difference between the total and absorption cross sections.

$$\left[\mu_n \frac{d}{dx} + \tilde{\sigma}_t(x)\right]\psi_n(x) = (\tilde{\sigma}_t(x) - \tilde{\sigma}_a(x))\sum_{m=1}^{N} w_m\psi_m(x) + Q(x), \quad n = 1,\ldots,N$$

(2.32)

To proceed with the asymptotic analysis the physical cross sections and external source (i.e. the tilde quantities) are scaled by the dimensionless parameter ε in the following manner:

$$\tilde{\sigma}_t(x) = \frac{\sigma_t(x)}{\varepsilon}, \tag{2.33a}$$

$$\tilde{\sigma}_a(x) = \varepsilon\sigma_a(x), \tag{2.33b}$$

$$\tilde{Q}(x) = \varepsilon Q(x). \tag{2.33c}$$

From this point on physical quantities will be represented using tildes while the ε independent components of these quantities are represented without tildes. The parameter ε is defined as the ratio of a typical mean free path to the scale length of the system. A more thorough discussion of ε and the chosen scalings can be found in Section II of [10]. However it is important to note that under this definition, the diffusion limit implies that the parameter $\varepsilon \to 0$ as the typical mean free path in the system diminishes compared to the system size, thus approaching 0. In highly diffusive systems the probability of neutron interaction is very large and so in highly diffusive systems the parameter ε tends toward 0.

The scalings in Eq. (2.33) were chosen so that as $\varepsilon \to 0$ the total cross section becomes large while the absorption cross section and external source become small. This describes a regime dominated by neutron scattering and defines the concept of the diffusion limit as it will be used in this work, i.e., the diffusion limit is the limit as $\varepsilon \to 0$. This work will also take advantage of standard asymptotic notation. Using this notation it is said that $\tilde{\sigma}_t$ is $O(\varepsilon)$, meaning $\tilde{\sigma}_t$ is at most some constant times the parameter ε. Likewise, it can be said σ_t is $O(1)$ because it is invariant to changes in ε and also that $\tilde{\sigma}_a$ is $O(\varepsilon^{-1})$.

The specific scaling chosen also has three very desirable properties, enumerated by Larsen [20], that should be briefly noted. Under this scaling both the infinite medium solution $\phi_\infty = \tilde{Q}/\tilde{\sigma}_a = Q/\sigma_a$ and the diffusion length,

$$L = \frac{1}{\sqrt{3\tilde{\sigma}_a \tilde{\sigma}_t}} = \frac{1}{\sqrt{3\sigma_a \sigma_t}} \tag{2.34}$$

are $O(1)$.

It can also be seen easily that if the selected scaling is applied to the diffusion approximation, Eq. (2.22), the resulting equation is independent of ε. When considering the transport problem in Eq. (2.32) under the given scaling the resulting equation is

$$\left[\mu_n \frac{d}{dx} + \frac{\sigma_t(x)}{\varepsilon}\right] \psi_n(x) = \left(\frac{\sigma_t(x)}{\varepsilon} - \varepsilon\sigma_a(x)\right) \sum_{m=1}^{N} w_m \psi_m(x) + \varepsilon Q(x), \quad n = 1, \ldots, N. \tag{2.35}$$

With having introduced the scaled parameters into the transport problem it is now possible to expand the angular flux in powers of ε as shown by

$$\psi_n(x) = \sum_{k=0}^{\infty} \varepsilon^k \psi_n^{(k)}(x). \tag{2.36}$$

By inserting the asymptotic expansion, Eq. (2.36), into Eq. (2.35) a system of equations for $0 \leq k \leq \infty$ is obtained. The resulting asymptotic relation is satisfied in the limit $\varepsilon \to 0$ for each power of ε. The first equation, equating the coefficients of ε^{-1}, is given by

$$\sigma_t(x) \left(\psi_n^{(0)}(x) - \sum_{m=1}^{N} w_m \psi_m^{(0)}(x)\right) = 0. \tag{2.37}$$

The solution to Eq. (2.37) is simply given by

$$\psi_n^{(0)}(x) = \phi^{(0)}(x), \tag{2.38}$$

where $\phi^{(0)}$ is the zero order asymptotic estimate of the scalar flux defined by

$$\phi^{(k)}(x) \equiv \sum_{m=1}^{N} w_m \psi_m^{(k)}(x). \tag{2.39}$$

Equation (2.37) clearly implies that the zero order asymptotic estimate of the angular flux, i.e. $\psi_n^{(0)}$, is isotropic. At this point $\phi^{(0)}(x)$ is still an unknown quantity. The asymptotic equation corresponding to the coefficients of the $O(1)$ terms again involves $\psi_n^{(0)}$ and is given by

$$\sigma_t(x) \left(\psi_n^{(1)}(x) - \sum_{m=1}^{N} w_m \psi_m^{(1)}(x) \right) = -\mu_n \frac{d}{dx} \phi^{(0)}(x). \tag{2.40}$$

For a solution of this equation, $\psi_n^{(1)}$, to exist a certain solvability condition needs to be satisfied. This condition is found by multiplying the equation by the quadrature weights, w_n and then summing over all of the discrete angles. This operation causes the left hand side of the equation to vanish, resulting in

$$0 = -\left(\sum_{m=1}^{N} \mu_m w_m \right) \frac{d}{dx} \phi^{(0)}(x), \tag{2.41}$$

which implies that for any non constant scalar flux it must be true that

$$0 = \sum_{m=1}^{N} \mu_m w_m. \tag{2.42}$$

Thus if the quadrature set chosen in the discrete-ordinates framework satisfies this condition the solution to Eq. (2.40) is given by

$$\psi_n^{(1)}(x) = \phi^{(1)}(x) - \frac{\mu_n}{\sigma_t(x)} \frac{d}{dx} \phi^{(0)}, \tag{2.43}$$

where we recognize that the Gauss-Legendre quadrature set does satisfy the condition given in Eq. (2.42) as explicitly stated in Eq. (2.3a).

Generating Eq. (2.43) has provided another equation involving $\phi^{(0)}(x)$, but another undetermined quantity, $\phi^{(1)}(x)$, has also been introduced. For this reason the expression equating the coefficients of ε is considered, written as

$$\sigma_t(x) \left(\psi_n^{(2)}(x) - \sum_{m=1}^{N} w_m \psi_m^{(2)}(x) \right) =$$

$$- \mu_n \frac{d}{dx} \left(\phi^{(1)}(x) - \frac{\mu_n}{\sigma_t(x)} \frac{d}{dx} \phi^{(0)}(x) \right) - \sigma_a(x)\phi^{(0)}(x) + Q(x). \quad (2.44)$$

Rather than solve Eq. (2.44) for $\psi_n^{(2)}(x)$, a solvability condition is imposed. It is easily seen that if Eq. (2.44) is multiplied by w_n and summed over all n the left hand side vanishes. This implies that the summation over the right hand side must also be equal to 0.

$$\sum_{n=1}^{N} \left[-\frac{d}{dx} \left(\mu_n \phi^{(1)}(x) - \frac{\mu_n^2}{\sigma_t(x)} \frac{d}{dx} \phi^{(0)}(x) \right) - \sigma_a(x)\phi^{(0)}(x) + Q(x) \right] w_n = 0 \quad (2.45)$$

After performing the summation it is shown that the solvability condition requires the following relation must hold:

$$-\frac{d}{dx} \frac{1}{3\sigma_t(x)} \frac{d}{dx} \phi^{(0)}(x) + \sigma_a(x)\phi^{(0)}(x) = Q(x). \quad (2.46)$$

Should the quadrature set chosen satisfy the condition

$$\sum_{n=1}^{N} w_n \mu_n^2 = \frac{1}{3},$$

which the previously chosen set does, as shown in Eq. (2.3b), it is easy to see that Eq. (2.46) is very similar to the standard diffusion approximation. In fact if Eq. (2.46) is multiplied by ε it can be written in terms of the physical cross sections and external source as

$$-\frac{d}{dx} \tilde{D}(x) \frac{d}{dx} \phi^{(0)}(x) + \tilde{\sigma}_a(x)\phi^{(0)}(x) = \tilde{Q}(x). \quad (2.47)$$

Comparing this with the diffusion theory equation given in Eq. (2.22) we observe they are identical with the diffusion coefficient set to $\tilde{D} = (3\tilde{\sigma}_t)^{-1}$. This analysis shows that the asymptotic solution to the transport problem in a diffusive

regime is given by

$$\psi_n(x, \varepsilon) = \phi^{(0)}(x) + O(\varepsilon). \tag{2.48}$$

The relationship stated above is a restatement of Eq. (2.38) with explicit acknowledgement that the angular anisotropy in the angular flux is of $O(\varepsilon^0)$. It has also now been shown that the zero order component of the scalar flux, $\phi^{(0)}$, satisfies the diffusion approximation given in Eq. (2.47). Thus, this relation states that in a diffusive regime the angular flux is approximately equal to the scalar flux, with an error term that is $O(\varepsilon)$, such that as ε goes to 0 the two fluxes approach one another. This relation is the basis for recognizing that the diffusion approximation is an asymptotic limit of transport theory.

2.4 Asymptotic Solutions of Discretized Transport Problems

The previous analysis shows that the continuous one-speed, diffusion equation is an asymptotic limit of the one-speed, isotropic-scattering transport equation in slab geometry. This result uncovers yet another link between transport and diffusion theory, however it begs one to question whether the same relationship holds true for the discrete versions of the transport and diffusion equations discussed in Sections 2.1 and 2.2. This question was thoroughly examined by Larsen, Morel, and Miller in an influential 1987 paper [10].

If this relationship did hold then one would expect the discretized transport equation to asymptotically limit to the discretized diffusion equation. However, it was shown in Section 2.1 that the discretization of the transport equation requires an auxiliary relationship or discretization scheme (e.g. Diamond Difference). It will be seen shortly that for some discretization schemes the discrete transport equation limits to a discrete diffusion equation and for others it does not. When discussing discretized problems it is also necessary to determine whether the analysis will be done in the "thick" or "intermediate" diffusion limit as defined by Larsen, Morel, and Miller [10].

In the thick diffusion limit the optical thickness of spatial cells become increas-

ingly thick as $\varepsilon \to 0$. This implies that in the scaling described in Sec. 2.3 the mesh spacing, h, is chosen in a manner that is independent of ε, i.e., h is $O(1)$, while σ_t provides the growth in the optical cell size as $\varepsilon \to 0$,

$$\tau_{\text{thick}} = \frac{\sigma_t h}{\varepsilon} = O(\varepsilon)^{-1} \tag{2.49}$$

In the thick diffusion limit the mesh spacing is said to be on the order of a "scale length", the typical distance by which the angular flux varies by an $O(1)$ amount. For problems in a diffusive regime the scale length can be roughly equated with the diffusion length, L.

Along with the scale length another natural measure of length is the mean free path, the typical distance a neutron travels between successive interactions. In the intermediate diffusion limit the mesh spacing is on the order of a typical mean free path, $O(\varepsilon)$, which implies that the optical thickness in this regime is given by

$$\tau_{\text{int}} = \sigma_t h = O(1). \tag{2.50}$$

With the concept of the thick and intermediate limits explained, Figure 2.2, adapted from [10], clarifies the relationships among continuum transport theory, continuum diffusion theory, discretized transport theory, and discretized diffusion theory. The solid lines in Figure 2.2 indicate relationships proven to be true. It was shown in Section 2.3 that the continuum, or analytic, S_N equations limit to the continuum diffusion equation in the limit $\varepsilon \to 0$. Truncation error analyses have been used in the past to prove that "good" discretizations of the diffusion equation and of the spatial dependence of the S_N equations limit to their respective analytic counterparts as the cell size, h, approaches 0.

The dotted lines indicate possible relationships, which may or may not hold for a given spatial discretization scheme. In the thick limit this relationship is said to hold if the discretized discrete-ordinates equations asymptotically limit to a legitimate diffusion discretization. A diffusion discretization is considered legitimate if the analytic diffusion equation is obtained from the discretized equation as $h \to 0$. If it is shown for a given discretization scheme that a relationship indicated by a dotted line holds then that spatial discretization is said to have the corresponding diffusion limit. Thus it is possible for any discretization scheme to possess both
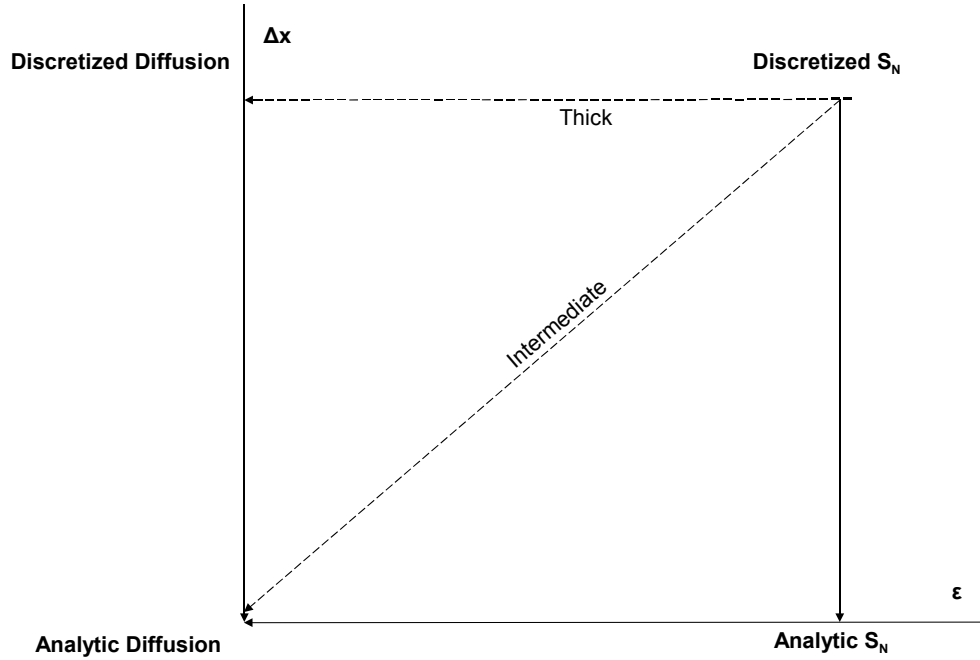
Figure 2.2. Comparison of Asymptotic Diffusion Limits

limits, neither limit, only the thick diffusion limit, or only the intermediate diffusion limit. Furthermore a distinction can be made between cell edge and cell center fluxes such that each flux quantity can individually be said to possess one, neither, or both of the limits.

Larsen, Morel, and Miller [10] investigated five different discretization schemes with regards to both the cell average and cell edge fluxes. The analyses they performed are concerned with the interior of the slab only and assume any boundary layers have been adequately resolved by the spatial mesh. The conclusions drawn from these analyses can be found in Table 1 of [10]. A portion of this table is reproduced in Table 2.1 to present the results obtained for the Diamond Difference and Step methods for later reference in this thesis. For the Diamond Difference cell edge fluxes in the thick diffusion limit the entry *maybe* means *yes* only if incident

Table 2.1. Selected Results from Larsen, Morel, and Miller [10]

	Intermediate		Thick	
	Edge	Average	Edge	Average
Diamond	yes	yes	maybe	yes
Step	maybe	maybe	maybe	maybe

boundary fluxes are isotropic and is *no* otherwise. The *maybe* entries for the Step method only become *yes* under the very restrictive conditions that $\sigma_{a,i} = Q_i = 0$ and also that the product $(\sigma_{t,i} h_i)$ is a constant for $1 \leq i \leq I$. If these conditions are not met then the Step method does not have the diffusion limit.

The analyses performed to obtain these results, specifically for the thick limit, are at the core of this thesis and are used extensively to re-analyze the Diamond Difference method and the AHOT-N0 and AHOT-N1 schemes. To understand the results adapted from [10] in Table 2.1 and the new results derived in this thesis a good foundation in the asymptotic analysis of the discretized equations is necessary. Therefore both the thick regime Step and Diamond Difference method derivations of Larsen, Morel, and Miller [10] will now be presented.

2.4.1 The Step Method

The Step method itself was described in Section 2.1 as a specific case of a WDD scheme with weights $\mu_n / |\mu_n|$. Writing the balance and Step equations using the scalings from Eqs. (2.33) yields

$$\frac{\mu_n}{h_i} \left(\psi_{n,i+1/2} - \psi_{n,i-1/2} \right) + \frac{\sigma_{t,i}}{\varepsilon} \psi_{n,i} = \left(\frac{\sigma_{t,i}}{\varepsilon} - \varepsilon \sigma_{a,i} \right) \sum_{m=1}^{M} w_m \psi_{m,i} + \varepsilon Q_i, \qquad (2.51)$$

$$\psi_{n,i} = \psi_{n,i \pm 1/2}, \quad \mu_n \gtrless 0. \qquad (2.52)$$

An asymptotic expansion similar to that given in Eq. (2.36) is now introduced through

$$\psi_n \approx \sum_{k=0}^{\infty} \varepsilon^k \psi_n^{(k)}. \qquad (2.53)$$

Inserting Eq. (2.53) into Eqs. (2.51) and (2.52), with the assumption that both the cell averaged and cell edge fluxes can be represented through this power series in ε we follow the same procedure used in the continuous case, equating the coefficients of the various powers of ε and recursively solving the resulting set of equations for coefficients of the orders of ε in the asymptotic expansion of the angular flux. The first power of ε considered is ε^{-1}, where by equating the coefficients of ε^{-1} we obtain

$$\sigma_{t,i}\left(\psi_{n,i}^{(0)} - \sum_{m=1}^{M} w_m \psi_{m,i}^{(0)}\right) = 0. \tag{2.54}$$

Therefore the following relation must be true, with the quantity $\phi_i^{(0)}$ still being undetermined,

$$\psi_{n,i}^{(0)} = \phi_i^{(0)}. \tag{2.55}$$

This relationship implies that the leading order component of the angular flux expansion is isotropic. Armed with this relationship between the zero order terms of the scalar and angular flux, the remaining task is then to find an expression for $\phi_i^{(0)}$. To find this expression the terms in the asymptotic expansion of the Step method of ε^0 are examined. By equating these coefficients we obtain

$$\sigma_{t,i}\left(\psi_{n,i}^{(1)} - \sum_{m=1}^{M} w_m \psi_{m,i}^{(1)}\right) = -\frac{\mu_n}{h_i}\left(\psi_{n,i+1/2}^{(0)} - \psi_{n,i-1/2}^{(0)}\right), \tag{2.56}$$

$$\psi_{n,i}^{(0)} = \psi_{n,i\pm1/2}^{(0)}. \tag{2.57}$$

Equations. (2.57) and (2.55) can now be substituted into Eq. (2.56) to produce

$$\sigma_{t,i}\left(\psi_{n,i}^{(1)} - \sum_{m=1}^{M} w_m \psi_{m,i}^{(1)}\right) = -\frac{\mu_n}{h_i}\left(\phi_{n,i+1/2\mp1/2}^{(0)} - \phi_{n,i-1/2\mp1/2}^{(0)}\right), \quad \mu_n \gtrless 0. \tag{2.58}$$

The solvability condition which is then applied to Eq. (2.58) consists of multiplying Eq. (2.58) by w_n and summing over all angles. with the result of this operation given by

$$0 = -\frac{1}{h_i} \left(\sum_{\mu_n > 0} \mu_n w_n \right) \left(\phi_{i-1}^{(0)} - 2\phi_i^{(0)} + \phi_{i+1}^{(0)} \right). \tag{2.59}$$

It is easy to see that Eq. (2.59) is comparable to the discretized diffusion equation, Eq. (2.30), only under the very restrictive conditions listed previously in this section. That is, it is necessary that $\sigma_a = Q = 0$ and the product $(\sigma_{t,i} h_i)$ is a constant for $1 \le i \le I$. Under these conditions it can be said the cell average fluxes in the Step method have the thick diffusion limit. The same can be said for the cell center fluxes since these can be directly related to $\phi_i^{(0)}$ by combining Eqs. (2.55) and (2.57).

These results show that in the thick diffusive regime the Step method does not generally limit to a legitimate discretization of the diffusion equation. The theory proposed by Larsen, Morel, and Miller [10] is that any scheme which does limit to a legitimate diffusion discretization will provide much more accurate results than a scheme which does not limit to a legitimate diffusion discretization. Thus these results imply that in the thick regime the Step method will produce inaccurate results unless the conditions given above are met. As it turns out the Step method is quite inaccurate in this regime as confirmed by numerical results generated by Larsen, Morel, and Miller which will be presented in Section 2.4.3. These numerical results will also confirm the predictions made by the results of the Diamond Difference analysis which will be presented next.

2.4.2   Diamond Difference

The asymptotic analysis of the Diamond Difference method developed by Larsen, Morel, and Miller [10] was expanded in the followup paper by Larsen, and Morel [11] to specifically account for unresolved boundary layers. Although to this point the boundaries have been ignored, the analysis including boundary layers will be included here for the sake of completeness. The analysis presented here is lengthy but essential for the understanding of the new work which will described in Chapter 4.

The Diamond Difference method was described in Section 2.1 as the WDD scheme with spatial weights of 0. Writing the balance and Diamond Difference

relations along with the boundary conditions and using the scalings from Eq. (2.33) results in the problem described by

$$\frac{\mu_n}{h_i}\left(\psi_{n,i+1/2} - \psi_{n,i-1/2}\right) + \frac{\sigma_{t,i}}{\varepsilon}\psi_{n,i} = \left(\frac{\sigma_{t,i}}{\varepsilon} - \varepsilon\sigma_{a,i}\right)\sum_{m=1}^{M} w_m\psi_{m,i} + \varepsilon Q_i, \qquad (2.60a)$$

$$\psi_{n,i} = \frac{1}{2}\left(\psi_{n,i+1/2} + \psi_{n,i-1/2}\right), \qquad (2.60b)$$

$$\psi_{n,1/2} = f_n, \quad \mu_n > 0 \qquad (2.60c)$$

$$\psi_{n,I+1/2} = g_n, \quad \mu_n < 0, \qquad (2.60d)$$

where the quadrature rules again adhere to the properties described by Eqs. (2.3).

This analysis will frequently use the operation of multiplying an equation by $\mu_n^k w_n$ and summing over all angles, which we term "taking the kth angular moment" of the equation. An angular cell edge or cell average quantity which has undergone this operation is also said to be the kth moment of the original quantity. Using this nomenclature the zeroth, first, and second angular moments of the angular flux are defined by

$$\phi^{(k)} = \sum_{m=1}^{M} w_m\psi_m^{(k)}, \qquad (2.61a)$$

$$\vartheta^{(k)} = \sum_{m=1}^{M} \mu_m w_m\psi_m^{(k)}, \qquad (2.61b)$$

$$\nu^{(k)} = \sum_{m=1}^{M} \mu_m^2 w_m\psi_m^{(k)}. \qquad (2.61c)$$

Again the analysis begins by inserting the asymptotic expansion of Eq. (2.53) into Eqs. (2.60). The coefficients of powers of ε are then equated creating a recursive set of equations. As with the Step method there is only one equation of $O(\varepsilon^{-1})$, given by

$$\sigma_{t,i}\left(\psi_{n,i}^{(0)} - \sum_{m=1}^{M} w_m\psi_{m,i}^{(0)}\right) = 0 \qquad (2.62)$$

Again the solution to Eq. (2.62) is isotropic,

$$\psi_{n,i}^{(0)} = \phi_i^{(0)}, \tag{2.63}$$

with the quantity $\phi_i^{(0)}$ still undetermined. There are four equations of $O(\varepsilon^0)$, given by

$$\phi_i^{(0)} = \frac{1}{2}\left(\psi_{n,i+1/2}^{(0)} + \psi_{n,i-1/2}^{(0)}\right), \tag{2.64a}$$

$$\sigma_{t,i}\left(\psi_{n,i}^{(1)} - \sum_{m=1}^{M} w_m \psi_{m,i}^{(1)}\right) = -\frac{\mu_n}{h_i}\left(\psi_{n,i+1/2}^{(0)} - \psi_{n,i-1/2}^{(0)}\right), \tag{2.64b}$$

$$\psi_{n,1/2}^{(0)} = f_n, \quad \mu_n > 0 \tag{2.64c}$$

$$\psi_{n,I+1/2}^{(0)} = g_n, \quad \mu_n < 0. \tag{2.64d}$$

In order to more easily analyze Eq. (2.64a), we define the quantity

$$\eta_{n,i+1/2}^{(0)} \equiv \psi_{n,i+1/2}^{(0)} - 3\nu_{i+1/2}^{(0)}, \tag{2.65}$$

where $\nu_{i+1/2}^{(0)}$ is the second angular moment of the angular flux at a cell edge as defined by Eq. (2.61c). This definition implies that the following is also true,

$$\sum_{n=1}^{M} \mu_n^2 \eta_{n,i+1/2}^{(0)} w_n = 0, \tag{2.66}$$

which also allows for Eq. (2.64a) to be written as the sum

$$\frac{1}{3}\phi_i^{(0)} = \frac{1}{2}\left(\nu_{i+1/2}^{(0)} + \nu_{i-1/2}^{(0)}\right) + \frac{1}{6}\left(\eta_{n,i+1/2}^{(0)} + \eta_{n,i-1/2}^{(0)}\right). \tag{2.67}$$

The second angular moment of Eq. (2.67) is then taken, producing

$$\frac{1}{3}\phi_i^{(0)} = \frac{1}{2}\left(\nu_{i+1/2}^{(0)} + \nu_{i-1/2}^{(0)}\right). \tag{2.68}$$

Substituting Eq. (2.68) into Eq. (2.67) also results in

$$0 = \eta_{n,i+1/2}^{(0)} + \eta_{n,i-1/2}^{(0)}, \tag{2.69}$$

which in term implies

$$\eta_{n,i+1/2}^{(0)} = (-1)^i \eta_n^{(0)}. \tag{2.70}$$

With the above relationships available it is possible to rewrite Eqs. (2.65) and (2.66), respectively, in terms of $\eta_n^{(0)}$ as

$$\psi_{n,i+1/2}^{(0)} = 3\nu_{i+1/2}^{(0)} + (-1)^i \eta_n^{(0)}, \tag{2.71}$$

$$\sum_{n=1}^{M} \mu_n^2 \eta_n^{(0)} w_n = 0. \tag{2.72}$$

Equation (2.71) now explicitly shows the leading order component of the angular edge flux split into an isotropic and an anisotropic component. This relationship can now be substituted into the $O(\varepsilon^0)$ neutron balance equation, Eq. (2.64b), resulting in

$$\sigma_{t,i} \left(\psi_{n,i}^{(1)} - \sum_{m=1}^{M} w_m \psi_{m,i}^{(1)} \right) = -\frac{\mu_n}{h_i} \left[3 \left(\nu_{i+1/2}^{(0)} - \nu_{i-1/2}^{(0)} \right) + 2(-1)^i \eta_n^{(0)} \right]. \tag{2.73}$$

If the zeroth angular moment of Eq. (2.73) is taken, the solvability condition given by

$$0 = \sum_{n=1}^{M} \mu_n \eta_n^{(0)} w_n \tag{2.74}$$

results. This is a condition which is required for the existence of a solution to Eq. (2.73), a solution expressed by

$$\psi_{n,i}^{(1)} = \phi_i^{(1)} - \frac{\mu_n}{h_i} \left[3 \left(\nu_{i+1/2}^{(0)} - \nu_{i-1/2}^{(0)} \right) + 2(-1)^i \eta_n^{(0)} \right]. \tag{2.75}$$

The quantity $\phi_i^{(1)}$ is still undetermined, along with $\phi_i^{(0)}$. Before considering any $O(\varepsilon)$ equations we consider the $O(\varepsilon^0)$ boundary equations. We begin by inserting the separated leading order edge angular flux, Eq. (2.71), into Eqs. (2.64c) and (2.64d), the left and right boundary conditions, respectively. This substitution results in the following equations,

$$3\nu_{1/2}^{(0)} + \eta_n^{(0)} = f_n, \quad \mu_n > 0 \tag{2.76a}$$

$$3\nu_{I+1/2}^{(0)} + (-1)^I \eta_n^{(0)} = g_n, \quad \mu_n < 0 \tag{2.76b}$$

which imply the following is true

$$\eta_n^{(0)} = \begin{cases} f_n - 3\nu_{1/2}^{(0)}, & \mu_n > 0 \\ (-1)^I (g_n - 3\nu_{I+1/2}^{(0)}), & \mu_n < 0. \end{cases} \tag{2.77}$$

From Eqs. (2.72) and (2.74) it is known that the first and second angular moments of $\eta_n^{(0)}$ are equal to zero. Substituting the expression for $\eta_n^{(0)}$, given by Eq. (2.77), into the two angular moment relations makes it possible to explicitly solve for $\nu_{1/2}^{(0)}$ and $\nu_{I+1/2}^{(0)}$, the second angular moment of the flux at the slab edges. Solving for these quantities yields the following expressions:

$$\nu_{1/2}^{(0)} = \sum_{\mu_n>0} \left(\frac{\mu_n}{6\gamma} + \mu_n^2 \right) f_n w_n + (-1)^I \sum_{\mu_n<0} \left(-\frac{|\mu_n|}{6\gamma} + \mu_n^2 \right) g_n w_n. \tag{2.78a}$$

$$\nu_{I+1/2}^{(0)} = \sum_{\mu_n<0} \left(\frac{|\mu_n|}{6\gamma} + \mu_n^2 \right) g_n w_n + (-1)^I \sum_{\mu_n>0} \left(-\frac{\mu_n}{6\gamma} + \mu_n^2 \right) f_n w_n. \tag{2.78b}$$

The constant, γ, is a function of the quadrature set, and is defined by

$$\gamma \equiv \sum_{\mu_n>0} \mu_n w_n \approx \frac{1}{4}. \tag{2.79}$$

Equations (2.78) effectively define the boundary conditions of the spatially discretized system of equations based on the second angular moments, $\nu_{i+1/2}^{(0)}$. Larsen and Morel examine the accuracy of these boundary conditions upon the completion of the Diamond Difference analysis. With the boundary values out of the way we direct our attention back toward the system interior by considering the $O(\varepsilon)$ equations of the Diamond Difference and balance equations,

$$\psi_{n,i}^{(1)} = \frac{1}{2} \left(\psi_{n,i+1/2}^{(1)} + \psi_{n,i-1/2}^{(1)} \right), \tag{2.80}$$

$$\sigma_{t,i} \left(\psi_{n,i}^{(2)} - \sum_{m=1}^{M} w_m \psi_{m,i}^{(2)} \right) = -\frac{\mu_n}{h_i} \left(\psi_{i+1/2}^{(1)} - \psi_{i-1/2}^{(1)} \right) - \sigma_{a,i} \phi_i^{(0)} + Q_i. \qquad (2.81)$$

We then take the zeroth angular moment of Eq. (2.81), which yields

$$\vartheta_{i+1/2}^{(1)} - \vartheta_{i-1/2}^{(1)} = h_i \left(-\sigma_{a,i} \phi_i^{(0)} + Q_i \right), \qquad (2.82)$$

where the first angular moment on the edge, $\vartheta_{i+1/2}^{(1)}$, is defined by Eq. (2.61b) .

We then proceed to write Eq. (2.82) for the $(i + 1)$th cell and add this result to equation Eq. (2.82) to obtain

$$\vartheta_{i+3/2}^{(1)} - \vartheta_{i-1/2}^{(1)} = - \left(\sigma_{a,i+1} h_{i+1} \phi_{i+1}^{(0)} + \sigma_{a,i} h_i \phi_i^{(0)} \right) + \left(h_{i+1} Q_{i+1} + h_i Q_i \right). \qquad (2.83)$$

The next step we take is to substitute Eq. (2.80) into Eq. (2.75) and take the first angular moment of this equation. Utilizing the condition given by Eq. (2.72) and subtracting the equation for the ith cell from the equation for the $(i + 1)$th cell yields

$$\begin{aligned}
\vartheta_{i+3/2}^{(1)} - \vartheta_{i-1/2}^{(1)} &= 2 \sum_{n=1}^{M} \mu_n \left(\psi_{n,i+1}^{(1)} - \psi_{n,i}^{(1)} \right) w_n \\
&= -\frac{2}{\sigma_{t,i+1} h_{i+1}} \left(\nu_{i+3/2}^{(0)} - \nu_{i+1/2}^{(0)} \right) + \frac{2}{\sigma_{t,i} h_i} \left(\nu_{i+1/2}^{(0)} - \nu_{i-1/2}^{(0)} \right). \qquad (2.84)
\end{aligned}$$

As previously mentioned, Eqs. (2.83) and (2.84) are valid in the slab interior, i.e., $i \in [2, I - 1]$. The first angular moment edge fluxes can be eliminated by equating the right hand side of both equations. The resulting expression is given by

$$-\frac{1}{3\sigma_{t,i+1}h_{i+1}}\left(\nu_{i+3/2}^{(0)}-\nu_{i+1/2}^{(0)}\right)+\frac{1}{3\sigma_{t,i}h_i}\left(\nu_{i+1/2}^{(0)}-\nu_{i-1/2}^{(0)}\right)$$
$$+\frac{1}{4}\left(\sigma_{a,i+1}h_{i+1}\left(\nu_{i+3/2}^{(0)}+\nu_{i+1/2}^{(0)}\right)+\sigma_{a,i}h_i\left(\nu_{i+1/2}^{(0)}+\nu_{i-1/2}^{(0)}\right)\right)$$
$$=\frac{1}{6}\left(h_{i+1}Q_{i+1}+h_iQ_i\right),\quad 2\le i\le I-1.\quad (2.85)$$

By inserting Eq. (2.68) into Eq. (2.63) the leading order cell average angular fluxes are then given by

$$\frac{1}{3}\psi_{n,i}=\frac{1}{2}\left(\nu_{i+1/2}^{(0)}+\nu_{i-1/2}^{(0)}\right)+O(\varepsilon).\qquad (2.86)$$

The cell edge fluxes are given by Eq. (2.71) and thus to leading order are given by

$$\frac{1}{3}\psi_{n,i+1/2}=\nu_{i+1/2}^{(0)}+\frac{1}{3}(-1)^i\eta_n^{(0)}+O(\varepsilon).\qquad (2.87)$$

The second angular moment edge flux, $\nu_{i+1/2}^{(0)}$, is now determined in the slab interior by Eq. (2.85) and on the boundaries by Eqs. (2.78). The quantity $\eta_n^{(0)}$ is determined by Eq. (2.77).

Equation (2.85) shows that to leading order the cell average angular flux calculated using the Diamond Difference method does limit to a legitimate diffusion discretization in the slab interior. This is true because Eq. (2.85) is an edge based discretization of the diffusion equation. Granted that we are convinced Eq. (2.85) is a legitimate diffusion discretization, i.e. that if $h\to 0$ Eq. (2.85) results in Eq. (2.22), then we can see from Eq. (2.87) that unless $\eta_n^{(0)}=0$ the cell edge angular fluxes do not generally have the thick diffusion limit. As $h\to 0$ the term $\eta_n^{(0)}$ is invariable and thus $(\nu_{i+1/2}^{(0)}+(-1)^i\eta_n^{(0)})$ will not be a legitimate discretization of the diffusion equation.

There are some peculiarities regarding this diffusion discretization. Most notable is that the second moment of the angular flux rather than the scalar flux itself is the unknown quantity in the diffusion discretization. The authors do explicitly mention that this choice was made for the sake of algebraic simplicity but the analysis itself is not restricted to the chosen definition of $\nu_{i+1/2}^{(0)}$. The discretization is

also based on cell edges as opposed to the cell average based discretization derived in Section 2.2. It is also noteworthy that the diffusion discretization in Eq. (2.85) differs from the previously developed discretization by including external sources and absorption terms from cells adjacent to cell i.

For the Diamond Difference method to fully possess the thick diffusion limit it is not sufficient to limit to a legitimate diffusion discretization in the slab interior. It is also necessary for any unresolved boundary layers to be accounted for. To determine the accuracy of the method on the system boundaries Larsen and Morel determine how closely the conditions given in Eqs. (2.78) approximate the appropriate diffusion boundary conditions, which they discuss thoroughly in the introduction to [11]. These boundary conditions rely on the Case W-function [2], a component included in solutions of half-space problems arising from formal boundary layer analysis of the diffusion limit to the transport problem. This type of analysis is necessary because the diffusion equation cannot adequately represent the correct transport boundary conditions [34]. Specifically these boundary conditions in the continuum are given by

$$\frac{1}{2}\phi(0) = \int_0^1 W(\mu)f(\mu)d\mu, \tag{2.88a}$$

$$\frac{1}{2}\phi(L) = \int_{-1}^0 W(-\mu)g(\mu)d\mu. \tag{2.88b}$$

Here L represents the x-coordinate of the slab edge and the W-function itself is given in terms of Chandrasekhar's X-function [7] by

$$W(\mu) = \frac{\mu}{X(-\mu)}\left[\int_0^1 \frac{s}{X(-s)}ds\right]^{-1}. \tag{2.89}$$

However, Larsen and Morel note that the W-function is smooth and can be represented fairly well by the polynomial

$$\tilde{W}(\mu) = 0.956\mu + 1.565\mu^2 \pm 0.0035 \approx \mu + \frac{3}{2}\mu^2. \tag{2.90}$$

Larsen and Morel then conclude that the boundary conditions derived in the asymptotic analysis, Eqs. (2.78) only closely approximate Eq. (2.90) if the following condition is true:

$$0 = \sum_{\mu_n > 0} \left(-\frac{\mu_n}{6\gamma} + \mu_n^2 \right) f_n w_n = \sum_{\mu_n < 0} \left(-\frac{|\mu_n|}{6\gamma} + \mu_n^2 \right) g_n w_n. \tag{2.91}$$

The authors note that this condition does not generally hold, but does for the case of isotropic incident flux. Thus for a homogeneous slab with vacuum boundaries it can be expected that both the cell average and cell edge angular fluxes have the thick diffusion limit. It should be recognized that even with vacuum boundaries a heterogeneous slab will not generally have the thick diffusion limit for either the cell average or cell edge fluxes due to possible anisotropy at the material interface.

For an anisotropic incident boundary flux, Eqs. (2.78) result in very highly distorted boundary conditions, where the distortion itself is dependent on whether the arbitrarily chosen number of cells, I, is even or odd. Larsen and Morel note that the variation on the left boundary is due solely to an anisotropic incident boundary flux on the right boundary while the variation on the right boundary is due solely to an anisotropic incident boundary flux on the left boundary.

The analytic predictions made by the asymptotic analyses of the Step and Diamond Difference methods have previously been summarized in Table 2.1 and have now been rigorously derived. To test these predictions numerically Larsen, Morel, and Miller [10] chose five problems while Larsen and Morel [11] chose two problems, composing a set of seven distinct numerical experiments. One problem from each set will be presented in the following section.

2.4.3 Numerical Results

Two numerical experiments have been chosen from among the seven conducted by Larsen, Morel, and Miller [10] and Larsen and Morel [11]. These two problems were specifically chosen because the boundary conditions are vacuum and the same numerical experiments will be used to test the new analyses being presented in following chapters. All of the problems were solved using the S_8 Gauss-Legendre quadrature set and the reference solutions were created using the Diamond Difference method on a uniform mesh containing 10^4 spatial cells. Solutions for Problem 1 were generated using the Diamond Difference and Step methods with the indicated mesh size and then compared to the reference solution.

Problem 1

The first numerical experiment consists of a purely scattering homogeneous slab containing an external source with vacuum boundaries, defined in the thick regime by the following problem:

$$\mu_n \frac{d\psi_n}{dx} + 100\psi_n = 100 \sum_{m=1}^{M} \psi_m w_m + 0.01, \quad 0 < x < 10$$

$$\psi_n(0) = 0, \quad \mu_n > 0$$

$$\psi_n(10) = 0, \quad \mu_n < 0$$

$$h = 1.0.$$

The theoretical predictions made suggest that even with such thick spatial cells (100 mean free paths) the Diamond Difference method will produce accurate results because it limits to a legitimate diffusion discretization. In contrast, the Step method analysis predicts that the Step method will not be accurate with such
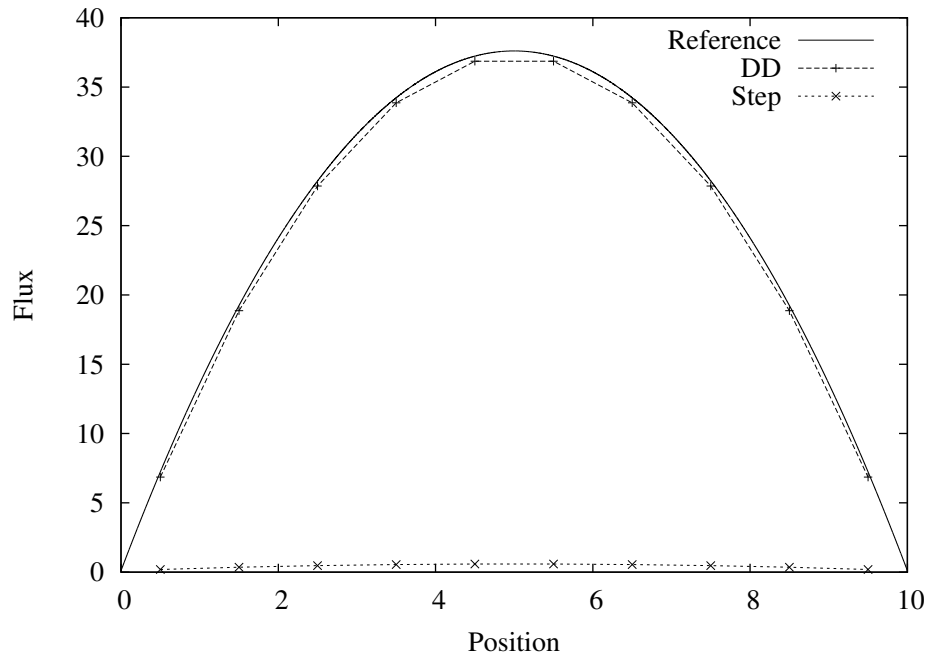
Figure 2.3. Problem 1: Larsen, Morel, and Miller [10] Cell Average Thick Regime Results
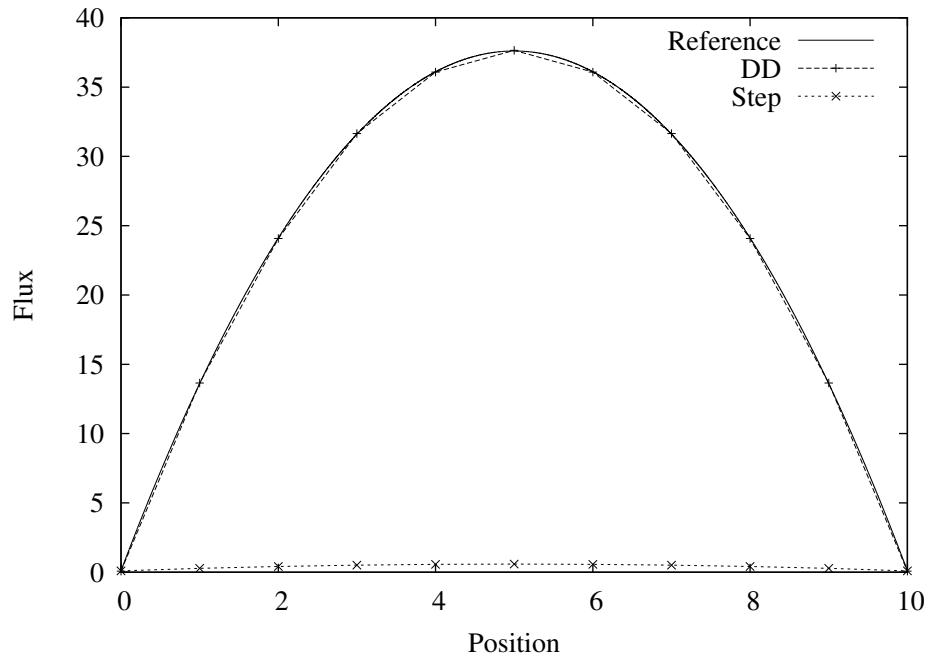
Figure 2.4. Problem 1: Larsen, Morel, and Miller [10] Cell Edge Thick Regime Results

optically thick cells. For this specific problem the predictions made with regard to each method are the same for both the cell edge and cell averaged fluxes. Figures 2.3 and 2.4 confirm the above predictions. It can be seen for both cell edge and cell average scalar fluxes that the Diamond Difference results are nearly identical to the reference solution while the results produced by the Step method are grossly inaccurate.

These numerical results support the hypothesis made by Larsen, Morel, and Miller [10] that a spatial discretization that possesses the thick diffusion limit will yield accurate results when using optically thick spatial cells. Thus the asymptotic analysis technique can be used to determine which transport spatial discretizations will result in solutions with accuracy comparable to diffusion theory and which spatial discretizations will fail to provide accurate solutions in the regime in which $h \to \infty$, well outside the realm of tradition truncation analyses.

Problem 2

The second numerical experiment consists of a two region slab with vacuum boundaries. One region contains a flat external source along with finite absorption while

the other region is purely scattering with no external source. The experiment is defined by the following problem:

$$\mu\frac{\partial}{\partial x}\psi(x,\mu) + \sigma_t(x)\psi(x,\mu) = \frac{\sigma_s(x)}{2}\int_{-1}^{1}\psi(x,\mu')d\mu' + \frac{Q(x)}{2}, \quad 0 < x < 20$$

$$\psi(0,\mu) = 0, \quad \mu > 0$$

$$\psi(20,\mu) = 0, \quad \mu < 0$$

$$\sigma_t(x) = 100,$$

$$\sigma_s(x) = \begin{cases} 90, & 0 < x < 10 \\ 100, & 10 < x < 20 \end{cases}$$

$$Q(x) = \begin{cases} 10, & 0 < x < 10 \\ 0, & 10 < x < 20 \end{cases}$$

$$h = \begin{cases} 10/N, & 1 < x < 10 \\ 1.0, & 10 < x < 20. \end{cases}$$

Figs. 2.5 and 2.6 show the results of the two region problem in terms of cell average and cell edge fluxes, respectively. It is quite apparent that the material interface introduces significant inaccuracy to the Diamond Difference results. The cell average fluxes oscillate slightly in the source region but are reasonably accurate. However, upon entrance to the scattering region there is a large degradation in the quality of the solution. Larsen and Morel state that the reason for these inaccuracies is the highly oscillatory nature of the edge fluxes, apparent in Fig. 2.6.

The authors conjecture that it is the oscillating behavior of the edge fluxes, specifically at the material interface, which leads to the inaccuracies in the cell average fluxes. The evidence for this is given by the two different values of N considered. For $N = 11$ the edge fluxes enter the scattering region well above the reference solution and subsequently the cell average fluxes in this case are also well above the reference solution. The converse is true for the case where $N = 10$,
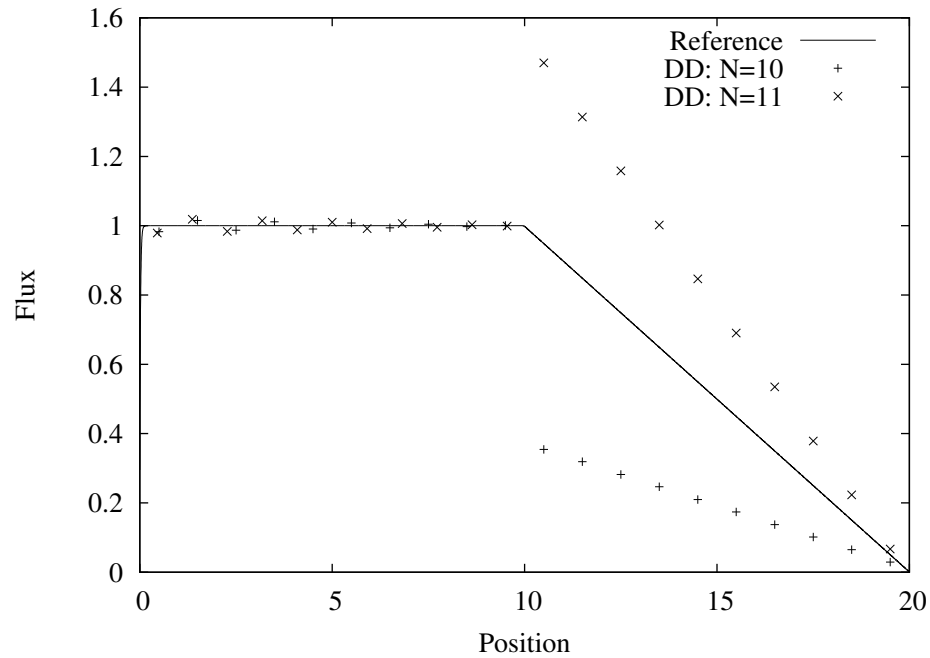
Figure 2.5. Problem 2: Larsen and Morel [11] Cell Average Thick Regime Results

the edge fluxes enter the scattering region below the reference solution and the cell average fluxes for the same case are well below the reference solution in the scattering region.

No satisfactory explanation for the origin of the oscillations present in the cell edge scalar fluxes is provided in [11]. The asymptotic analysis suggests that for this problem the cell-edge fluxes will be accurate since the prescribed incident (vacuum) fluxes are isotropic, although it is possible that the oscillations arise solely due to the anisotropy of the flux at the material interface. Although it is not a certainty that the asymptotic analysis is applicable in the source region since as the authors note, the region is not diffusive in an asymptotic sense because of the magnitude of σ_a. However they also go on to state that the diffusion approximation produces accurate results in this region. The behavior of the Diamond Difference method in this numerical experiment will be re-examined in more detail in Chapter 4, and a potential explanation for the oscillation seen in the edge fluxes will also be provided.

To this point the relevant background has been presented as has the theory and mechanics of the asymptotic analysis on discretized transport problems. The
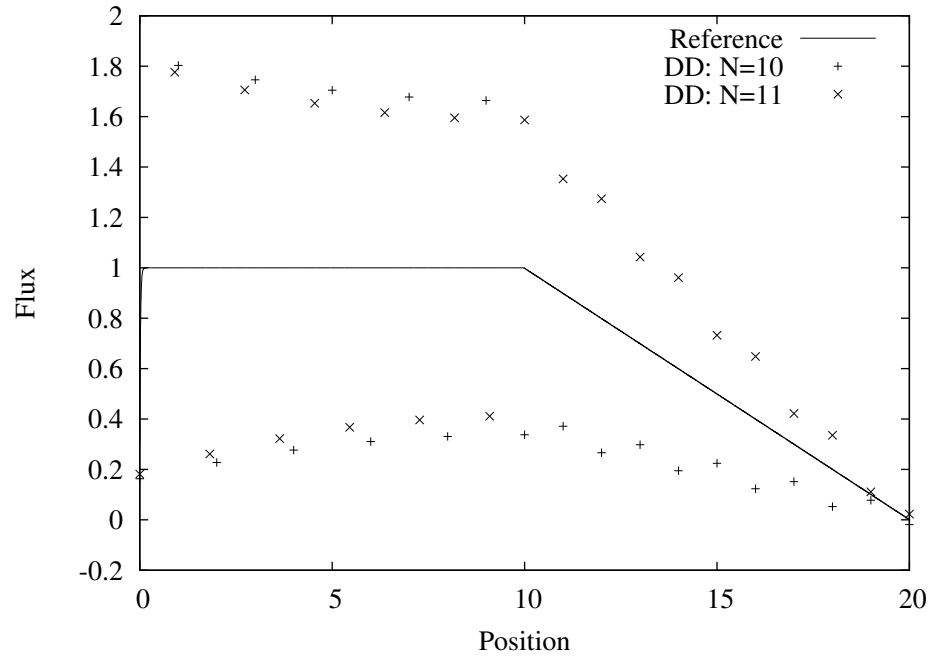
Figure 2.6. Problem 2: Larsen and Morel [11] Cell Edge Thick Regime Results

following chapters will extend this analysis to the AHOT-N0 method and also show that the analysis of the Linear Discontinuous method, performed by Larsen and Morel [11], applies to the first order nodal method, AHOT-N1, as well. Finally the asymptotic limit of the Diamond Difference method will be rederived in terms of cell average rather than cell edge scalar fluxes. Problems 1 and 2 will again be used to test predictions arising from the asymptotic analyses regarding the behavior of the spatial discretizations.

Asymptotic Analyses of Low Order Nodal Methods

3.1   Introduction

The class of Arbitrarily High Order Transport methods of the Nodal type (AHOT-N) was introduced in Section 1.1.4 and the low order methods, AHOT-N0 and AHOT-N1, were specifically formulated in Section 2.1. In this chapter the solutions to these methods are now considered for transport problems in thick, diffusive regimes. The same methods used to analyze and classify the Step and Diamond Difference methods can be applied to these low order nodal methods.

AHOT-N0 is the lowest order nodal method and in slab geometry is exact aside from the representation of the scattering source. In the AHOT-N0 approximation the scattering source is represented mathematically by polynomials of order zero (constants) in a spatial cell. The AHOT-N0 discretization can be written as a weighted Diamond Difference scheme with one distinct spatial weight, $\alpha_{n,i}$, per spatial cell, per discrete ordinate, as given in Eq. (3.1c), where $0 \leq |\alpha_{n,i}| \leq 1$. Thus the spatial weights of the AHOT-N0 method lie between the extremes of the Diamond Difference and Step methods.

The AHOT-N1 method uses a linear approximation of the spatial dependence and in slab geometry the AHOT-N1 equations also are exact aside from the repre-

sentation of the scattering source by polynomials of order one (linear functions) in a spatial cell. The AHOT-N1 discretization can also be written as a WDD scheme with one distinct spatial weight, $\alpha_{n,i}$, per spatial cell, per discrete ordinate, given by Eq. (3.13d). The AHOT-N1 method differs from the WDD schemes considered so far by possessing multiple balance equations. This method includes both a zero and first spatial moment of the scalar flux and so a balance equation for each of these quantities is necessary.

The same asymptotic analysis performed previously on the Step and Diamond Difference methods will now be applied to the AHOT-N0 and AHOT-N1 discretizations. Initial hopes were that the AHOT-N0 method, being "more exact" than the Step and Diamond Difference methods, would possess the thick diffusion limit unconditionally for both the cell average and cell edge fluxes. Unfortunately, the asymptotic analysis shows and numerical results confirm that AHOT-N0 only possesses the thick diffusion limit under the same restrictive conditions as the Step method. It can be shown however that AHOT-N1 rigorously possesses the thick diffusion limit for cell average and cell edge fluxes, even in the presence of unresolved boundary layers. The AHOT-N1 equations can actually be written in such a manner that the Larsen and Morel [11] analysis of the Linear Moments method is directly applicable and the results then inferred. The conclusions drawn regarding both nodal methods will be confirmed using two numerical experiments presented in Sec. 2.4.3.

This chapter will close with a brief examination of the the Explicit Slope (ES) discretization, derived by Hanshaw and Larsen [35]. This discretization seeks to emulate the accuracy of the AHOT-N1 method in the thick limit while only requiring the same amount of storage as the AHOT-N0 method. This is accomplished by approximating the scattering source as a linear function with an explicitly defined slope.

3.2 AHOT-N0 Thick Limit Analysis

The AHOT-N0 method is completely characterized by the balance equation, auxiliary relation, and spatial weight given by

$$\frac{\mu_n}{h_i}\left(\psi_{n,i+1/2}-\psi_{n,i-1/2}\right)+\tilde{\sigma}_{t,i}\psi_{n,i}=\tilde{\sigma}_{s,i}\sum_{m=1}^{M}w_m\psi_{m,i}+\tilde{Q}_i, \qquad (3.1\text{a})$$

$$\psi_{n,i}=\left(\frac{1+\tilde{\alpha}_{n,i}}{2}\right)\psi_{n,i+1/2}+\left(\frac{1-\tilde{\alpha}_{n,i}}{2}\right)\psi_{n,i-1/2}, \qquad (3.1\text{b})$$

$$\tilde{\alpha}_{n,i}=\coth\left(\frac{\tilde{\sigma}_{t,i}h_i}{2\mu_n}\right)-\left(\frac{1}{\frac{\tilde{\sigma}_{t,i}h_i}{2\mu_n}}\right). \qquad (3.1\text{c})$$

We have foregone the inclusion of the boundary conditions for simplicity and also because the outcome of the analysis indicates including the boundary conditions would be unnecessary.

As in previous analyses the first step is to replace the scattering cross section by the difference of the total and absorption cross sections, and then scale the cross sections and fixed source by the parameter ε using Eqs. (2.33). The scaled system of equations is then given by

$$\frac{\mu_n}{h_i}\left(\psi_{n,i+1/2}-\psi_{n,i-1/2}\right)+\frac{\sigma_{t,i}}{\varepsilon}\psi_{n,i}=\left(\frac{\sigma_{t,i}}{\varepsilon}-\varepsilon\sigma_{a,i}\right)\sum_{m=1}^{M}w_m\psi_{m,i}+\varepsilon Q_i, \qquad (3.2\text{a})$$

$$\psi_{n,i}=\left(\frac{1+\alpha_{n,i}}{2}\right)\psi_{n,i+1/2}+\left(\frac{1-\alpha_{n,i}}{2}\right)\psi_{n,i-1/2}, \qquad (3.2\text{b})$$

$$\alpha_{n,i}=\coth\left(\frac{\sigma_{t,i}h_i}{2\mu_n\varepsilon}\right)-\left(\frac{2\mu_n\varepsilon}{\sigma_{t,i}h_i}\right). \qquad (3.2\text{c})$$

We now include the previously used asymptotic expansion, Eq. (2.53), which expands the cell average and cell edge angular fluxes in power series in the asymptotic variable ε. However, we can see from Eq. (3.2c) that simply equating the coefficients of ε is not possible in this case due to the presence of the hyperbolic cotangent. To amend this it is necessary to find an expansion for the AHOT-N0 spatial weights as $\varepsilon \to 0$. The first step in this expansion is to rewrite the spatial weights as

$$\alpha_{n,i} = \begin{cases} + \left(\dfrac{1+e^{\left(-\frac{\sigma_{t,i}h_i}{|\mu_n|\varepsilon}\right)}}{1-e^{\left(-\frac{\sigma_{t,i}h_i}{|\mu_n|\varepsilon}\right)}} - \left(\dfrac{2|\mu_n|\varepsilon}{\sigma_{t,i}h_i}\right) \right), & \mu_n > 0 \\[3em] - \left(\dfrac{1+e^{\left(-\frac{\sigma_{t,i}h_i}{|\mu_n|\varepsilon}\right)}}{1-e^{\left(-\frac{\sigma_{t,i}h_i}{|\mu_n|\varepsilon}\right)}} - \left(\dfrac{2|\mu_n|\varepsilon}{\sigma_{t,i}h_i}\right) \right), & \mu_n < 0. \end{cases} \qquad (3.3)$$

We can now split the first term into two components as shown by

$$\alpha_{n,i} = \begin{cases} + \left(\dfrac{1}{1-e^{\left(-\frac{\sigma_{t,i}h_i}{|\mu_n|\varepsilon}\right)}} + \dfrac{e^{\left(-\frac{\sigma_{t,i}h_i}{|\mu_n|\varepsilon}\right)}}{1-e^{\left(-\frac{\sigma_{t,i}h_i}{|\mu_n|\varepsilon}\right)}} - \left(\dfrac{2|\mu_n|\varepsilon}{\sigma_{t,i}h_i}\right) \right), & \mu_n > 0 \\[3em] - \left(\dfrac{1}{1-e^{\left(-\frac{\sigma_{t,i}h_i}{|\mu_n|\varepsilon}\right)}} + \dfrac{e^{\left(-\frac{\sigma_{t,i}h_i}{|\mu_n|\varepsilon}\right)}}{1-e^{\left(-\frac{\sigma_{t,i}h_i}{|\mu_n|\varepsilon}\right)}} - \left(\dfrac{2|\mu_n|\varepsilon}{\sigma_{t,i}h_i}\right) \right), & \mu_n < 0. \end{cases} \qquad (3.4)$$

We now expand the first two terms in each case about the exponential term as $\varepsilon \to 0$, which, when combined with the remaining linear term, results in the asymptotic spatial weights given by

$$\alpha_{n,i} = \pm \left(1 - \frac{2|\mu_n|\varepsilon}{\sigma_{t,i}h_i} \right) + O\left(e^{-\frac{\sigma_{t,i}h_i}{|\mu_n|\varepsilon}} \right). \qquad (3.5)$$

With this expression for the AHOT-N0 spatial weights in hand we can proceed to substitute the asymptotic expansion of Eq. (2.53) into Eqs. (3.2). We also now substitute the expansion developed for the spatial weights, Eq. (3.5) into Eq. (3.2c). These substitutions result in the equation set

$$\varepsilon^{-1}\sigma_{t,i}\left(\psi_{n,i}^{(0)} - \sum_{m=1}^{M} w_m \psi_{m,i}^{(0)} \right) +$$

$$\varepsilon^{0}\left[\sigma_{t,i}\left(\psi_{n,i}^{(1)} - \sum_{m=1}^{M} w_m \psi_{m,i}^{(1)} \right) + \frac{\mu_n}{h_i}\left(\psi_{n,i+1/2}^{(0)} - \psi_{n,i-1/2}^{(0)} \right) \right] + O(\varepsilon) = 0, \quad (3.6a)$$

$$\varepsilon^{0}\left(\psi_{n,i}^{(0)} - \psi_{n,i\pm1/2}^{(0)} \right) + O(\varepsilon) = 0. \qquad (3.6b)$$

We can easily see here that up to $0(\varepsilon)$, Eqs. (3.6) are identical to those of the Step method. If the $O(\varepsilon)$ components were considered then the differences

between the two methods would begin to appear. However since the $O(\varepsilon^{-1})$ and the $O(\varepsilon^0)$ terms sufficed to determine $\phi_i^{(0)}$ for the Step method the same will hold true for AHOT-N0. To verify this reasoning we can now collect and equate the coefficients of ε^{-1} and ε^0. The lone $O(\varepsilon^{-1})$ equation, Eq. (3.7) comes from the neutron balance relation,

$$\sigma_{t,i}\left(\psi_{n,i}^{(0)} - \sum_{m=1}^{M} w_m \psi_{m,i}^{(0)}\right) = 0. \tag{3.7}$$

This relation implies that the quantity, $\phi_i^{(0)}$ is given by

$$\psi_{n,i}^{(0)} = \phi_i^{(0)}. \tag{3.8}$$

At this point $\phi_i^{(0)}$ itself is still an undetermined quantity. We again proceed to the relations for the next order of epsilon in the hopes of finding an expression for $\phi_i^{(0)}$. The auxiliary relation for $O(\varepsilon^0)$ is given by

$$\psi_{n,i}^{(0)} = \psi_{n,i\pm1/2}^{(0)}, \quad \mu_n \gtrless 0 \tag{3.9}$$

which is readily seen to be the same as the $O(\varepsilon^0)$ Step relation.

The balance relation at $O(\varepsilon^0)$ is then specified by

$$\sigma_{t,i}\left(\psi_{n,i}^{(1)} - \sum_{m=1}^{M} w_m \psi_{m,i}^{(1)}\right) = -\frac{\mu_n}{h_i}\left(\psi_{n,i+1/2}^{(0)} - \psi_{n,i-1/2}^{(0)}\right). \tag{3.10}$$

Just as with the Step method we can now substitute Eq. (3.8) and Eq. (3.9) into the $O(\varepsilon^0)$ balance relation, Eq. (3.10), resulting in

$$\sigma_{t,i}\left(\psi_{n,i}^{(1)} - \sum_{m=1}^{M} w_m \psi_{m,i}^{(1)}\right) = -\frac{\mu_n}{h_i}\left(\phi_{i+1/2\mp1/2}^{(0)} - \phi_{i-1/2\mp1/2}^{(0)}\right). \tag{3.11}$$

If we now take the zeroth angular moment of Eq. (3.11) the resulting relation contains only the unknown $\phi^{(0)}$,

$$0 = -\frac{1}{h_i}\left(\sum_{\mu_n>0} \mu_n w_n\right)\left(\phi_{i-1}^{(0)} - 2\phi_i^{(0)} + \phi_{i+1}^{(0)}\right). \tag{3.12}$$

It is clear that Eq. (3.12) is identical to Eq. (2.59) and thus also comparable to

the discretized diffusion equation, Eq. (2.30), only under the same very restrictive conditions given for the Step method. AHOT-N0 limits to a legitimate diffusion discretization if $\sigma_a = Q = 0$ and the product $(\sigma_{t,i} h_i)$ is a constant for $1 \leq i \leq I$. Only under these conditions can it be said that the cell average fluxes in the AHOT-N0 method have the thick diffusion limit. The same can be said for the cell edge fluxes since these can be directly related to $\phi^{(0)}$ by combining Eqs. (3.8) and (3.9).

This result is disappointing but also somewhat expected since the AHOT-N0 spatial weights are easily shown to limit to the Step method weights for increasingly optically thick cells such that in the thick diffusive regime it should be expected the AHOT-N0 and Step discretizations behave similarly. With the failure of this nodal method we now ask whether AHOT-N1 will fail to have the thick diffusion limit as well. This analysis will be carried out in the following section. Numerical results will then be given in Section 3.4 to support the predictions made by both analyses.

3.3   AHOT-N1 Thick Limit Analysis

The AHOT-N1 method is fundamentally different from the Diamond Difference, Step, and AHOT-N0 methods because it utilizes a linear in-cell representation of the scattering source, as well as the angular and scalar fluxes. However, AHOT-N1 is not unique among discretization schemes in this sense. Larsen and Morel [11] have previously analyzed the Linear Discontinuous (LD) and Linear Moments discretization methods which also use linear functions within the spatial cell. The Linear Moments method itself is a one dimensional version of the Linear-Linear Nodal Method which in one dimension is equivalent to the AHOT-N1 method. Larsen and Morel state that the Linear Moments analysis is identical to the LD analysis, so the claim can be made that results drawn by Larsen and Morel for the LD method also hold true for the AHOT-N1 method. Although the equations are not identical, just as AHOT-N0 was not identical to the Step method, they are asymptotically equivalent up to $O(\varepsilon)$ and so the asymptotic limit which describes the LD method also describes the AHOT-N1 method.

Larsen and Morel show that the LD method does limit to a legitimate diffu-

sion discretization for both cell average and cell edge fluxes. Their analysis also shows that unlike Diamond Difference the LD boundary conditions asymptotically approach the correct diffusion boundary conditions. This means that even in the presence of unresolved boundary layers the LD method will still *unconditionally* limit to a diffusion discretization in the thick regime. Interestingly Larsen and Morel find that by introducing a free parameter, θ, into the LD equations they can force the method to limit to a "more desirable" diffusion discretization in the thick regime. Problem 2 of Section 2.4.3 is considered using the LD method and it is shown that the results are far superior to the Diamond Difference results. The analysis performed by Larsen and Morel and the numerical experiments will be duplicated here with regards to the AHOT-N1 method.

The boundary condition analysis will not be included here for the sake of brevity, instead only the results will be discussed. See [11] and its corrigendum for this portion of the analysis. The AHOT-N1 method is now rewritten here to include Larsen and Morel's free parameter θ and in the spirit of consistency with previous notation the first moment of the flux will be represented by $\hat{\psi}_{n,i}$ while the zeroth moment of the flux will be denoted by $\psi_{n,i}$. Thus the AHOT-N1 method without boundary conditions, which has also been scaled by the asymptotic parameter ε per Eqs. (2.33) is given by

$$\frac{\mu_n}{h_i}\left(\psi_{n,i+1/2} - \psi_{n,i-1/2}\right) + \frac{\sigma_{t,i}}{\varepsilon}\psi_{n,i} = \left(\frac{\sigma_{t,i}}{\varepsilon} - \varepsilon\sigma_{a,i}\right)\sum_{m=1}^{M} w_m\psi_{m,i} + \varepsilon Q_i, \quad (3.13\text{a})$$

$$\frac{\mu_n}{\theta h_i}\left(\psi_{n,i+1/2} - 2\psi_{n,i} + \psi_{n,i-1/2}\right) + \frac{\sigma_{t,i}}{\varepsilon}\hat{\psi}_{n,i} = \left(\frac{\sigma_{t,i}}{\varepsilon} - \varepsilon\sigma_{a,i}\right)\sum_{m=1}^{M} w_m\hat{\psi}_{m,i} + \varepsilon\hat{Q}_i,$$
$$(3.13\text{b})$$

$$\left(\frac{1+\alpha_{n,i}}{2}\right)\psi_{n,i+1/2} + \left(\frac{1-\alpha_{n,i}}{2}\right)\psi_{n,i-1/2} = \psi_{n,i} + \alpha_{n,i}\hat{\psi}_{n,i}, \quad (3.13\text{c})$$

$$\alpha_{n,i} = \frac{\left[\coth\left(\frac{\delta_{n,i}}{\epsilon}\right) - \frac{\varepsilon}{\delta_{n,i}}\right]}{\left[1 - \frac{3\varepsilon}{\delta_{n,i}}\left(\coth\left(\frac{\delta_{n,i}}{\varepsilon}\right) - \frac{\varepsilon}{\delta_{n,i}}\right)\right]}. \quad (3.13\text{d})$$

The $\delta_{n,i}$ found in the AHOT-N1 spatial weights is defined by Eq. (2.14). We can also see when comparing Eq. (3.13b) to Eq. (2.15) that $\theta = 1/3$ corresponds

to the AHOT-N1 discretization described in Chapter 2.

As with the AHOT-N0 method it is also necessary to expand the AHOT-N1 spatial weights. Inspection of Eq. (3.13d) shows that as with the AHOT-N0 spatial weights, the AHOT-N1 spatial weights are odd functions of $\delta_{n,i}$, or more specifically odd functions of μ_n, thus we can make the replacement, $\delta_{n,i} \rightarrow |\delta_{n,i}|$. We also recognize that the AHOT-N0 spatial weights themselves show up in both the numerator and denominator of Eq. (3.13d) so that we can use the previous expansion of the AHOT-N0 weights to rewrite this equation as $\varepsilon \rightarrow 0$ as

$$\alpha_{n,i} = \pm \frac{\left[1 - \frac{\varepsilon}{|\delta_{n,i}|} + \mathcal{O}(e^{-\frac{2|\delta_{n,i}|}{\varepsilon}})\right]}{\left[1 - \frac{3\varepsilon}{|\delta_{n,i}|}\left(1 - \frac{\varepsilon}{|\delta_{n,i}|} + \mathcal{O}(e^{-\frac{2|\delta_{n,i}|}{\varepsilon}})\right)\right]}.$$

Here the exponential terms have been removed since they approach 0 much quicker than any polynomial. The remaining terms are now expanded as

$$\alpha_{n,i} = \pm \frac{\left[1 - \frac{\varepsilon}{|\delta_{n,i}|}\right]}{\left[1 - \frac{3\varepsilon}{|\delta_{n,i}|}\left(1 - \frac{\varepsilon}{|\delta_{n,i}|}\right)\right]} \approx \pm \left(1 - \frac{\varepsilon}{|\delta_{n,i}|}\right)\left(1 + \frac{3\varepsilon}{|\delta_{n,i}|} + O\left(\varepsilon\right)^2\right).$$

The final asymptotic expression for the AHOT-N1 spatial weights is then given by

$$\alpha_{n,i} = \pm \left(1 + \frac{2\varepsilon}{|\delta_{n,i}|}\right) + O\left(\varepsilon\right)^2. \tag{3.14}$$

After successfully expanding the spatial weights the asymptotic expansion of Eq. (2.53) is introduced for the zeroth and first moment cell average and for the cell edge fluxes. The coefficients of the ε^{-1}, ε^0, and ε^1 terms can now be equated and the system of equations solved as in previous analyses.

There are now two $O(\varepsilon^{-1})$ contributions, resulting from Eqs. (3.13a) and (3.13b) and given by

$$\sigma_{t,i}\left(\psi_{n,i}^{(0)} - \sum_{m=1}^{M} w_m \psi_{m,i}^{(0)}\right) = 0, \tag{3.15a}$$

$$\sigma_{t,i} \left(\hat{\psi}_{n,i}^{(0)} - \sum_{m=1}^{M} w_m \hat{\psi}_{m,i}^{(0)} \right) = 0. \tag{3.15b}$$

As before the solutions of these equations are isotropic quantities, where $\hat{\phi}$ has been used to represent the first moment of the scalar flux.

$$\psi_{n,i}^{(0)} = \phi_i^{(0)} \tag{3.16a}$$

$$\hat{\psi}_{n,i}^{(0)} = \hat{\phi}_i^{(0)} \tag{3.16b}$$

Each of the AHOT-N1 equations contributes at $O(1)$ and when substituting in Eqs. (3.16) the resulting equations are given by

$$\sigma_{t,i} \left(\psi_{n,i}^{(1)} - \sum_{m=1}^{M} w_m \psi_{m,i}^{(1)} \right) = -\frac{\mu_n}{h_i} \left(\psi_{n,i+1/2}^{(0)} - \psi_{n,i-1/2}^{(0)} \right), \tag{3.17a}$$

$$\sigma_{t,i} \left(\hat{\psi}_{n,i}^{(1)} - \sum_{m=1}^{M} w_m \hat{\psi}_{m,i}^{(1)} \right) = -\frac{\mu_n}{\theta h_i} \left(\psi_{n,i+1/2}^{(0)} - 2\psi_{n,i}^{(0)} + \psi_{n,i-1/2}^{(0)} \right), \tag{3.17b}$$

$$\psi_{n,i+1/2}^{(0)} = \begin{cases} \phi_i^{(0)} + \hat{\phi}_i^{(0)}, & 1 \leq i \leq I, & \mu_n > 0 \\ \phi_{i+1}^{(0)} - \hat{\phi}_{i+1}^{(0)}, & 0 \leq i \leq I-1, & \mu_n < 0. \end{cases} \tag{3.17c}$$

Substituting Eq. (3.16a) into Eq. (3.17b) and taking the zeroth angular moment of Eqs. (3.17a) and (3.17b), while keeping in mind the quadrature rules of Eq. (2.3) yields the following two solvability conditions,

$$\sum_{n=1}^{M} w_n \mu_n \psi_{n,i+1/2}^{(0)} - \sum_{n=1}^{M} w_n \mu_n \psi_{n,i-1/2}^{(0)} = 0,$$

$$\sum_{n=1}^{M} w_n \mu_n \psi_{n,i+1/2}^{(0)} + \sum_{n=1}^{M} w_n \mu_n \psi_{n,i-1/2}^{(0)} = 0,$$

which imply the following condition must hold if a solution to Eqs. (3.17) is to exist:

$$\sum_{n=1}^{M} w_n \mu_n \psi_{n,i+1/2}^{(0)} = 0. \tag{3.18}$$

By substituting Eq. (3.17c) into the condition given by Eq. (3.18), and impos-

ing continuity of the angular flux across the cell edge at $x_{i+1/2}$, separating cells i and $i+1$, it is then seen that

$$\phi_i^{(0)} + \hat{\phi}_i^{(0)} = \phi_{i+1}^{(0)} - \hat{\phi}_{i+1}^{(0)}, \quad 1 \leq i \leq I - 1. \tag{3.19}$$

We then take the zeroth angular moment of Eq. (3.17c), resulting in

$$\phi_{i+1/2}^{(0)} \equiv \phi_i^{(0)} + \hat{\phi}_i^{(0)} = \phi_{i+1}^{(0)} - \hat{\phi}_{i+1}^{(0)}, \tag{3.20}$$

thus implying

$$\phi_i^{(0)} = \frac{1}{2}\left(\phi_{i+1/2}^{(0)} + \phi_{i-1/2}^{(0)}\right), \quad 1 \leq i \leq I, \tag{3.21a}$$

$$\hat{\phi}_i^{(0)} = \frac{1}{2}\left(\phi_{i+1/2}^{(0)} - \phi_{i-1/2}^{(0)}\right), \quad 1 \leq i \leq I. \tag{3.21b}$$

Using the expressions in Eqs. (3.21), Eq. (3.17c) can now be written as

$$\psi_{n,i+1/2}^{(0)} = \phi_{i+1/2}^{(0)}, \quad i \in \begin{cases} 1 \leq i \leq I, & \mu_n > 0 \\ 0 \leq i \leq I - 1, & \mu_n < 0. \end{cases} \tag{3.22}$$

Assuming the condition given in Eq. (3.18) holds, a general solution to Eq. (3.17a) is given by

$$\psi_{n,i}^{(1)} = -\frac{\mu_n}{\sigma_{t,i} h_i}\left(\phi_{i+1/2}^{(0)} - \phi_{i-1/2}^{(0)}\right) + \phi_i^{(1)}, \quad 1 \leq i \leq I, \tag{3.23}$$

where the angular edge fluxes have been replaced using the relation given in Eq. (3.22). The unknown quantity, $\phi_i^{(1)}$, can be "integrated" out by taking the first angular moment of Eq. (3.23), resulting in

$$\vartheta_i^{(1)} = -\frac{1}{3\sigma_{t,i} h_i}\left(\phi_{i+1/2}^{(0)} - \phi_{i-1/2}^{(0)}\right), \tag{3.24}$$

where ϑ is the first angular moment of the flux as defined by Eq. (2.61b).

It still remains to find an expression to represent the unknown quantity $\phi_{i+1/2}^{(0)}$. To do so it is necessary to consider the $O(\varepsilon)$ components of both the zeroth and first moment balance equation. The expressions resulting from these contributions are

$$\sigma_{t,i}\left(\psi_{n,i}^{(2)} - \sum_{m=1}^{M} w_m \psi_{m,i}^{(2)}\right) = -\frac{\mu_n}{h_i}\left(\psi_{n,i+1/2}^{(1)} - \psi_{n,i-1/2}^{(1)}\right) - \sigma_{a,i}\phi_i^{(0)} + Q_i, \quad (3.25a)$$

$$\sigma_{t,i}\left(\hat{\psi}_{n,i}^{(2)} - \sum_{m=1}^{M} w_m \hat{\psi}_{m,i}^{(2)}\right) = -\frac{\mu_n}{\theta h_i}\left(\psi_{n,i+1/2}^{(1)} - 2\psi_{n,i}^{(1)} + \psi_{n,i-1/2}^{(1)}\right) - \sigma_{a,i}\hat{\phi}_i^{(0)} + \hat{Q}_i.$$
$$(3.25b)$$

Taking the zeroth angular moment of Eq. (3.25a) and adding the resulting expression for the ith cell to that for the $(i+1)$th cell yields

$$\left(\vartheta_{i+3/2}^{(1)} - \vartheta_{i-1/2}^{(1)}\right) = -h_i \sigma_{a,i}\phi_i^{(0)} + h_i Q_i - h_{i+1}\sigma_{a,i+1}\phi_{i+1}^{(0)} + h_{i+1}Q_{i+1}. \quad (3.26)$$

Taking the zeroth angular moment of Eq. (3.25b) and subtracting the resulting expression for the ith cell to that for the $(i+1)$th cell results in

$$\left(\vartheta_{i+3/2}^{(1)} - \vartheta_{i-1/2}^{(1)}\right) = 2\left(\vartheta_{i+1}^{(1)} - \vartheta_{i}^{(1)}\right) + h_i \sigma_{a,i}\theta\phi_i^{(0)} - h_i\theta Q_i$$
$$- h_{i+1}\sigma_{a,i+1}\theta\phi_{i+1}^{(0)} + h_{i+1}\theta Q_{i+1}. \quad (3.27)$$

Equations (3.26) and (3.27) can now be equated and then combined with Eq. (3.24) to yield

$$-\frac{1}{3\sigma_{t,i+1}h_{i+1}}\left(\phi_{i+3/2}^{(0)} - \phi_{i+1/2}^{(0)}\right) + \frac{1}{3\sigma_{t,i}h_i}\left(\phi_{i+1/2}^{(0)} - \phi_{i-1/2}^{(0)}\right) +$$
$$\frac{1}{4}\left(h_i\sigma_{a,i}\left((1-\theta)\phi_{i-1/2}^{(0)} + (1+\theta)\phi_{i+1/2}^{(0)}\right)\right.$$
$$\left. + h_{i+1}\sigma_{a,i+1}\left((1+\theta)\phi_{i+1/2}^{(0)} + (1-\theta)\phi_{i+3/2}^{(0)}\right)\right)$$
$$= \frac{1}{2}\left(h_{i+1}\left(Q_{i+1} - \theta\hat{Q}_{i+1}\right) + h_i\left(Q_i - \theta\hat{Q}_i\right)\right), \quad 1 \le i \le I \quad (3.28)$$

after further algebraic simplification. Eq. (3.28) is an expression solely in terms of the unknown $\phi_{i+1/2}^{(0)}$.

This equation is a legitimate discretization in an edge-based diffusion equation, giving AHOT-N1 the thick diffusion limit. Larsen and Morel [11] also show that the boundary conditions of the linear method are excellent approximations to the boundary conditions given by Eqs. (2.88). Thus, it can be expected that the AHOT-N1 method will provide accurate solutions using optically thick cells, even in the presence of unresolved boundary layers.

Equation (3.28) also shows the benefit of including the θ parameter in the first moment balance equation. If θ is given the actual value of $1/3$, or more generally any value not equal to 1, then the resulting expression contains a three-point absorption scheme. Larsen and Morel observe that using a θ value of 1 will collapse this three-point removal term to a more standard one-point removal term, which they state results in a more robust discretization.

The effect of the θ parameter becomes more obvious if we look at Eq. (3.28) for a homogeneous medium with a piecewise constant fixed source (so that $\hat{Q}_i = 0$). For $\theta = 1/3$ the expression simplifies to

$$-\left(\frac{1}{3\sigma_t h^2} - \frac{\sigma_a}{6}\right)\left(\phi_{i-1/2}^{(0)} - 2\phi_{i+1/2}^{(0)} + \phi_{i+3/2}^{(0)}\right) + \sigma_a \phi_{i+1/2}^{(0)} = Q_i, \qquad (3.29)$$

while for $\theta = 1$ we obtain

$$-\frac{1}{3\sigma_t h^2}\left(\phi_{i-1/2}^{(0)} - 2\phi_{i+1/2}^{(0)} + \phi_{i+3/2}^{(0)}\right) + \sigma_a \phi_{i+1/2}^{(0)} = Q_i. \qquad (3.30)$$

We can see that for the case where $\theta = 1/3$ there is an unexpected absorption term in the diffusion coefficient. In fact for sufficiently large absorption or mesh size, h, we can see that there is even the possibility of the diffusion coefficient taking on an unphysical negative value. Specifically if $h > \sqrt{6}L$ then the effective diffusion coefficient will become negative. Here L is the diffusion length, given by Eq (2.34). However this instability is not present in Eq. (3.30), where $\theta = 1$, the value which Larsen and Morel highly recommend in thick diffusive regimes.

Regardless of the value of θ, AHOT-N1 does have the thick diffusion limit for cell edge and cell average fluxes. This can be formally shown by recognizing that $\phi_{i+1/2}^{(0)}$ satisfies the legitimate diffusion discretization given by Eq. (3.28) and using Eqs. (3.22), Eq. (3.21a), and Eq. (3.16a) to formulate the relations

Table 3.1. AHOT-N0 and AHOT-N1 Asymptotic Limits

	Thick	
	Edge	Average
AHOT-N0	maybe	maybe
AHOT-N1	yes	yes

$$\psi_{n,i}^{(0)} = \frac{1}{2}\left(\phi_{i+1/2}^{(0)} + \phi_{i-1/2}^{(0)}\right) + O(\varepsilon), \tag{3.31a}$$

$$\psi_{n,i+1/2}^{(0)} = \phi_{i+1/2}^{(0)} + O(\varepsilon). \tag{3.31b}$$

The AHOT-N0 and AHOT-N1 results are summarized in Table 3.1. The *maybes* in the AHOT-N0 columns indicate that this discretization possesses the thick diffusion limit only under the same restrictive conditions as the Step method. The AHOT-N1 method possesses the thick limit for both edge and average fluxes without any conditions imposed regarding fluxes incident on the system, unlike the previous Diamond Difference results. The analytical conclusions for these low order nodal methods are tested using the previously described numerical experiments in the following section.

3.4   Numerical Results

The predictions made from the asymptotic analyses of the AHOT-N0 and AHOT-N1 methods were tested using the previously defined numerical experiments. The AHOT-N0 method was used for the homogeneous experiment, Problem 1. The AHOT-N0 average and edge scalar fluxes are displayed in Fig. 3.1. These results confirm the analytical predictions. It is easily seen that the AHOT-N0 method is quite inaccurate in thick diffusive media. The results are nearly identical to the results generated by the Step method for the same problem. However, the results are *not* identical, but instead slightly differ. This is also to be expected since the methods are only the same in the asymptotic limit. Since ε is not *equal* to 0 the difference between the solutions will be at most $O(\varepsilon)$.

Interestingly if we consider the AHOT-N0 method, and the Step method as
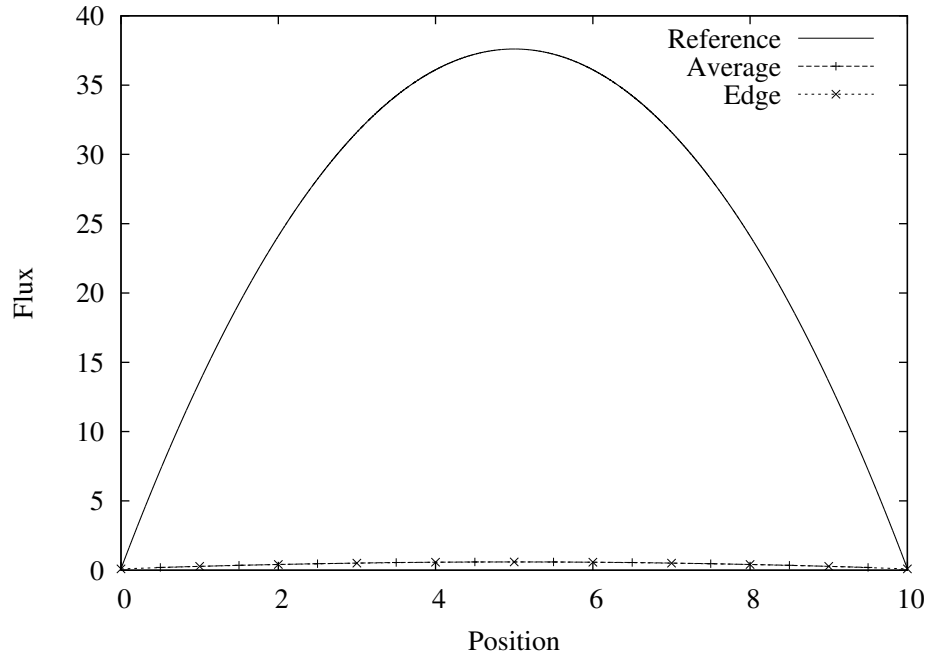
Figure 3.1. Problem 1: AHOT-N0 Cell Average and Edge Scalar Fluxes

well, for the two-region heterogeneous slab described in Chapter 2 we see much different results. The AHOT-N0, Step, and DD cell average and cell edge scalar fluxes are plotted along with the same reference solution used previously, in Figures 3.2 and 3.3 respectively. Since the AHOT-N0 and Step methods do not display the oscillatory behavior that DD does, only the case where N=10 was plotted as there is nothing to gain by plotting the case where N=11. We do see that for this problem the AHOT-N0 and Step methods perform nearly identically and much better than DD! This may seem like it contradicts the results of the asymptotic analysis, but instead it actually supports the conclusions. We know that the left half of the slab, the source region, has an external source and absorption cross section sufficiently large that the asymptotic analysis is not strictly applicable in this region. Lewis and Miller [4] have also shown that for h values sufficiently large the DD method can be expected to actually provide less accurate solutions than the Step method, thus in this region which is dominated by local balance, the AHOT-N0 and Step methods perform well.

Since AHOT-N0 and Step do not oscillate like the DD method, they reach the material interface at nearly the correct solution. The right half of the slab
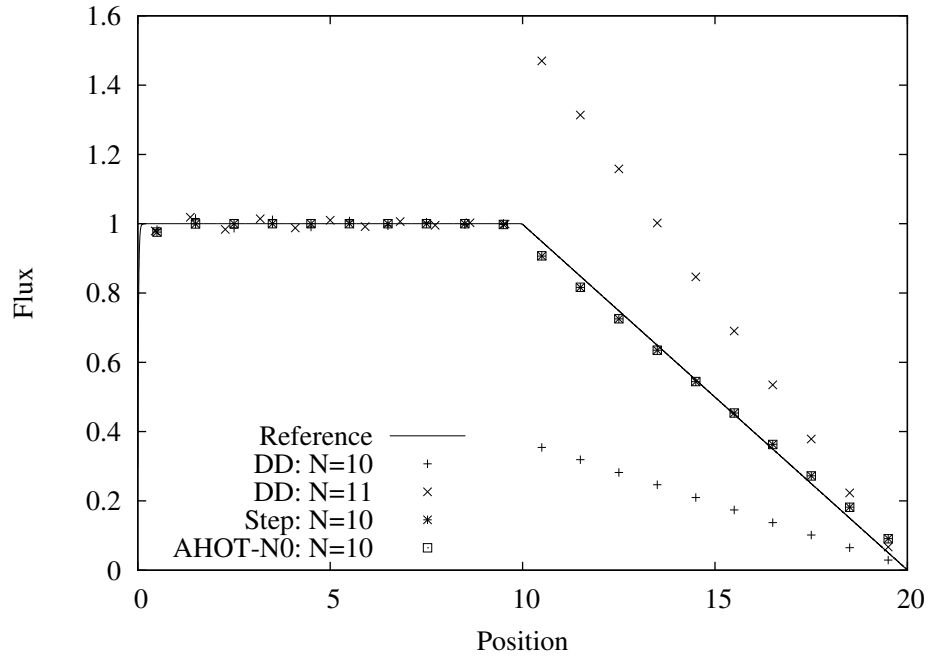
Figure 3.2. Problem 2: AHOT-N0 Cell Average Scalar Fluxes

is certainly in the thick diffusion limit and so we would generally expect that AHOT-N0 and Step would perform poorly. However the right half of the slab meets the restrictive conditions under which the AHOT0-N0 and Step methods possess the thick diffusion limit since $\sigma_a = Q = 0$ and $(\sigma_t h)$ is constant throughout the material. So in fact, we should expect these methods to perform well in this leakage dominated region. The same reasoning can be used to explain the cell edge scalar flux results for the AHOT-N0 and Step methods as well.

Figure 3.4 shows the average and edge scalar fluxes generated using the AHOT-N1 method for Problem 2, the heterogeneous slab. The AHOT-N1 results are quite accurate for this problem and do not display any of the gross inaccuracies which characterized the Diamond Difference method. There are slight inaccuracies displayed by the AHOT-N1 method near the boundary in the absorbing portion of the slab, however as Larsen and Morel note, the magnitude of the absorption in this reason is large enough so that this region cannot be considered an optically thick, diffusive region.

These figures show that numerical solutions from both nodal methods agree with the analytical predictions made. This further supports the original thesis of
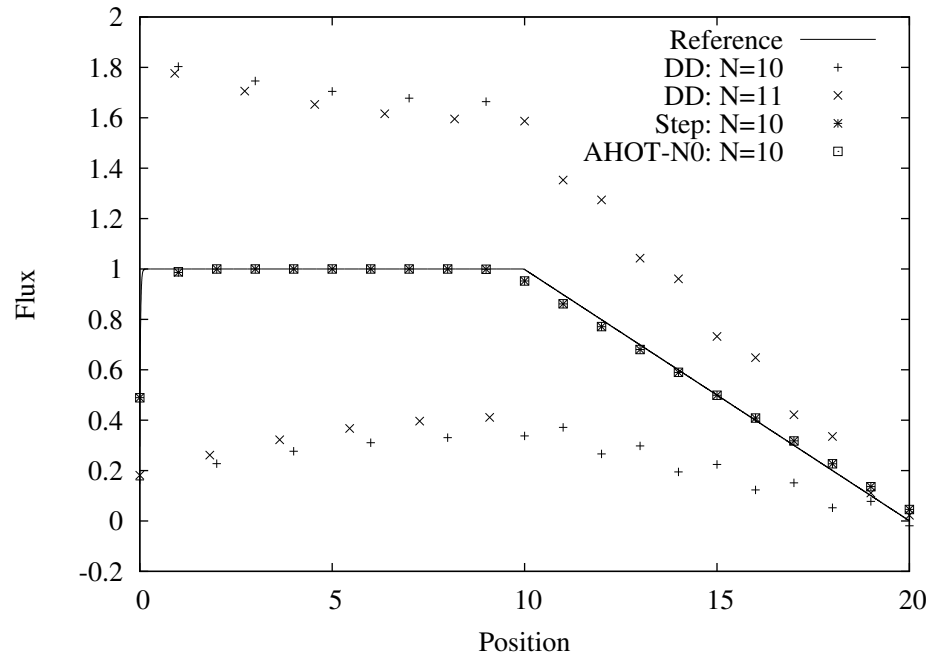
Figure 3.3. Problem 2: AHOT-N0 Cell Edge Scalar Fluxes
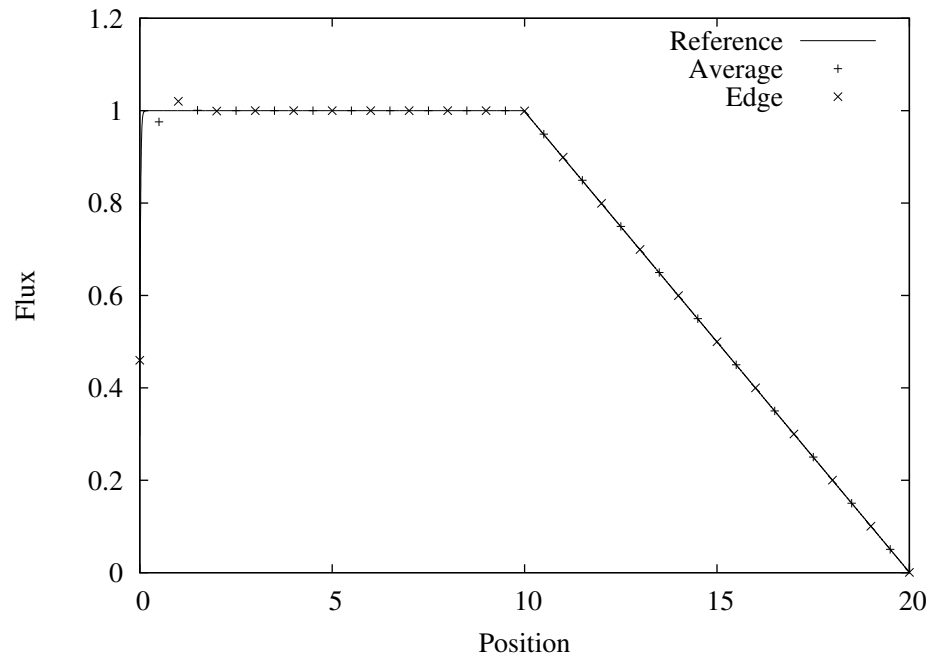
Figure 3.4. Problem 2: AHOT-N1 Cell Average and Edge Scalar Fluxes

Larsen, Morel, and Miller [10] that discretizations possessing the thick diffusion limit can be expected to generate accurate solutions in optically thick, diffusive regimes. Though the AHOT-N1 method shows itself to be superior in this limit to the Step, Diamond Difference, and AHOT-N0 methods, this increase in accuracy comes at the cost of requiring larger storage. This leads to the question of whether it is possible to derive a discretization scheme requiring only one unknown per cell (e.g. Step, Diamond Difference, and AHOT-N0) while possessing the accuracy of AHOT-N1 in the thick diffusion limit. This question was addressed by Hanshaw and Larsen in a 2003 paper [35].

Explicit Slope S_N Discretization Method

The Explicit Slope (ES) discretization was derived by Hanshaw and Larsen [35] with the intention of finding a discretization which would have the accuracy of a linear method in the thick limit but require the storage of only one fundamental unknown. To accomplish this goal Hanshaw and Larsen represent the scattering source as a linear function in space but explicitly approximate the slope of the linear function in terms of the cell average scalar flux. This reduces the number of unknowns to put the method on par with Step and Diamond Difference.

A full derivation of the method can be found in [35]. The method itself however is characterized by the auxiliary relation below.

$$\psi_{n,i} = \left(\frac{1 + \alpha_{n,i}}{2}\right)\psi_{n,i+1/2} + \left(\frac{1 - \alpha_{n,i}}{2}\right)\psi_{n,i-1/2} - \frac{\alpha_{n,i}}{4\sigma_{t,i}}\left(\sigma_{s,i}\hat{\phi}_{n,i} + \hat{Q}_i\right) \quad (3.32)$$

In this relation $\alpha_{n,i}$ represents the spatial weights used by AHOT-N0, given by Eq. (3.1c). The quantities $\hat{\phi}_{n,i}$ and $\hat{Q}_i$ represent "slopes." These are explicitly defined by Hanshaw and Larsen through

$$\hat{\phi}_{n,i} = \hat{\phi}_{\pm,i} = \begin{cases} \frac{2\sigma_{t,i}h_i}{\sigma_{t,i}h_i + \sigma_{t,i+1}h_{i+1}}\left(\phi_{i+1} - \phi_i\right), & \mu_n > 0 \\ \frac{2\sigma_{t,i}h_i}{\sigma_{t,i}h_i + \sigma_{t,i-1}h_{i-1}}\left(\phi_i - \phi_{i-1}\right), & \mu_n < 0. \end{cases} \quad (3.33)$$

This representation of the slope results from imposing the condition that the discrete net current across cell boundaries be continuous.

Performing the same asymptotic analysis we have seen many times to this point on the ES method yields a legitimate diffusion discretization. In this case however the diffusion discretization has no multiple-cell removal schemes or conditional requirements. The diffusion discretization is in fact the standard cell-centered diffusion discretization given by Eq. (2.26), which was fully derived in Section 2.2. Hanshaw and Larsen present numerical results which confirm that the ES method is accurate in diffusive regimes. They also impose what they term a "slope limiter" to force the method to perform adequately at material interfaces where the explicitly defined slope of Eq. (3.33) can be quite inaccurate.

This is the first method which has been examined that asymptotically limits to a cell-centered based diffusion discretization, along the lines of what was derived in Section 2.2. This is a desirable diffusion discretization because it can be physically interpreted as a balance of neutrons across the spatial cell, while an edge based discretization does not lend itself to this idea easily. The remainder of this work revisits the Diamond Difference method but approaches the asymptotic analysis with the intent of deriving the ε limit in terms of cell average scalar fluxes and thus ending up with a variant of the cell-centered based diffusion discretization. This derivation leads to many interesting results and allows for a further analysis of the inadequacies of Diamond Difference in the thick diffusion limit.

Asymptotic Analysis of the Diamond Difference Method

Our asymptotic analysis of the DD method will use the scalings described by Eqs. (2.33) and the quadrature rules given by Eq. (2.3). To begin our analysis of the DD method we consider the same problem described in Section 2.4.2, which for the indicated quadrature set is described by

$$\frac{\mu_n}{h_i} \left(\psi_{n,i+1/2} - \psi_{n,i-1/2} \right) + \frac{\sigma_{t,i}}{\varepsilon} \psi_{n,i} = \left(\frac{\sigma_{t,i}}{\varepsilon} - \varepsilon \sigma_{a,i} \right) \sum_{m=1}^{N} w_m \psi_{m,i} + \varepsilon Q_i, \qquad (4.1a)$$

$$\psi_{n,i} = \frac{1}{2} \left(\psi_{n,i+1/2} + \psi_{n,i-1/2} \right), \qquad (4.1b)$$

$$\psi_{n,1/2} = f_n, \quad \mu_n > 0, \qquad (4.1c)$$

$$\psi_{n,I+1/2} = g_n, \quad \mu_n < 0. \qquad (4.1d)$$

At this point we will only consider the system interior, and return to the boundary conditions at a later point. Again using the asymptotic expansion of Eq. (2.53) to expand the cell edge and cell average angular fluxes in a power series about ε we can equate the coefficients of different powers of ε to obtain the following system of equations,

$$\sigma_{t,i} \left(\psi_{n,i}^{(k)} - \sum_{m=1}^{N} w_m \psi_{m,i}^{(k)} \right) = -\frac{\mu_n}{h_i} \left(\psi_{n,i+1/2}^{(k-1)} - \psi_{n,i-1/2}^{(k-1)} \right)$$

$$- \sigma_{a,i} \sum_{m=1}^{N} w_m \psi_{m,i}^{(k-2)} + \delta_{k,2} Q_i, \quad k \geq 0, \quad (4.2a)$$

$$\psi_{n,i}^{(k)} = \frac{1}{2} \left(\psi_{n,i+1/2}^{(k)} + \psi_{n,i-1/2}^{(k)} \right), \quad k \geq 0, \tag{4.2b}$$

with the quantities $\psi^{(-1)}$ and $\psi^{(-2)}$ being equal to zero.

We first consider Eq. (4.2a) for $k = 0$. As in previous analyses this relation shows that the leading order component of the cell average angular flux is isotropic, where the quantity $\phi^{(0)}$ is still undetermined at this point.

$$\psi_{n,i}^{(0)} = \phi_i^{(0)} \tag{4.3}$$

We proceed by considering the DD relation for $k = 0$. Replacing $\psi_{n,i}^{(0)}$ with $\phi_i^{(0)}$ and taking the second angular moment of the resulting equation yields

$$\frac{1}{3} \phi_i^{(0)} = \frac{1}{2} \left(\nu_{i+1/2}^{(0)} + \nu_{i-1/2}^{(0)} \right). \tag{4.4}$$

If we now proceed to the case of $k = 2$ and take the zeroth angular moment of Eq. (4.2a) the following relation results,

$$-\frac{1}{h_i} \left(\vartheta_{i+1/2}^{(1)} - \vartheta_{i-1/2}^{(1)} \right) - \sigma_{a,i} \phi_i^{(0)} + Q_i = 0. \tag{4.5}$$

At this point our system of equations contains two equations and five unknowns: two unknown first angular moment edge quantities, two second angular moment edge quantities, and the cell average scalar flux. Another relationship can be developed in terms of the previous unknowns by using both the DD and balance equations for $k = 1$ to eliminate the quantity $\psi_{n,i}^{(1)}$. Taking the first angular moment of the resulting expression yields

$$\frac{1}{2} \left(\vartheta_{i+1/2}^{(1)} + \vartheta_{i-1/2}^{(1)} \right) = -\frac{1}{\tau_i} \left(\nu_{i+1/2}^{(0)} - \nu_{i-1/2}^{(0)} \right), \tag{4.6}$$

where the cell optical thickness, τ_i is given by

$$\tau_i = \sigma_{t,i} h_i. \tag{4.7}$$

This linear system is now comprised of three relations with five unknowns. To eliminate the first and second angular moment quantities it is necessary to consider adjacent spatial cells. Below we write the three equation system for cells $i-1$, i, and $i+1$, creating a system of nine equations, which utilizes the continuity of the angular flux and its angular moments at a cell interface. This algebraic system contains 11 unknown quantities and 9 equations and can be reduced to only one equation containing the three unknown cell average scalar flux quantities through subsequent manipulation. The system follows in its entirety to make the elimination steps as clear as possible and so certain expressions can be later used to assist in the derivation of boundary conditions in terms of cell average scalar fluxes.

$$-\frac{1}{h_{i-1}}\left(\vartheta_{i-1/2}^{(1)} - \vartheta_{i-3/2}^{(1)}\right) - \sigma_{a,i-1}\phi_{i-1}^{(0)} + Q_{i-1} = 0 \tag{4.8a}$$

$$\frac{1}{3}\phi_{i-1}^{(0)} = \frac{1}{2}\left(\nu_{i-1/2}^{(0)} + \nu_{i-3/2}^{(0)}\right) \tag{4.8b}$$

$$\frac{1}{2}\left(\vartheta_{i-1/2}^{(1)} + \vartheta_{i-3/2}^{(1)}\right) = -\frac{1}{\tau_{i-1}}\left(\nu_{i-1/2}^{(0)} - \nu_{i-3/2}^{(0)}\right) \tag{4.8c}$$

$$-\frac{1}{h_i}\left(\vartheta_{i+1/2}^{(1)} - \vartheta_{i-1/2}^{(1)}\right) - \sigma_{a,i}\phi_i^{(0)} + Q_i = 0 \tag{4.9a}$$

$$\frac{1}{3}\phi_i^{(0)} = \frac{1}{2}\left(\nu_{i+1/2}^{(0)} + \nu_{i-1/2}^{(0)}\right) \tag{4.9b}$$

$$\frac{1}{2}\left(\vartheta_{i+1/2}^{(1)} + \vartheta_{i-1/2}^{(1)}\right) = -\frac{1}{\tau_i}\left(\nu_{i+1/2}^{(0)} - \nu_{i-1/2}^{(0)}\right) \tag{4.9c}$$

$$-\frac{1}{h_{i+1}}\left(\vartheta_{i+3/2}^{(1)} - \vartheta_{i+1/2}^{(1)}\right) - \sigma_{a,i+1}\phi_{i+1}^{(0)} + Q_{i+1} = 0 \tag{4.10a}$$

$$\frac{1}{3}\phi_{i+1}^{(0)} = \frac{1}{2}\left(\nu_{i+3/2}^{(0)} + \nu_{i+1/2}^{(0)}\right) \tag{4.10b}$$

$$\frac{1}{2}\left(\vartheta^{(1)}_{i+3/2} + \vartheta^{(1)}_{i+1/2}\right) = -\frac{1}{\tau_{i+1}}\left(\nu^{(0)}_{i+3/2} - \nu^{(0)}_{i+1/2}\right) \qquad (4.10c)$$

We choose to begin by eliminating the second angular moment quantities, $\nu^{(0)}$. This is accomplished by summing Eqs. (4.8b) and (4.8c) and taking the difference of Eqs. (4.10b) and (4.10c), then eliminating the second angular moment quantities on the outer edges of the three-cell system, which results in explicit expressions for $\nu^{(0)}_{i-1/2}$ and $\nu^{(0)}_{i+1/2}$, respectively. By taking the sum and the difference of Eqs. (4.9b) and (4.9c) we can also find two explicit expressions for $\nu^{(0)}_{i-1/2}$ and $\nu^{(0)}_{i+1/2}$. Equating these four expressions completely eliminates the second angular moment quantities and leaves us a system of five equations comprised of

$$\frac{1}{3}\phi^{(0)}_{i-1} - \frac{\tau_{i-1}}{4}\left(\vartheta^{(1)}_{i-1/2} + \vartheta^{(1)}_{i-3/2}\right) = \frac{1}{3}\phi^{(0)}_i + \frac{\tau_i}{4}\left(\vartheta^{(1)}_{i+1/2} + \vartheta^{(1)}_{i-1/2}\right), \qquad (4.11a)$$

$$\frac{1}{3}\phi^{(0)}_{i+1} - \frac{\tau_{i+1}}{4}\left(\vartheta^{(1)}_{i+3/2} + \vartheta^{(1)}_{i+1/2}\right) = \frac{1}{3}\phi^{(0)}_i - \frac{\tau_i}{4}\left(\vartheta^{(1)}_{i+1/2} + \vartheta^{(1)}_{i-1/2}\right), \qquad (4.11b)$$

and Eqs. (4.8a), (4.9a), and (4.10a). We now reduce this system to three equations by solving Eqs. (4.8a) and (4.10a) for the quantities $\vartheta^{(1)}_{i-3/2}$ and $\vartheta^{(1)}_{i+3/2}$ respectively and using the result to eliminate the quantities in Eqs. (4.11a) and (4.11b). The system has now been reduced to three equations, given by

$$\frac{1}{3}\phi^{(0)}_{i-1} - \frac{\tau_{i-1}}{4}\left(\vartheta^{(1)}_{i-1/2} + h_{i-1}\sigma_{a,i-1}\phi^{(0)}_{i-1} - h_{i-1}Q_{i-1}\right)$$
$$= \frac{1}{3}\phi^{(0)}_i + \frac{\tau_i}{4}\left(\vartheta^{(1)}_{i+1/2} + \vartheta^{(1)}_{i-1/2}\right), \quad (4.12a)$$

$$\frac{1}{3}\phi^{(0)}_{i+1} - \frac{\tau_{i+1}}{4}\left(\vartheta^{(1)}_{i+1/2} + h_{i+1}\sigma_{a,i+1}\phi^{(0)}_{i+1} - h_{i+1}Q_{i+1}\right)$$
$$= \frac{1}{3}\phi^{(0)}_i - \frac{\tau_i}{4}\left(\vartheta^{(1)}_{i+1/2} + \vartheta^{(1)}_{i-1/2}\right), \quad (4.12b)$$

and Eq. (4.9a). The remaining unknown quantities are the three cell average $\phi^{(0)}$'s and the two first angular moment quantities $\vartheta^{(1)}_{i-1/2}$ and $\vartheta^{(1)}_{i+1/2}$. The two first angular moment quantities can then be eliminated from the system of three

equations resulting in one expression containing only the unknown $\phi^{(0)}$ quantities. By utilizing the shorthand notation of Eq. (2.27) and the definition of ξ provided below the previously undetermined quantity $\phi^{(0)}$ is now determined by,

$$
-a_{i,i-1} \left[1 - \frac{3}{4} \left((h\sigma_a)_{i-1} \tau_{i-1} \right) \right] \phi_{i-1}^{(0)}
$$
$$
+ \left[a_{i,i-1} \left(1 - \frac{3}{4} \left((h\sigma_a)_i \tau_{i-1} \right) \right) + a_{i,i+1} \left(1 - \frac{3}{4} \left((h\sigma_a)_i \tau_{i+1} \right) \right) \right] \phi_i^{(0)}
$$
$$
- a_{i,i+1} \left[1 - \frac{3}{4} \left((h\sigma_a)_{i+1} \tau_{i+1} \right) \right] \phi_{i+1}^{(0)} + \left(\xi_{i-1} + \xi_{i+1} \right) \sigma_{a,i} \phi_i^{(0)}
$$
$$
= \frac{1}{2h_i} \left((hQ)_{i-1} \xi_{i-1} + (hQ)_i \left(\xi_{i-1} + \xi_{i+1} \right) + (hQ)_{i+1} \xi_{i+1} \right), \quad 1 \leq 1 \leq I, \quad (4.13)
$$

$$
\xi_{i\pm 1} = \frac{\tau_{i\pm 1}}{\tau_{i\pm 1} + \tau_i}. \tag{4.14}
$$

The notation $(hQ)_i$ is used as shorthand to signify the product $h_i Q_i$ and likewise for $(h\sigma_a)_i$. We can see that Eq. (4.13) is a legitimate discretization of the diffusion equation, but it is also easy to see that it may not be the most ideal diffusion discretization. While this expression does resemble Eq. (2.26) there are many notable differences, which will be discussed in detail once this analysis has been completed.

We now turn our attention to analyzing the system boundaries in the asymptotic diffusion limit. As discussed previously, in the asymptotic limit we hope that the boundary conditions resemble the diffusion boundary conditions described by Eqs. (2.88). To start we wish to find an explicit expression for the outgoing angular flux at cells 1 and I so that the edge flux at $x_{1/2}$ and $x_{I+1/2}$ can be written as the sum of the outgoing flux and the known incident fluxes f_n and g_n. One manner in which the outgoing flux can be written for the DD method is to use the expressions

$$
\psi_{n,1/2}^{out} = \sum_{i=1}^{I} v_{n,i} \left(\tilde{c}_i \phi_i + \frac{\tilde{Q}_i}{\tilde{\sigma}_{t,i}} \right) + v_{n,n} g_n, \tag{4.15a}
$$

$$\psi_{n,I+1/2}^{out} = \sum_{i=1}^{I} w_{n,i} \left(\tilde{c}_i \phi_i + \frac{\tilde{Q}_i}{\tilde{\sigma}_{t,i}} \right) + w_{n,n} f_n, \tag{4.15b}$$

which can be derived by considering the neutron balance in a one dimensional slab in terms of multiple discrete cell balance equations. The parameters v and w used in the outgoing angular flux expression are defined for the DD method by

$$v_{n,1} = \left(\frac{2}{1 + 2\tilde{\kappa}_{n,i}} \right), \tag{4.16a}$$

$$w_{n,I} = \left(\frac{2}{1 + 2\tilde{\kappa}_{n,I}} \right), \tag{4.16b}$$

$$v_{n,n} = w_{n,n} = \prod_{i=1}^{I} \left(\frac{2\tilde{\kappa}_{n,i} - 1}{2\tilde{\kappa}_{n,i} + 1} \right), \tag{4.17}$$

$$v_{n,i} = \left(\frac{2}{1 + 2\tilde{\kappa}_{n,i}} \right) \prod_{j=1}^{i-1} \left(\frac{2\tilde{\kappa}_{n,j} - 1}{2\tilde{\kappa}_{n,j} + 1} \right), \quad 2 \leq i \leq I, \tag{4.18a}$$

$$w_{n,i} = \left(\frac{2}{1 + 2\tilde{\kappa}_{n,i}} \right) \prod_{j=i+1}^{I} \left(\frac{2\tilde{\kappa}_{n,j} - 1}{2\tilde{\kappa}_{n,j} + 1} \right), \quad 1 \leq i \leq I - 1, \tag{4.18b}$$

$$\tilde{\kappa}_{n,i} = \frac{|\mu_n|}{\tilde{\sigma}_{t,i} h_i}. \tag{4.19}$$

We now wish to expand this expression into components of varying orders of ε. This is achieved through the same means used in previous analyses, expanding the angular flux in a power series using the asymptotic expansion of Eq. (2.53) which in turn implies the scalar flux can be expanded in a similar series. We will also scale $\tilde{\sigma}_{t,i}$ and $\tilde{Q}_i$ as described by Eq. (2.33), which implies that the scattering ratio, c, is scaled like,

$$\tilde{c}_i \rightarrow 1 - \varepsilon^2 (1 - c_i).$$

It is also necessary to expand the parameters v and w in Taylor series in the asymptotic variable ε. We first scale the total cross section in the $\tilde{\kappa}_{n,i}$ parameter in the now standard manner so that under this scaling we can replace $\tilde{\kappa}_{n,i}$ with $\varepsilon \kappa_{n,i}$ where

$$\kappa_{n,i} = \frac{|\mu_n|}{\sigma_{t,i} h_i},$$

is now independent of ε. We can easily expand the two factors which appear in the v and w definitions as

$$\frac{2}{1 + 2\varepsilon\kappa_{n,i}} = 2 + O(\varepsilon), \tag{4.20a}$$

$$\frac{2\varepsilon\kappa_{n,i} - 1}{2\varepsilon\kappa_{n,i} + 1} = -1 + O(\varepsilon). \tag{4.20b}$$

By substituting the above expansions into the definitions of v and w we find that the parameters are asymptotically defined by

$$v_{n,1} = 2 + O(\varepsilon), \tag{4.21a}$$

$$w_{n,I} = 2 + O(\varepsilon), \tag{4.21b}$$

$$v_{n,n} = w_{n,n} = (-1)^I + O(\varepsilon), \tag{4.22}$$

$$v_{n,i} = \begin{cases} -2 + O(\varepsilon), & i = \text{odd} \\ 2 + O(\varepsilon), & i = \text{even} \end{cases} \quad 2 \leq i \leq I, \tag{4.23a}$$

$$w_{n,i} = \begin{cases} -2(-1)^I + O(\varepsilon), & i = \text{odd} \\ 2(-1)^I + O(\varepsilon), & i = \text{even} \end{cases} \quad 1 \leq i \leq I - 1. \tag{4.23b}$$

If we now take the expanded v and w parameters, the scaled external source, scattering ratio, and total cross section, as well as the expanded angular and scalar fluxes and substitute them into Eqs. (4.15) we find the expressions for the outgoing angular flux at the system edges in the asymptotic diffusion limit given by

$$\psi_{n,1/2}^{out} = 2\left(\bar{\phi}_{1 \to I}\right) + (-1)^I g_n + O(\varepsilon), \tag{4.24a}$$

$$\psi_{n,I+1/2}^{out} = 2(-1)^{I+1}\left(\bar{\phi}_{1 \to I}\right) + (-1)^I f_n + O(\varepsilon), \tag{4.24b}$$

where we have defined the quantity

$$\bar{\phi}_{1\to I} \equiv \left(\phi_1^{(0)} - \phi_2^{(0)} + \phi_3^{(0)} - \phi_4^{(0)} + \ldots + (-1)^{I+1}\phi_I^{(0)}\right). \tag{4.25}$$

We now have an explicit expression for the outgoing angular flux in terms of the known incident flux at the system boundary and the interior scalar fluxes defined by Eq. (4.13). We will now replace the $\bar{\phi}_{1\to I}$ expression using a relationship we derive from the recursive system of equations given by Eqs. (4.2).

We begin by taking the first angular moment of Eq. (4.2a) for $k = 0$ which trivially shows that $\vartheta_i^{(0)} = 0$. If we subsequently take the first angular moment of Eq. (4.2b) for $k = 1$ and substitute the previous result we find that $\vartheta_{i+1/2}^{(0)} = -\vartheta_{i-1/2}^{(0)}$. However, when we take the zeroth angular moment of Eq. (4.2a) for $k = 1$ we find that $\vartheta_{i+1/2}^{(0)} = \vartheta_{i-1/2}^{(0)}$, implying

$$\vartheta_{i+1/2}^{(0)} = \vartheta_{i-1/2}^{(0)} = 0 \tag{4.26}$$

We now write an expression for $\vartheta_{i+1/2}^{(0)}$, recognizing that it is equal to zero, and separately consider the incoming and outgoing flux at the cell face, yielding,

$$\vartheta_{1/2}^{(0)} = \sum_{\mu_n > 0} w_n |\mu_n| f_n - \sum_{\mu_n < 0} w_n |\mu_n| \psi_{n,1/2}^{out} = 0, \tag{4.27}$$

where f_n is the known incident angular flux. We now substitute the expression given by Eq. (4.24a) and extract all isotropic quantities from the summations, resulting in

$$\sum_{\mu_n > 0} w_n |\mu_n| f_n - 2\gamma\left(\bar{\phi}_{1\to I}\right) - (-1)^I \sum_{\mu_n < 0} w_n |\mu_n| g_n = 0, \tag{4.28}$$

where γ is again defined by Eq. (2.79), such that $\bar{\phi}_{1\to I}$ is given by

$$\bar{\phi}_{1\to I} = \frac{1}{2\gamma}\left(\sum_{\mu_n > 0} w_n |\mu_n| f_n - (-1)^I \sum_{\mu_n < 0} w_n |\mu_n| g_n\right). \tag{4.29}$$

We can now use this relation to replace $\bar{\phi}_{1\to I}$ in the outgoing angular flux expressions, resulting in

$$\psi_{n,1/2}^{out} = \frac{1}{\gamma} \left(\sum_{\mu_n>0} w_n|\mu_n|f_n - (-1)^I \sum_{\mu_n<0} w_n|\mu_n|g_n \right) + (-1)^I g_n + O(\varepsilon), \quad (4.30a)$$

$$\psi_{n,I+1/2}^{out} = \frac{1}{\gamma} \left(\sum_{\mu_n<0} w_n|\mu_n|g_n - (-1)^I \sum_{\mu_n>0} w_n|\mu_n|f_n \right) + (-1)^I f_n + O(\varepsilon). \quad (4.30b)$$

Although this provides us with an expression for the outgoing angular flux solely in terms of the flux incident on the system it still does not provide us with a relation which will allow us to determine the values of $\phi_i^{(0)}$. To find such a relation we begin by writing $\nu_{1/2}^{(0)}$ in the same manner in which we previously wrote $\vartheta_{1/2}^{(0)}$, that is

$$\nu_{1/2}^{(0)} = \sum_{\mu_n>0} w_n\mu_n^2 f_n + \sum_{\mu_n<0} w_n\mu_n^2 \psi_{n,1/2}^{out}. \quad (4.31)$$

If we now introduce Eq. (4.30a) into the above relation we can write $\nu_{1/2}^{(0)}$ as shown below, where we have also shown the analogous expression for $\nu_{I+1/2}^{(0)}$.

$$\nu_{1/2}^{(0)} = \sum_{\mu_n>0} \left(\frac{\mu_n}{6\gamma} + \mu_n^2 \right) f_n w_n + (-1)^I \sum_{\mu_n<0} \left(-\frac{|\mu_n|}{6\gamma} + \mu_n^2 \right) g_n w_n. \quad (4.32a)$$

$$\nu_{I+1/2}^{(0)} = \sum_{\mu_n<0} \left(\frac{|\mu_n|}{6\gamma} + \mu_n^2 \right) g_n w_n + (-1)^I \sum_{\mu_n>0} \left(-\frac{\mu_n}{6\gamma} + \mu_n^2 \right) f_n w_n. \quad (4.32b)$$

These equations are identical to the previously derived asymptotic boundary conditions for the DD method. Thus we can expect the same conclusions drawn regarding their accuracy to hold for this system. More specifically, for Eqs. (4.32) to closely resemble the appropriate boundary condition in Eq. (2.90) it must again be true that

$$0 = \sum_{\mu_n>0} \left(-\frac{\mu_n}{6\gamma} + \mu_n^2 \right) f_n w_n = \sum_{\mu_n<0} \left(-\frac{|\mu_n|}{6\gamma} + \mu_n^2 \right) g_n w_n. \quad (4.33)$$

We recognize that generally this condition is not true, although under certain instances such as isotropic incident fluxes, the condition is satisfied. As in the scalar

edge flux based DD analysis, vacuum conditions at the slab edges will result in asymptotic boundary conditions that agree well with the correct diffusion boundary conditions.

We are now in possession of an expression that describes the second angular moment of the angular flux at the slab interface. However we need to relate this quantity to $\phi^{(0)}$ in order to allow the algebraic system defined by Eq. (4.13) to be fully solved. To find the remaining relations we return to the 9 equation system given by Eqs. (4.8) – (4.10). Through a substantial amount of algebraic manipulation, which will not be repeated here, we are able to condense the system down to two expressions containing two adjacent cell average scalar flux values, $\phi_{i-1}^{(0)}$ and $\phi_i^{(0)}$, and the second moment edge quantity $\nu_{i+1/2}^{(0)}$ or $\nu_{i-1/2}^{(0)}$. We then consider the expression for $\nu_{i+1/2}^{(0)}$ specifically for the value of $i = I$ and the expression for $\nu_{i-1/2}^{(0)}$ specifically for $i = 1$, yielding

$$
\nu_{1/2}^{(0)} = \frac{\left(8\tau_1 + 4\tau_2 + 3\left(h\sigma_a\right)_1 \tau_1\tau_2\right)}{12\left(\tau_1 + \tau_2\right)}\phi_1^{(0)}
$$
$$
+ \frac{\left(-4\tau_1 + 3\left(h\sigma_a\right)_2 \tau_1\tau_2\right)}{12\left(\tau_1 + \tau_2\right)} - \frac{\tau_1\tau_2}{4\left(\tau_1 + \tau_2\right)}\left(h_1 Q_1 + h_2 Q_2\right), \quad \text{(4.34a)}
$$

$$
\nu_{I+1/2}^{(0)} = \frac{\left(8\tau_I + 4\tau_{I-1} + 3\left(h\sigma_a\right)_I \tau_{I-1}\tau_I\right)}{12\left(\tau_{I-1} + \tau_I\right)}\phi_I^{(0)}
$$
$$
+ \frac{\left(-4\tau_I + 3\left(h\sigma_a\right)_{I-1} \tau_{I-1}\tau_I\right)}{12\left(\tau_{I-1} + \tau_I\right)}\phi_{I-1}^{(0)} - \frac{\tau_{I-1}\tau_I}{4\left(\tau_{I-1} + \tau_I\right)}\left(h_{I-1} Q_{I-1} + h_I Q_I\right). \quad \text{(4.34b)}
$$

We now have two explicit expressions for the second moment of the angular flux at each system boundary, one expression involving only the known incident fluxes and the other involving only the cell average scalar flux unknowns, $\phi_i^{(0)}$. We finally equate the two expression at each interface, eliminating the second angular moment and providing us with the final two equations necessary to form a closed algebraic system. These two equations are given by the following expressions,

$$\sum_{\mu_n>0} \left(\frac{\mu_n}{6\gamma} + \mu_n^2 \right) f_n w_n + (-1)^I \sum_{\mu_n<0} \left(-\frac{|\mu_n|}{6\gamma} + \mu_n^2 \right) g_n w_n$$

$$+ \frac{\tau_1 \tau_2}{4(\tau_1 + \tau_2)} (h_1 Q_1 + h_2 Q_2)$$

$$= \frac{(8\tau_1 + 4\tau_2 + 3(h\sigma_a)_1 \tau_1 \tau_2)}{12(\tau_1 + \tau_2)} \phi_1^{(0)} + \frac{(-4\tau_1 + 3(h\sigma_a)_2 \tau_1 \tau_2)}{12(\tau_1 + \tau_2)} \phi_2^{(0)}, \quad (4.35a)$$

$$\sum_{\mu_n<0} \left(\frac{|\mu_n|}{6\gamma} + \mu_n^2 \right) g_n w_n + (-1)^I \sum_{\mu_n>0} \left(-\frac{\mu_n}{6\gamma} + \mu_n^2 \right) f_n w_n$$

$$+ \frac{\tau_{I-1} \tau_I}{4(\tau_{I-1} + \tau_I)} (h_{I-1} Q_{I-1} + h_I Q_I)$$

$$= \frac{(8\tau_I + 4\tau_{I-1} + 3(h\sigma_a)_I \tau_{I-1} \tau_I)}{12(\tau_{I-1} + \tau_I)} \phi_I^{(0)} + \frac{(-4\tau_I + 3(h\sigma_a)_{I-1} \tau_{I-1} \tau_I)}{12(\tau_{I-1} + \tau_I)} \phi_{I-1}^{(0)}. \quad (4.35b)$$

Eq. (4.13) along with the two expressions above uniquely define the cell average scalar flux $\phi^{(0)}$ for all cells i, $1 \leq i \leq I$. We can summarize the results of the analysis by the statement

$$\psi_{n,i}^{(0)} = \phi_i^{(0)} + O(\varepsilon), \quad (4.36)$$

where $\phi_i^{(0)}$ is now completely defined on the interval $1 \leq i \leq I$, by Eq. (4.13) and Eqs. (4.35). We can see that the system of I equations which defines $\phi_i^{(0)}$ will result in a tridiagonal linear system of the form described by Eq. (2.29), however the elements of matrix $\mathbf{A}$ and vector $\vec{Q}$ will differ from those described in Chapter 2.

This asymptotic limit differs from the limit previously derived in [10] and [11] mainly by the fact that the newly derived limit of the DD scheme is based on cell average and not cell edge quantities. This allows us to directly compare the interior tridiagonal stencil of the standard diffusion system to the altered tridiagonal stencil described by the DD asymptotic limit and to also directly compare the boundary conditions derived. Sections 4.1 and 4.2 compare both the standard and asymptotic cell average diffusion discretizations, for homogeneous media and heterogeneous media, respectively. Some interesting numerical effects due to the

disparity between the asymptotic and standard cell average diffusion discretizations are discussed for each case material regime and a variety of methods attempting to "fix" these numerical effects are presented.

4.1   Homogeneous Media

Analyzing the interior equation and boundary conditions of the linear system given by the asymptotic limit of the DD discretization, Eq. (4.13) and Eqs. (4.35), is considerably less complicated when considering a homogeneous media with no incident flux, constant mesh spacing and a uniform external source. Thus in this section the quantities $\sigma_{t,i}$, $\sigma_{a,i}$, Q_i, and h_i are simply given by σ_t, σ_a, Q, and h since they are constant throughout the problem domain, which also implies that $\tau_i = \tau$ and $\xi_i = \xi$. Under these assumptions $\phi_i^{(0)}$ is determined in the slab interior by

$$-\left(D - \frac{h^2 \sigma_a}{4}\right) \frac{\left(\phi_{i-1}^{(0)} - 2\phi_i^{(0)} + \phi_{i+1}^{(0)}\right)}{h^2} + \sigma_a \phi_i^{(0)} = Q, \quad 2 \le i \le I - 1, \quad (4.37)$$

where the off-diagonal absorption terms have been lumped in to the diffusion coefficient to form an "effective" diffusion coefficient. The boundary conditions in a homogeneous medium in the instance of vacuum are given by

$$\left(\frac{3D}{h^2} + \frac{\sigma_a}{4}\right) \phi_1 + \left(-\frac{D}{h^2} + \frac{\sigma_a}{4}\right) \phi_2 = \frac{Q}{2}, \qquad (4.38\text{a})$$

$$\left(-\frac{D}{h^2} + \frac{\sigma_a}{4}\right) \phi_{I-1} + \left(\frac{3D}{h^2} + \frac{\sigma_a}{4}\right) \phi_I = \frac{Q}{2}. \qquad (4.38\text{b})$$

We can see that Eq. (2.30) and Eq. (4.37) have the same general form with the exception of the "effective" diffusion coefficient present in the DD asymptotic limit set of equations. The boundary conditions given by Eqs. (2.31) and Eqs. (4.38) are also remarkably similar aside from the factor of 1/2 applied to the external source term, Q, and the factor of 1/4 applied to σ_a. Thus we can make the statement that the only circumstances under which the DD method will asymptotically limit to the exact diffusion discretization described in Chapter 2 are when

- $\sigma_t = $ constant,

- $h = $ constant,

- $Q = $ constant,

- $\sigma_a = 0$.

It is important to note here that this concept is different than the concept of legitimacy as defined by Larsen, Morel, and Miller [10]. Assuming that the system given by Eq. (4.13) and Eqs. (4.35) does limit to Eq. (2.22) as $h \rightarrow 0$, and thus the asymptotic limit of the DD scheme is a legitimate diffusion discretization, it still cannot be claimed that it is an accurate diffusion discretization. By an accurate diffusion discretization we mean that the solutions of the linear system described by the DD asymptotic limit are good approximations to the solutions of the standard discretized diffusion equation. By this definition we would expect the asymptotic DD limit to be an accurate discretization only under the limiting conditions listed above. We will explore this idea more thoroughly through numerical experiment, however we will briefly show that this simplified form of the cell average based asymptotic limit of the DD method is equivalent with the cell edge based form of the limit derived in [10] and [11].

We begin by considering the same homogeneous medium with uniform source and mesh spacing used above such that Eq. (2.85) can be shown to simplify to

$$
-\left(D - \frac{h^2 \sigma_a}{4}\right) \frac{\left(\nu_{i-1/2}^{(0)} - 2\nu_{i+1/2}^{(0)} + \nu_{i+3/2}^{(0)}\right)}{h^2} + \sigma_a \nu_{i+1/2}^{(0)} = \frac{1}{3}Q, \quad 2 \leq i \leq I - 1.
$$
(4.39)

Writing the previous equation for cell $i-1$ and cell i and summing the resulting expressions together yields

$$
-\left(D - \frac{h^2 \sigma_a}{4}\right) \left[\frac{\left(\nu_{3-1/2}^{(0)} + \nu_{i-1/2}^{(0)}\right) - 2\left(\nu_{i-1/2}^{(0)} + \nu_{i+1/2}^{(0)}\right) + \left(\nu_{i+1/2}^{(0)} + \nu_{i+3/2}^{(0)}\right)}{h^2}\right] +
$$
$$
\sigma_a \left(\nu_{i+1/2}^{(0)} + \nu_{i-1/2}^{(0)}\right) = \frac{2}{3}Q, \quad 2 \leq i \leq I - 1, \quad (4.40)
$$

after a slight manipulation of the leakage term. If we now use the relation given by Eq. (2.68), we can replace all of the cell edge quantities in the above equation with cell average quantities, resulting in the same expression as that given by Eq. (4.37). Thus we have shown that the asymptotic limit of the DD method derived in terms of cell edge scalar fluxes is consistent with that derived in terms of cell average scalar fluxes, for the specialized case considered above. We have also previously shown the equivalence of the boundary conditions which is independent of any assumptions regarding the problem parameters. However, under less restrictive conditions we are not able to demonstrate such a relationship between Eq. (2.85) and Eq. (4.13), determining a cell average based asymptotic limit instead requires a separate analysis as performed in this work.

4.1.1 Effective Diffusion Coefficient

We have previously seen that for both the cell average and cell edge based asymptotic limits of the DD method, the standard diffusion coefficient has been replaced by what we have termed an effective diffusion coefficient. This is because the factor

$$D_{eff} = \left(D - \frac{(h^2 \sigma_a)}{4} \right), \tag{4.41}$$

now multiplies the leakage, so that regardless of the physical value of D the numerical solution will behave as if D were D_{eff}. Thus in the asymptotic limit D_{eff} will never equal D unless $\sigma_a = 0$. We can also see that should h or σ_a be sufficiently large then D_{eff} will take on a completely unphysical negative value. In fact, when the mesh spacing satisfies the inequality,

$$h > 2\sqrt{\frac{D}{\sigma_a}} = 2L, \tag{4.42}$$

D_{eff} will be negative. In the above condition L represents the diffusion length, given by Eq. (2.34). This statement is consistent with the asymptotic analysis employed as it demands an h that is $O(1)$, since L is $O(1)$, which is true by the definition of the thick diffusion limit. We will now look at the effect that the magnitude and sign of D_{eff} has on the solution accuracy in a homogeneous region. The numerical experiment which we will use is given by

$$\mu_n \frac{d\psi_n}{dx} + 100\psi_n = \left(100 - 10^{-\omega}\right) \sum_{m=1}^{N} \psi_m w_m + 10^{-3}, \quad 0 < x < 20$$

$$\psi_n(0) = 0, \quad \mu_n > 0$$

$$\psi_n(20) = 0, \quad \mu_n < 0$$

$$h = 1.0,$$

where the S_8 quadrature set is used for all solutions and the reference solution is found using the DD method on a mesh of $2 * 10^4$ spatial cells. Note that in this problem we will be using a fixed mesh spacing, $h = 1$, but will be varying the absorption cross section so that D_{eff} will vary, taking on values both positive and negative. We will primarily be interested in plotting the relative error in the scalar flux which is calculated on a cell wise basis, where the fine-mesh reference solutions has been averaged in a way such that it can be directly compared to the thick cell DD solution. The edge errors are calculated using point-wise differences at each point being plotted. It should also be noted that when $\omega = 0$ the reference solution is very flat, saturating at $Q/\sigma_a = 10^{-3}$ throughout the slab interior, but tends toward a parabolic shaped solution as $\omega \to \infty$. The specific values of ω used and the resulting D_{eff} value are listed in Table 4.1, where we have also given the mesh spacing in terms of the diffusion length, L, for the particular ω value. The results of this numerical experiment for cell average and cell edge fluxes respectively are shown in Figures 4.1 and 4.2 for the left half of the slab, with the right half results being identical due to the problem symmetry.

Table 4.1. D_{eff} for Varying σ_a Values

ω	h/L	σ_t	σ_a	D_{eff}
0	17.32	100	1.00E+00	-2.466667E-01
1	5.48	100	1.00E-01	-2.166667E-02
2	1.73	100	1.00E-02	8.333333E-04
3	0.55	100	1.00E-03	3.083333E-03
4	0.17	100	1.00E-04	3.308333E-03
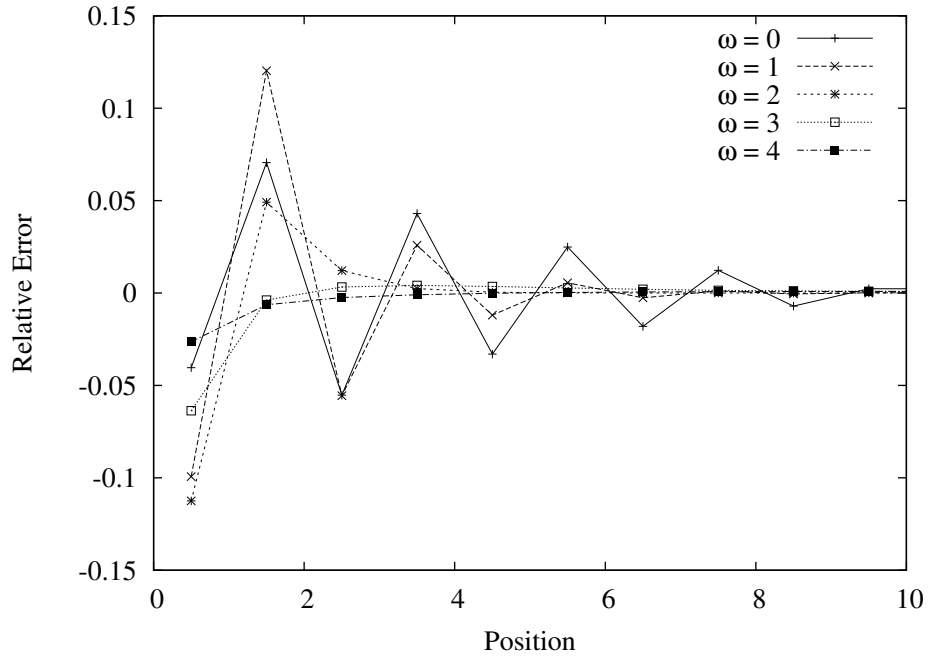
Figure 4.1. Cell Average Absorption Regimes Resulting from D_{eff}

We can see that the relative error saturates to practically zero at the slab midpoint while the boundary cell typically has the largest error, for all of the ω values. We can also see that there are roughly two different regimes that appear when considering the relative error in the cell average fluxes, coinciding with the magnitude of the absorption cross section. For the largest values of σ_a considered ($\omega = 0, 1$) the relative error is generally large at the boundary cell and oscillates about zero while for smaller values of σ_a ($\omega = 3, 4$) the error at the boundary cell has decreased while in the interior the error can be seen to be flat and practically zero. In the instance where $\omega = 2$ the error at the boundary cell is very large but instead of oscillating about zero the error saturates to zero by cell 4, from which point on it is practically indistinguishable from the $\omega = 4$ and $\omega = 5$ cases.

The cases in which the relative error of the cell average scalar flux oscillate about zero are also the cases where D_{eff} takes on negative values, which in effect describes a diffusion process that lumps particles together rather than smoothing their spatial distribution. We must recall here that D_{eff} only describes the behavior in the system interior, i.e. away from the slab edges. We also recall that we have previously shown the inequality of the asymptotic DD boundary conditions
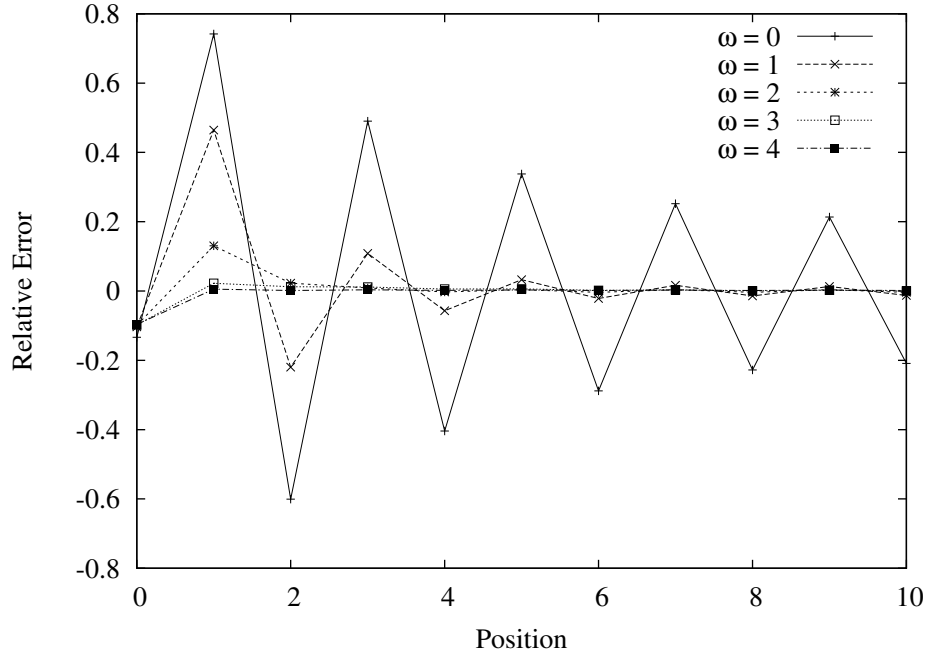
Figure 4.2. Cell Edge Absorption Regimes Resulting from D_{eff}

and the analogous diffusion boundary conditions, so that near the system edges we expect this to be a source of error in the solution. Thus, when we consider the numerical effect of D_{eff} it makes sense to ignore the first few cells in the problem. Doing so we see that the largest oscillations occur for $\omega = 0$, the case where we have the most negative D_{eff} and note that each increase in ω causes a decrease in the magnitude of the oscillations.

We are able to make the same observations regarding the behavior of the cell edge fluxes, but we should note that in this case the oscillations are *much* larger than in the case of the cell average flux errors. We do however see the same relationship between the oscillation magnitude and D_{eff}, supporting the conclusion that the larger the difference between D_{eff} and D the larger the error in the system interior will be.

To attempt to "fix" the error introduced by D_{eff} we consider replacing σ_t and c with $\bar{\sigma}_t$ and $\bar{c}$, respectively. The new values, $\bar{\sigma}_t$ and $\bar{c}$, will be chosen so that they preserve the absorption cross section σ_a but so that $D_{eff} = D$. The quantities are then defined by

Table 4.2. $\bar{\sigma}_t$ and $\bar{c}$ Values

| ω	h	σ_t	σ_a	c	$\bar{\sigma}_t$	$\bar{c}$
0	1	100	1.00E+00	0.990000	1.31579	0.240000000
1	1	100	1.00E-01	0.999000	11.76471	0.991500000
2	1	100	1.00E-02	0.999900	57.14286	0.999825000
3	1	100	1.00E-03	0.999990	93.02326	0.999989250
4	1	100	1.00E-04	0.999999	99.25558	0.999998993

$$\bar{\sigma}_t = \left(\frac{1}{\sigma_t} + \frac{3h^2\sigma_a}{4} \right)^{-1}, \tag{4.43}$$

$$\bar{c} = c - \frac{3h^2\sigma_a^2}{4}. \tag{4.44}$$

In Table 4.2 the $\bar{\sigma}_t$ and $\bar{c}$ values corresponding to the previous problem are given. These altered values are quite different from the actual values for $\omega = 0$. We can see that as ω increases, and the overall absorption thus decreases, the altered values approach the actual values. It is also interesting to note that had we considered the case of $\omega = -1$ then $\bar{c}$ would have actually been *negative*! A negative scattering ratio value is not only unintuitive but generally will introduce numerical instability into any iterative calculation. For this reason even though good results may be obtained it is generally undesirable to consider problems with a negative $\bar{c}$.

If we consider the numerical experiment previously defined where σ_t and c are replaced with the $\bar{\sigma}_t$ and $\bar{c}$ given in Table 4.2 then we obtain Figures 4.3 and 4.4.

The most obvious effect of altering the cross section and scattering ratio was greatly increasing the error at the system boundary. However we have already discussed how D_{eff} is a quantity that only describes the diffusion process on the system interior. By changing these parameters at the system edge we are basically describing an entirely different problem whereas by changing the parameters in the slab interior we are "correcting" the effective diffusion coefficient. Accepting that we have greatly increased the error at the boundary we will not display these points on the plots so that the scales can be kept consistent with those used in
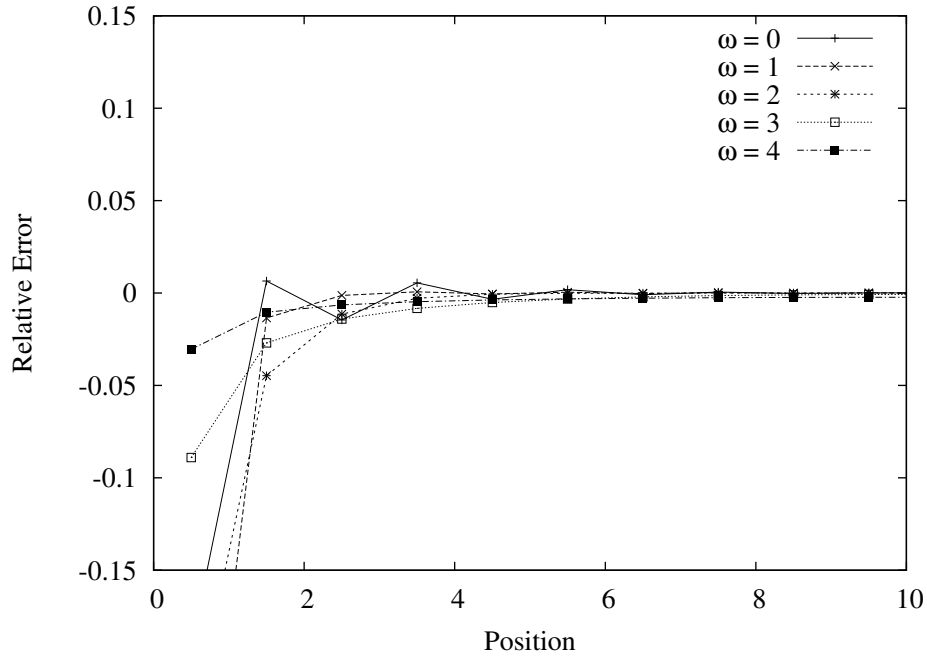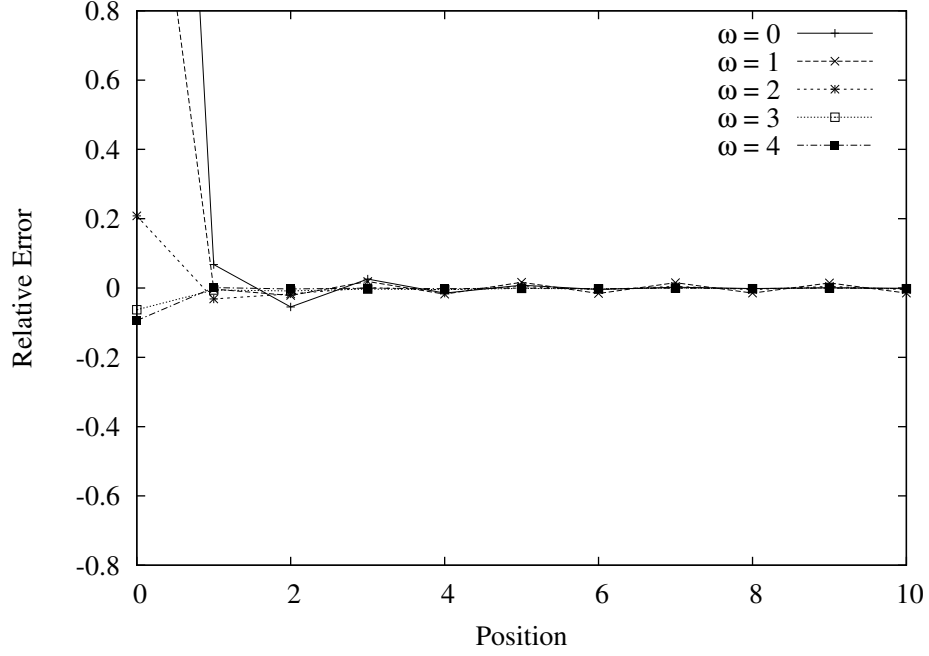
Figure 4.3. Cell Average Scalar Flux Relative Error with $D_{eff} = D$, $\sigma_a \to 0$

Figures 4.1 and 4.2.

We can see that away from the boundary we have generally reduced the error for both the cell average and cell edge fluxes by using the altered parameters, with the effect being much more drastic in the case of the cell edge fluxes. These plots show that it is possible to "fix" the diffusion discretization described by the thick asymptotic limit of the DD method on the system interior. However, the problem remains that imposing this fix greatly deteriorates the quality of the solution at the system edges. As it turns out there is no simple way to deal with this situation. One might consider using the actual σ_t and c values in the first cell and then the altered parameters in the interior, however there is no reason to expect this to work given that D_{eff} is only defined in a homogeneous environment. If we consider problems with non-constant total scattering cross sections and scattering ratios then we cannot simplify Eq. (4.13) in a manner such that D_{eff} results.

Previously we considered the case where we held h, Q, and σ_t constant while varying σ_a, meaning that as $\sigma_a \to 0$ we asymptotically approach the case of pure scattering, in which case $D_{eff} = D$. However it is important to realize that for each σ_a value considered we were actually solving a problem with a completely different
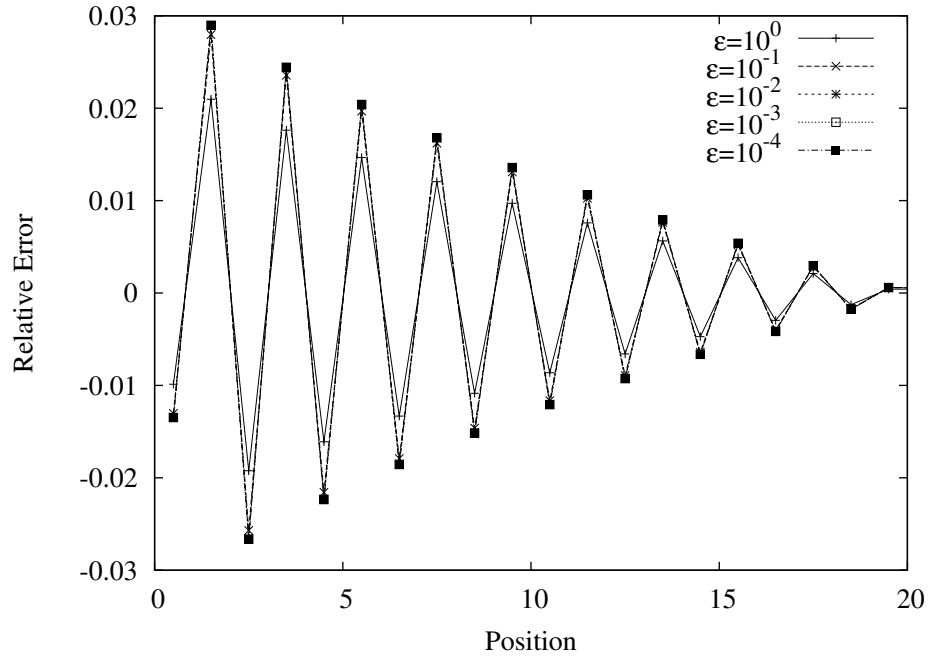
Figure 4.4. Cell Edge Scalar Flux Relative Error with $D_{eff} = D$, $\sigma_a \to 0$

solution than for the following and preceding σ_a values. In other words, as $\sigma_a \to 0$ the solution transitioned from a relatively flat solution where the external source was balanced by the absorption to a parabolic solution dominated by leakage.

Instead we now consider a problem where h, Q, σ_t, and σ_a are all given a particular initial value and then scaled by ε in the manner described by Eq. (2.33). In this scenario the shape of the solution will not approach a parabola, but rather the solution will approach the solution to Eqs. (4.13) and (4.35) for the initial h, Q, σ_t, and σ_a values as $\varepsilon \to 0$. It is also interesting to look at this scenario because we can specifically pick a problem that puts us in the absorption regime where we would expect the largest oscillations and then examine the solution error as $\varepsilon \to 0$.

The problem that we create is given by

$$\mu_n \frac{d\psi_n}{dx} + \frac{100}{\varepsilon}\psi_n = \left(\frac{100}{\varepsilon} - \varepsilon 10\right) \sum_{m=1}^{M} \psi_m w_m + \varepsilon, \quad 0 < x < 40$$

$$\psi_n(0) = 0, \quad \mu_n > 0$$

$$\psi_n(20) = 0, \quad \mu_n < 0$$

Figure 4.5. Cell Average Scalar Flux Relative Error, $\varepsilon \to 0$

$$h = 1.0.$$

The solution to this problem is *extremely* flat away from the immediate vicinity of the boundary, and is given by $\tilde{Q}/\tilde{\sigma}_a = 0.1$. In Figure 4.5 we show the relative error in the cell average scalar fluxes when using DD to solve the above problem, and in Figure 4.6 the relative error is shown when using DD along with the asymptotically corrected parameters $\bar{\sigma}_t$ and $\bar{c}$. Again due to the problem symmetry we have only plotted half of the slab, $0 < x < 20$.

We can see that when $\varepsilon = 1$ the oscillations are slightly smaller than the other cases, but as ε decreases the solution approaches the asymptotic limit solution very quickly and we have a nearly constant amplitude in the oscillations. We can also see that again by using the asymptotically corrected parameters $\bar{\sigma}_t$ and $\bar{c}$ we have effectively killed the oscillations. As in the previous case we see that by doing so we have *greatly* increased the error at the system boundary, although this is not perfectly clear in Figure 4.6 since the points have been cut-off so that the scales could be kept constant between Figure 4.6 and Figure 4.5. Still these figures clearly display the effect of the additional absorption terms in the thick diffusion limit of the DD method.
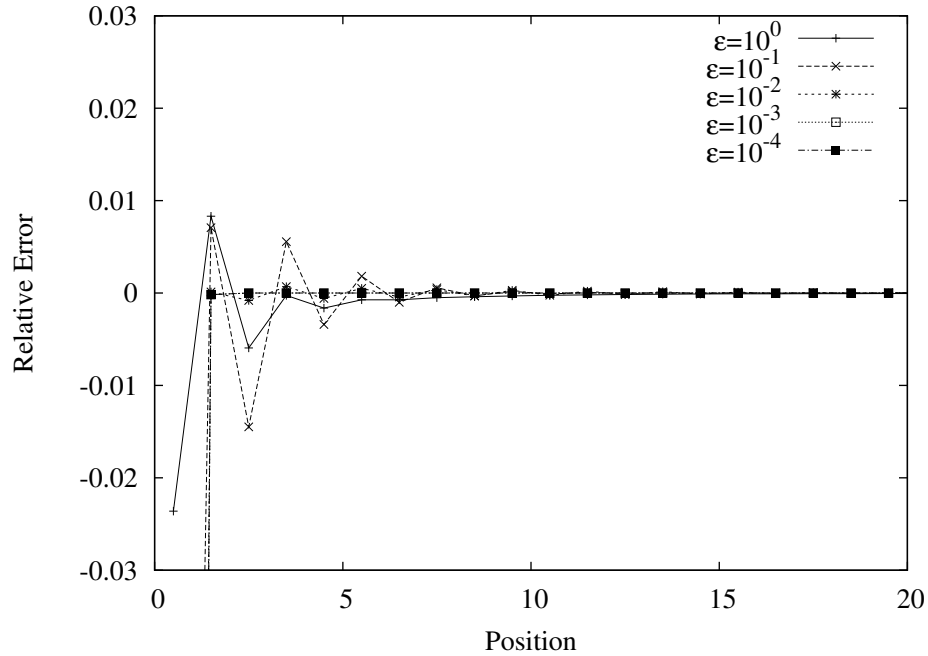
Figure 4.6. Cell Average Scalar Flux Relative Error with $D_{eff} = D$, $\varepsilon \to 0$

Eventually we would also like to know whether the diffusion discretization given in Chapter 2 provides a good representation of the solution to spatially continuous diffusion theory. To do so we now develop a discrete node based solution to the diffusion equation in a homogeneous medium which is still *exact*. In this manner we can compare the earlier finite-difference discretization with the exact discretization and decide whether altering the DD problem to more closely emulate the finite-difference diffusion discretization is a worthwhile endeavor.

4.1.2 Discrete Diffusion Solution

Homogeneous Case with $c = 1$

Again we will assume that the material properties and node sizes are constant in this problem and also that the distributed source is uniform throughout the slab. The notation and definitions used in Chapter 2 to discretize the diffusion equation via finite differencing also apply equal to the discretization technique being presented here.

The continuous diffusion equation that we are solving and its boundary condi-

tions are given by

$$\phi''(x) = -\frac{Q}{D}, \tag{4.45a}$$

$$\phi(x_{1/2}) = 0, \tag{4.45b}$$

$$\phi(x_{I+1/2}) = 0, \tag{4.45c}$$

where $x_{1/2}$ and $x_{I+1/2}$ again denote the x–coordinates of the slab end points. The general solution to this differential is easily found in terms of the constants c_1 and c_2 to be

$$\phi(x) = -\frac{Q}{2D}x^2 + c_1 x + c_2. \tag{4.46}$$

Now we now solve for the constants c_1 and c_2 in terms of the unknown edge fluxes, $\phi(x_{i-1/2}) = \phi_{i-1/2}$ and $\phi(x_{i+1/2}) = \phi_{i+1/2}$, which will become the edges of a spatial cell in this discretization, where we have again used h to denote the cell width. The point-wise flux can now be represented by

$$\phi(x) = -\frac{Q}{2D}x^2 + \left(\frac{-Q\left(x_{i-1/2}\right)^2 + Q\left(x_{i+1/2}\right)^2 - 2D\left(\phi_{i-1/2}\right) + 2D\left(\phi_{i+1/2}\right)}{2Dh}\right)x$$

$$- \left(\frac{Q\left(x_{i+1/2}\right)\left(x_{i-1/2}\right)}{2D}\right) - \frac{\left(\phi_{i+1/2}\right)\left(x_{i-1/2}\right) - \left(x_{i+1/2}\right)\left(\phi_{i-1/2}\right)}{h}. \tag{4.47}$$

This solution remains exact throughout the entire domain of the slab. If we were to set $\phi_{i-1/2}$ and $\phi_{i+1/2}$ to zero and choose $x_{i-1/2}$ and $x_{i+1/2}$ to be $x_{1/2}$ and $x_{I+1/2}$ respectively then the original problem would be completely solved. However, we would like to split the problem into discrete nodes so that a node averaged solution can be found. If we define the node average scalar flux as

$$\phi_i = \frac{1}{h}\int_{x_{i-1/2}}^{x_{i+1/2}} \phi(x), \tag{4.48}$$

then integrating Eq. (4.47) over the node, i.e. $[x_{i-1/2}, x_{i+1/2}]$, results in

$$\phi_i = \frac{1}{2}\left(\phi_{i-1/2} + \phi_{i+1/2}\right) + \frac{Qh^2}{12D}.$$

To simplify the above expression to this point it is necessary to recognize that the node edge x–coordinates can be written in terms of the midpoint value as $x_{i\pm1/2} = x_i \pm h/2$.

We would also like to impose the condition that the current is continuous across a node interface. This is done by differentiating the analytic expression for the flux in a node in two adjacent nodes, evaluating them at the x value of the shared interface and setting them equal, such that

$$\left.\frac{d}{dx}\phi_i(x)\right|_{x=x_{i+1/2}} = \left.\frac{d}{dx}\phi_{i+1}(x)\right|_{x=x_{i+1/2}} \tag{4.49}$$

If we use $\phi(x)$ from (4.47) we find that this operation yields the relation

$$\left(\phi_{i-1/2} - 2\phi_{i+1/2} + \phi_{i+3/2}\right) = -\frac{Qh^2}{D}$$

Still waiting to address the boundary conditions, we now have the linear system of equations given by

$$\phi_i = \frac{Qh^2}{12D} + \frac{1}{2}\left(\phi_{i-1/2} + \phi_{i+1/2}\right), \quad i = 1,\ldots,I \tag{4.50a}$$

$$\left(\phi_{i-1/2} - 2\phi_{i+1/2} + \phi_{i+3/2}\right) = -\frac{Qh^2}{D}, \quad i = 1,\ldots,I-1. \tag{4.50b}$$

We know that we would like to solve a system of node averaged equations in ϕ_i, so we will eliminate the edge quantities. If we take (4.50b) for node i and add it to (4.50b) for node $i-1$ we find the expression

$$\left(\phi_{i-3/2} - \phi_{i-1/2} - \phi_{i+1/2} + \phi_{i+3/2}\right) = -\frac{2Qh^2}{D}. \tag{4.51}$$

It is now possible to use (4.50a) to eliminate all edge quantities. This is done by writing (4.50a) for nodes $i-1$, i, and $i+1$. If we then take the linear combination of $\phi_{i-1} - 2\phi_i + \phi_{i+1}$ we see that we can use it to eliminate the left side of (4.51). This leaves us with the following expression for *only* the node averaged fluxes, in the slab interior,

$$(\phi_{i-1} - 2\phi_i + \phi_{+1}) = -\frac{Qh^2}{D}, \quad i = 2, \dots, I. \tag{4.52}$$

This is expression is identical to the finite difference equations for the slab interior, derived in Chapter 2, with this solution being *exact* for all of the node average fluxes, no truncation error has been incurred. To close the system we need to find boundary conditions in terms of these node average fluxes. We begin by writing (4.50a) for nodes 1 and 2 and (4.50b) for node 1 and finally setting $\phi_{1/2} = 0$ due to the imposed vacuum condition.

$$\phi_1 = \frac{Qh^2}{12D} + \frac{1}{2}\phi_{3/2}$$

$$\phi_2 = \frac{Qh^2}{12D} + \frac{1}{2}\left(\phi_{3/2} + \phi_{\frac{5}{2}}\right)$$

$$\left(-2\phi_{3/2} + \phi_{5/2}\right) = -\frac{Qh^2}{D}$$

Using all three equations we can eliminate the edge quantities $\phi_{3/2}$ and $\phi_{5/2}$ to find the boundary condition for the left edge of the system. The same process is applied to nodes I and $I-1$ to find the corresponding right edge condition. The complete closed system is now defined by

$$-\frac{D}{h^2}\left(\phi_{i-1} - 2\phi_i + \phi_{i+1}\right) = Q, \quad i = 2, \dots, I, \tag{4.53a}$$

$$-\frac{D}{h^2}\left(3\phi_1 - \phi_2\right) = \frac{2Q}{3}, \tag{4.53b}$$

$$-\frac{D}{h^2}\left(3\phi_I - \phi_{I-1}\right) = \frac{2Q}{3}. \tag{4.53c}$$

This set of equations is remarkably similar to the finite-differenced diffusion equation in a homogeneous medium with the zero boundary condition. The interior equations are in fact identical with the only difference in the systems being the factor of 2/3 applied to the right hand side of each boundary condition. Thus we see that even the vacuum bounds for the finite differenced diffusion equation previously derived are deficient when compared to the exact diffusion theory solution, although this can be fixed very easily in any one-dimensional diffusion implemen-

tation. It is not easy, and perhaps not possible, to alter the DD method in a manner such that the vacuum boundary conditions will asymptotically limit to those given above. However, we must remember these results are for the specialized circumstance of a purely scattering medium. We now proceed to determine an analytically exact discrete diffusion solution in the presence of absorption.

Homogeneous Case with $c < 1$

When we consider a finite amount of absorption in the previous problem the second order ordinary differential equation we are solving is given by

$$\phi''(x) - \frac{1}{L^2}\phi(x) = -\frac{Q}{D}, \tag{4.54a}$$

$$\phi(x_{1/2}) = 0, \tag{4.54b}$$

$$\phi(x_{M+1/2}) = 0, \tag{4.54c}$$

This derivation turns out to be a special case of a more generalized multidimensional nodal integral method derived in [36]. To find the analog to (4.50b) for the $c < 1$ case we can directly substitute the relation

$$\frac{\phi_{m+1}(+a) - 2\phi_m(+a) + \phi_m(-a)}{\left(\frac{2\sinh(\gamma a)}{\gamma}\right)^2} - \gamma^2\phi_m(+a) = \frac{S_m + S_{m+1}}{2}, m = 1, \ldots, M-1,$$

from the previously mentioned paper, which after making the necessary notation substitutions yields

$$\frac{\left(\phi_{i-1/2} - 2\phi_{i+1/2} + \phi_{i+3/2}\right)}{(2L\sinh(\frac{h}{2L}))^2} - \frac{1}{L^2}\phi_{i+1/2} = -\frac{Q}{D}, \quad i = 1, \ldots, I-1, \tag{4.55}$$

where L is the diffusion length. If we now average Azmy's [36] analytic solution for the nodal flux over the length of a node and again make the necessary notation changes we find that,

$$\phi_i = \frac{L}{h}\left(\phi_{i-1/2} + \phi_{i+1/2}\right)\tanh\left(\frac{h}{2L}\right) + \frac{Q}{\sigma_a}\left(1 - \frac{2L}{h}\tanh\left(\frac{h}{2L}\right)\right), \quad i = 1,\ldots,I. \tag{4.56}$$

To actually carry out the integration for this step the interval considered was $[-a_i, a_i]$ as in the work by Azmy, with the fact that in our notation $h = 2a$ being substituted in after the integration. This greatly simplifies the algebra involved because it allows for the cancellation of many of the hyperbolic terms existing on the node edge. Using (4.55) and (4.56) we can now carry out the exact same procedure as we did earlier to eliminate all edge quantities from the interior equations, although the algebra is slightly more complicated. The resulting equation in terms of node averaged fluxes is,

$$-\frac{D}{(2L\sinh(\frac{h}{2L}))^2}\left(\phi_{i-1} - 2\phi_i + \phi_{i+1}\right) + \sigma_a\phi_i = Q, \quad i = 2,\ldots,I-1 \tag{4.57}$$

We note here that to if we were to expand the hyperbolic function to leading order this equation is identical to the standard three point discretized diffusion scheme. To close this system we would like to find vacuum boundary conditions on both edges in the exact same manner as for the case where $c = 1$. Again there is a good deal more algebraic manipulation involved here, but the process is identical. The resulting closed system of equations is,

$$-\frac{D}{(2L\sinh(\frac{h}{2L}))^2}\left(\phi_{i-1} - 2\phi_i + \phi_{i+1}\right) + \sigma_a\phi_i = Q, \quad i = 2,\ldots,I-1, \tag{4.58a}$$

$$\left(2\cosh\left(\frac{h}{L}\right) + 1\right)\phi_1 - \phi_2 = \frac{2Q}{\sigma_a}\left(\cosh\left(\frac{h}{L}\right) - \frac{L}{h}\sinh\left(\frac{h}{L}\right)\right), \tag{4.58b}$$

$$\left(2\cosh\left(\frac{h}{L}\right) + 1\right)\phi_I - \phi_{I-1} = \frac{2Q}{\sigma_a}\left(\cosh\left(\frac{h}{L}\right) - \frac{L}{h}\sinh\left(\frac{h}{L}\right)\right). \tag{4.58c}$$

If we rewrite the diffusion length, L, in terms of only D and σ_a and then consider $\sigma_a \to 0$, we find that this closed set of equations derived for $c < 1$ limits exactly to the closed set of equations found in for the case where $c = 1$, as expected.

We can see then that the diffusion discretization described in Chapter 2 reasonably approximates the exact diffusion theory solution for c near one, with the exception of the equations on the system boundary. So it would seem that it is worthwhile to attempt to alter the DD method so that in the limit it behaves more like the finite-differenced diffusion equation. However, we must remember that all of the analysis done here is for the very restrictive case of a homogeneous region. We should also consider problems containing more than one material region so that we can look at the behavior of the DD method and diffusion theory across material interfaces.

4.2   Heterogeneous Media

In this section we will consider Problem 2, given in 2.4.3, a two-region problem dominated on the left by local balance and on the right by neutron leakage. We will primarily be focusing on numerical results for this problem since Eq. (4.13) cannot be simplified in any meaningful manner in the vicinity of the material interface. We have solved Problem 2 using three solutions methods: Diamond Difference, "asymptotically corrected" Diamond Difference (using $\bar{\sigma}_t$ and $\bar{c}$), and the finite-differenced diffusion discretization described in Chapter 2. We will also consider three different spatial meshes for this problem with the first spatial mesh considered being being termed thick (each cell 100 mfp). The next spatial mesh considered uses a fine mesh at the slab boundaries such that the first and last 100 cells are only a single mean free path thick. The final mesh uses a fine mesh both in the vicinity of each boundary and the material interface, specifically the first and last 100 cells are again a single mean free path thick while the the 100 cells to both the left and right of the material interface are also of this thickness. To analyze the behavior of the different solution methods for a given mesh we will plot the magnitude of the relative error in the scalar flux. All solutions were calculated using the S_{16} quadrature set with the reference solutions for each case calculated using a mesh composed of 10^4 spatial cells.

In the case of the thick mesh we have already actually seen the results for the DD method in Figure 2.5, although in that case we plotted the spatial distribution of the scalar flux and not the error in the scalar flux solution in Figure 4.7. We
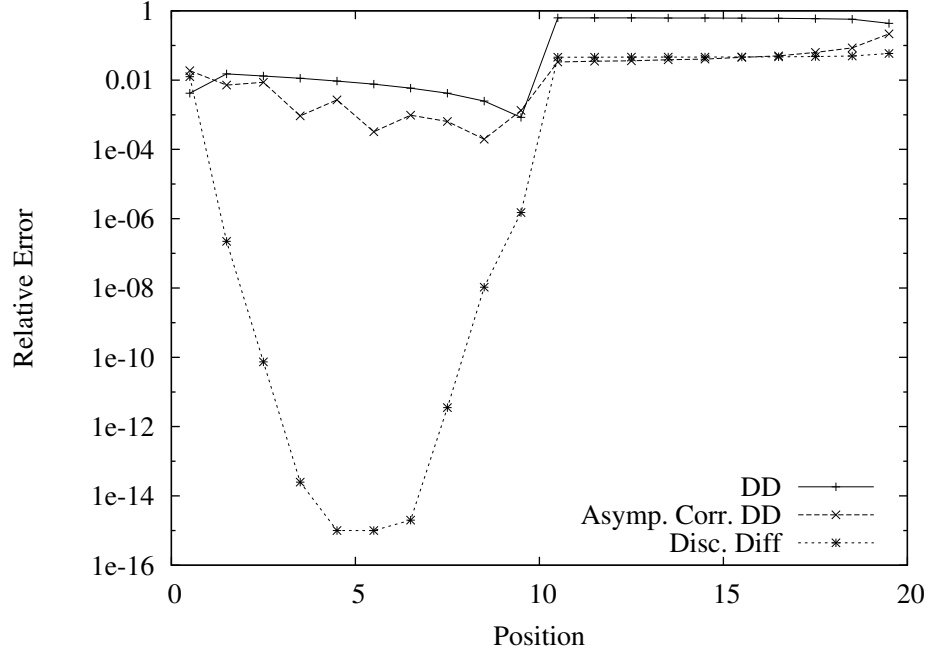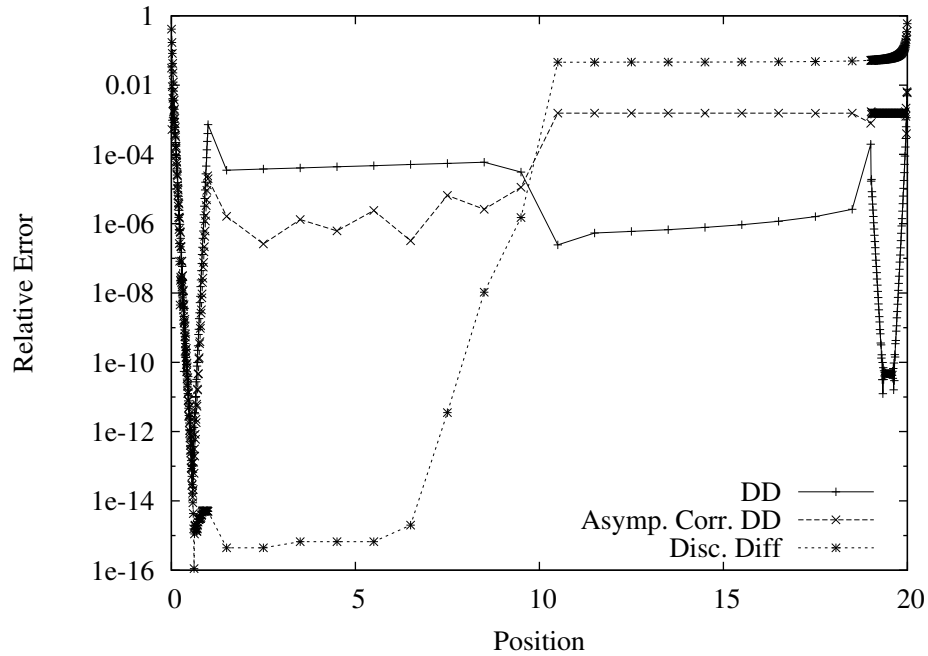
Figure 4.7. Thick Mesh Cell Average Scalar Flux Relative Error for Two-Region Problem

can see that in this case the DD method on its own performs the worst of the three methods tested, with the discretized diffusion solution performing the best in the source region and being comparable to the asymptotically fixed DD in the scattering region. It is worthwhile to note that in this two-region problem for the asymptotically fixed solution we have used $\bar{\sigma}_t$ and $\bar{c}$ as defined through Eqs. (4.43) and (4.44), respectively, even though we know that the quantity D_{eff} does not describe the diffusion process near the system edges or the material interface. Still this solution shows a considerable improvement over the standard DD solution since it does not display the flux jump at the material interface. In fact, in the scattering region the error is nearly two orders of magnitude lower as a result of using the asymptotically corrected parameters. This does show that even in two-region problems using thick spatial meshes the asymptotically corrected DD parameters can be beneficial. Still we see that the discretized diffusion results for this spatial mesh are *much* better than both DD solutions.

We now consider a mesh that spatially resolves the boundary layer at the each boundary of the slab, which is done by using 100 cells which are each a single

Figure 4.8. Resolved Boundary Mesh Cell Average Scalar Flux Relative Error for Two-Region Problem

mean free path thick and then returning to cells 100 mean free paths thick for the remaining interior of the slab. The relative error plots for each solution method on this spatial mesh are given by Figure 4.8. We again see that in the region dominated by local balance the discretized diffusion solution is extremely accurate when compared to both of the DD solutions. For this spatial mesh and the thick spatial mesh we also see a large increase in the discretized diffusion error across the material interface, which is expected as diffusion theory does not allege to provide accurate solutions near material interfaces or system boundaries. In the source region we also see again that the asymptotically corrected DD solution is more accurate than the standard DD solution, although this is not true in the scattering region. We do note though that even though the asymptotically corrected DD error increases across the material interface, in the scattering region it is still nearly two orders of magnitude better than the discretized diffusion solution in this region. We also note that the standard DD error actually decreases when the scattering region is encountered. These DD results suggest that it is not only the presence of D_{eff} which causes problems in this solution as we can see that by merely resolving
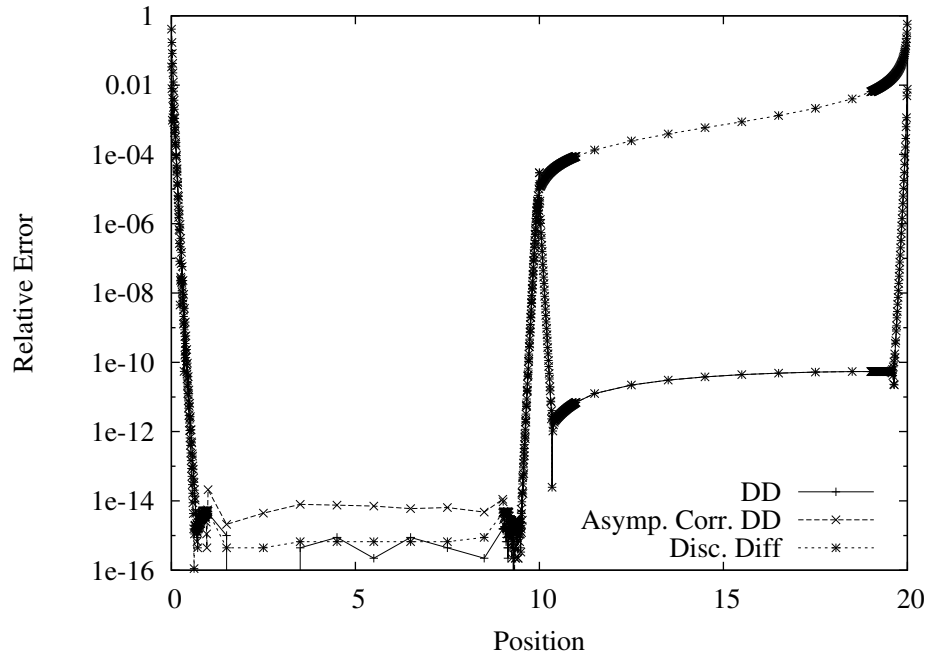
Figure 4.9. Resolved Interface and Boundary, Cell Average Scalar Flux Relative
Error for Two-Region Problem

the boundary layer the thick cell DD solution is much more accurate throughout
than in the case of the thick spatial mesh.

It is possible that the previously noted difference between the vacuum boundary
conditions for the diffusion discretization described in Chapter 2 and the asymp-
totic limit of the DD method is responsible for this behavior. By resolving the
boundary layer we are removing this component of the error which would other-
wise propagate throughout the problem and make the errors in Figure 4.8 more
closely resemble those in Figure 4.7. We can then explain the increase in error for
the asymptotically corrected DD solution across the interface by recalling that the
asymptotic corrections were defined for homogeneous media and so should not be
expected to work in the presence of material interfaces. In any case, Figure 4.8
shows that without the error component introduced at the slab boundary the DD
method is better than diffusion theory at handling material interfaces, even with
optically thick spatial cells.

In the final numerical experiment for the two-region problem we use a a spatial
mesh that again resolves the each boundary layer but also resolves the material

interface by using 100 cells, each a mean free path thick, to the left and right of the interface. The results of this experiment are plotted in Figure 4.9 and are quite different from the results given in Figure 4.8. We see that when both the material interface and boundaries are resolved using fine spatial meshes that both the DD and discretized diffusion error within the source region is 0 to within machine precision, while the asymptotically corrected DD error is a bit larger, but still extremely small. This error is most likely introduced by the heterogeneity in applying the correction to the optically thick cells while applying no correction to the optically thin cells boundary cells. We see now that in the scattering region the DD error is considerably smaller than with either of the previously discussed spatial meshes. The asymptotically corrected DD error is actually coincident with the DD error in this case, no error is propagated across the boundary because of the fine spatial mesh and there is no asymptotic corrections to make in the pure scattering medium, so in this region the solutions are identical.

We see now that for this problem D_{eff} has little or no effect in the interior given that any boundary layers and interfaces are suitably resolved. The asymptotically corrected DD was only truly beneficial in the case of the thick mesh, where the corrections were able to diminish the wild oscillations of the edge fluxes so that error did not propagate from the source region to the scattering region.

We also see that while resolving the material interface greatly reduces the DD error in each region, it has little effect on reducing the discretized diffusion error across the interface and in the scattering region. It is interesting to consider at this point that at the material interface in this problem Eq. (4.33) is most likely not satisfied and so the asymptotic analysis predicts that in the thick limit the DD method will not limit to the appropriate diffusion boundary condition. We can see from Figure 4.9 that even if we were to limit to the correct diffusion boundary condition, in this case it would be undesirable because diffusion theory itself cannot accurately describe the scalar flux across the material interface. Thus any attempt to correct the DD method to more accurately represent the correct diffusion discretization in the thick diffusion limit will ultimately lead to results that can only be as good as those shown by the discretized diffusion curve in Figure 4.9.

In fact, we could alter the work done in 4.1.2 so that the exact analytic dif-

fusion solution could be constructed, in which case we would see results that are practically identical to those shown in Figure 4.9 for the discretized diffusion curve. Accepting that diffusion theory itself, even in slab geometry, has serious drawbacks we consider the discrete-ordinates transport equation itself. Is it possible to construct a one-dimensional auxiliary relation that effectively divides the transport equation into analytically exact node-wise solutions as we did with the diffusion equation in 4.1.2? Some preliminary work along these lines has been conducted and is briefly presented in the following chapter.

Discrete $\mathbf{S}_N$ Transport Solution

Attaining an analytic solution for the one-dimensional, discrete-ordinates equations is considerably more difficult than solving the one-dimensional diffusion equation, however the topic has been thoroughly covered in the literature, notably by Chandrasekhar [7]. Davison [1] and Keller [37] considered the problem specifically for the case of neutron transport, with Keller actually providing generalized solutions in matrix form. Warsa [38] authored a 2002 article where he reviews solution methods to the problem with the ultimate goal of implementing the solutions in the symbolic mathematical software, MAPLE. The paper also provides the MAPLE scripts necessary to fully solve the problem in a heterogeneous media with anisotropic scattering and a choice of boundary conditions. It is also possible to compute the solution using a distributed source with any spatial dependence for which a particular solution can be found.

Although generalized prescriptions for the solutions of the one-dimensional, discrete-ordinates equations are available they often depend on numerically determined eigenvalues and are generally complicated for higher order quadrature sets. Here we will only set up the problem for the S_2 case in a homogeneous medium, considering both $c = 1$ and $c < 1$. The one-dimensional, steady-state, monoenergetic S_2 equations are then given by

$$\mu_n \frac{d}{dx}\psi_n + \sigma_t \psi_n = \sigma_t c \left(w_1 \psi_1 + w_2 \psi_2 \right) + Q, \quad n = 1, 2 \tag{5.1}$$

where Q is assumed to be constant in space and the quadrature set used follows the rules given by Eqs. (2.3), in which case the above equations simplify to

$$\frac{d}{dx}\psi_n + \frac{\sigma_t}{\mu_n}\psi_n = \frac{\sigma_t c}{2\mu_n}\left(\psi_1 + \psi_2\right) + \frac{Q}{\mu_n}, \quad n = 1, 2. \tag{5.2}$$

Recalling the assumption that the the quadrature set is even about $\mu = 0$ such that $\mu_1 = \mu$ and $\mu_2 = -\mu$, and utilizing matrix notation we can rewrite the above equations as

$$\frac{d}{dx}\vec{\psi} = \mathbf{A}\vec{\psi} + \begin{pmatrix} Q\mu^{-1} \\ -Q\mu^{-1} \end{pmatrix}, \tag{5.3}$$

where the vector $\vec{\psi}$ is of length 2 having the elements ψ_1 and ψ_2 and the 2 x 2 matrix $\mathbf{A}$ is given by

$$\mathbf{A} = \begin{pmatrix} \frac{\sigma_t(c-2)}{2\mu} & \frac{\sigma_t c}{2\mu} \\ -\frac{\sigma_t c}{2\mu} & -\frac{\sigma_t(c-2)}{2\mu} \end{pmatrix} \tag{5.4}$$

Calculating the eigenvalues, g, of $\mathbf{A}$ we find that

$$g_1 = \frac{\sigma_t}{\mu}\sqrt{1-c} \tag{5.5a}$$

$$g_2 = -\frac{\sigma_t}{\mu}\sqrt{1-c} \tag{5.5b}$$

For the case where $c < 1$ this provides two real, unique roots of equal magnitude with opposite sign. However, when $c = 1$ these two roots become a a double root at the origin, which requires a special solution procedure. A particular solution for the S_2 problem must also be included due to the presence of the external source. Rather than perform these derivations by hand we will utilize the computer algebra system *Mathematica* and by doing so we can easily solve the S_2 problem, including boundary conditions, for both $c = 1$ and $c < 1$.

5.1 The S_2 Problem for $c = 1$

We have seen previously with diffusion theory that the $c = 1$ case is often distinct from the $c < 1$ case, and this is just as true for the S_2 solution. *Mathematica* easily

gives us the general solution to Eq. (5.3) where the vacuum boundary conditions have imposed at the arbitrary endpoint A through the relations

$$\psi_n(-A) = 0, \quad \mu_n > 0 \tag{5.6a}$$

$$\psi_n(A) = 0, \quad \mu_n < 0 \tag{5.6b}$$

and ψ_1 and ψ_2 are given by the quadratic functions

$$\psi_1(x) = \frac{Q}{\mu} \left(\frac{A(2\mu + A\sigma_t)}{2\mu} + x - \frac{\sigma_t}{2\mu} x^2 \right) \tag{5.7a}$$

$$\psi_2(x) = \frac{Q}{\mu} \left(\frac{A(2\mu + A\sigma_t)}{2\mu} - x - \frac{\sigma_t}{2\mu} x^2 \right) \tag{5.7b}$$

We now define the average angular flux, $\bar{\psi}_n$ over the spatial range $[x_{in}, x_{out}]$, where $h = x_{out} - x_{in}$, by

$$\bar{\psi}_n = \frac{1}{h} \int_{x_{in}}^{x_{out}} \psi_n(x), \quad n = 1, 2. \tag{5.8}$$

At this point we would like to consider taking three adjacent nodes, defined in relation to an arbitrary point x_i as depicted in Figure 5.1, such that for $\mu > 0$,

$$x_{in} = x_i - \tfrac{3h}{2}, x_i - \tfrac{h}{2}, \quad \text{and} \quad x_i + \tfrac{h}{2}$$
$$x_{out} = x_i - \tfrac{h}{2}, x_i + \tfrac{h}{2}, \quad \text{and} \quad x_i + \tfrac{3h}{2},$$

and for $\mu < 0$, x_{in} and x_{out} are just the opposite of above.
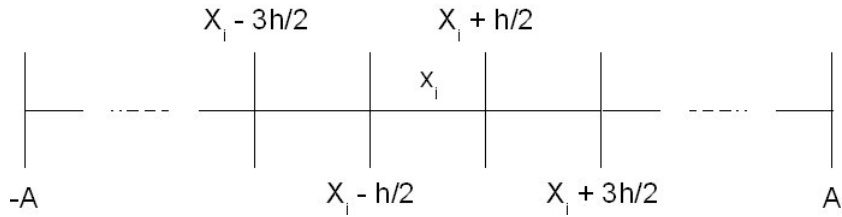
Figure 5.1. Arbitrary Discretization into Three Adjacent Nodes

We can now average both of Eqs. (5.7) over each of the three nodes depicted in Figure 5.1. So for each of these nodes we now have an analytically defined node average and we can evaluate Eqs. (5.7) at x_{in} and x_{out} to find the angular flux values at the edge. At this point we propose an auxiliary relation which has the

form

$$\alpha \bar{\psi}_n = [\psi_n(x_{out}) - \psi_n(x_{in})] + \beta [\psi_n(x_{out}) + \psi_n(x_{in})] + \gamma \bar{\phi} \qquad (5.9)$$

where α, β, and γ are at this point unknown constants and the scalar flux $\bar{\phi}$ for this problem is defined as

$$\bar{\phi} = \frac{1}{2} \left(\bar{\psi}_1 + \bar{\psi}_2 \right).$$

We will now attempt to find an auxiliary relation which along with the balance equation,

$$\frac{|\mu|}{h\sigma_t} [\psi_n(x_{out}) - \psi_n(x_{in})] + \bar{\psi}_n = \bar{\phi} + \frac{Q}{\sigma_t}, \qquad (5.10)$$

will result in node average fluxes which are analytically *exact*. This is achieved through writing the auxiliary relation given by Eq. (5.9) for each of the three nodes depicted in Figure 5.1 and solving for the α, β, and γ which satisfy the three equation linear system. *Mathematica* easily performs this operation, with the resulting expressions given by

$$\alpha = \left(\frac{12\mu}{h\sigma_t} - \frac{h\sigma_t}{\mu} \right), \qquad (5.11a)$$

$$\beta = \frac{6\mu}{h\sigma_t}, \qquad (5.11b)$$

$$\gamma = -\frac{h\sigma_t}{\mu}. \qquad (5.11c)$$

where the *Mathematica* notebook used to calculate the parameters α, β, and γ is provided in Appendix A for convenience.

If we were to now implement the same iterative algorithm used for DD, Step, and AHOT-N0 to solve the spatially and angularly discretized transport problem in slab geometry for a purely scattering medium, using the balance equation given by Eq. (5.10) with the auxiliary relation in Eq. (5.9) which uses the parameter definitions given by Eqs. (5.11), the resulting solution would be *exact*, in the discrete-ordinates formulation. In other words, the auxiliary equation we have derived does not commit any truncation errors due to the specific choice of α, β,
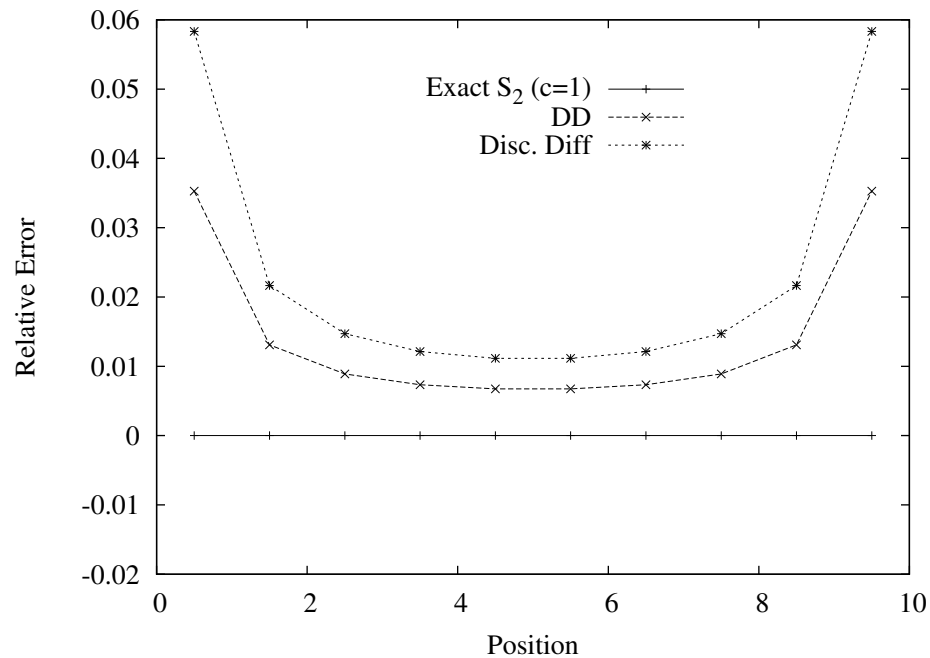
Figure 5.2. Exact S_2 Discretization ($c = 1$) Relative Error

and γ.

One of the downsides to this auxiliary relation is that the method used to determine α, β, and γ is in no way mathematically rigorous. We would like to be able to directly derive these parameters and also have some assurance that they are invariant across a homogeneous slab, as numerical evidence suggests. Still the numerical results do confirm that for the specific problem considered the solution is exact. This discretization scheme was implemented by altering a preexisting one-dimensional iterative S_N code and used to calculate the solution to Problem 1, described in Chapter 2. The S_2 quadrature set is used for all solutions and the relative error between the discretization and a fine-mesh (10^4 spatial cells) reference solution is given in Figure 5.2, where the DD and discretized diffusion results are also provided for the sake of comparison.

We see that the error is exactly equal to zero throughout the slab domain as expected, confirming that for the case of $c = 1$ and the S_2 quadrature set this discretization scheme results in exact solutions. Preliminary numerical evidence also suggests that the same α, β, and γ can be used for higher order quadrature sets without dramatically increasing the error. In the cases tested applying the exact

S_2 discretization for quadrature orders up to S_8 still resulted relative errors nearly two orders of magnitude lower than DD solutions calculated on the same spatial mesh with the same quadrature order. However we realize that there is no reason to believe we will generally witness this behavior, and ideally we would hope that α, β, and γ values could be found which can be used to calculate the exact solution to the discrete-ordinates problem with quadrature sets larger than S_2. We must also realize that these parameters were found for the very special case of $c = 1$ and that the development of more general parameters, which can describe the solution to problems containing finite amounts of absorption, are desirable, with the early work done in this area being presented briefly in the following section.

5.2 The S_2 Problem for $c < 1$

For the S_2 problem with $c < 1$ we do not have the luxury of working with polynomial functions. The presence of two real and unique roots to the characteristic equation implies that the homogeneous solution will be exponential in nature. Again we use *Mathematica* to find the general solution, after imposing the vacuum boundary conditions, Eqs. (5.6), on the problem. ψ_1 and ψ_2 are again easily found, but in this case the resulting expressions are too unwieldy to explicitly write below. In this case we were not able to use the arbitrary 3 cell discretization shown in Figure 5.1 because of a failure by *Mathematica* to simplify the final expression. The notebook used to determine the α, β, and γ values in this section is provided in Appendix B. As the process is identical for the most part to last time the majority of it will be skipped.

For the $c < 1$ case we are able to solve for the exact α, β, and γ which satisfy the auxiliary relation given by

$$\frac{|\mu|}{h\sigma_t} \left[\psi_n(x_{out}) - \psi_n(x_{in}) \right] + \bar{\psi}_n = c\bar{\phi} + \frac{Q}{\sigma_t}, \qquad (5.12)$$

but the expressions are enormous and extremely complex which makes them basically impossible to work with. To overcome this problem we have expanded the expressions for α, β, and γ in Taylor series centered on $c = 0$. *Mathematica* can perform the series expansion and then simplify the resulting terms into forms we

are more capable of working with. Below we show the values which were calculated using the attached *Mathematica* notebook.

$$\alpha = \frac{2h\sigma_T}{h\coth\left(\frac{h\sigma_T}{2\mu}\right)\sigma_T - 2\mu}$$
$$+ \frac{h^2\sigma_T^2\left(3\mu\sinh\left(\frac{h\sigma_T}{\mu}\right) - h\left(\cosh\left(\frac{h\sigma_T}{\mu}\right) + 2\right)\sigma_T\right)c}{2\mu\left(h\cosh\left(\frac{h\sigma_T}{2\mu}\right)\sigma_T - 2\mu\sinh\left(\frac{h\sigma_T}{2\mu}\right)\right)^2} + O\left(c^2\right), \quad \text{(5.13a)}$$

$$\beta = \frac{\left(-1 + e^{\frac{h\sigma_T}{\mu}}\right)h\sigma_T}{\left(1 + e^{\frac{h\sigma_T}{\mu}}\right)h\sigma_T - 2\left(-1 + e^{\frac{h\sigma_T}{\mu}}\right)\mu}$$
$$- \left[\frac{\left(h\sigma_T\left(-4\left(-1 + e^{\frac{h\sigma_T}{\mu}}\right)^2\mu^2 + \left(-1 + e^{\frac{2h\sigma_T}{\mu}}\right)h\sigma_T\mu + 2e^{\frac{h\sigma_T}{\mu}}h^2\sigma_T^2\right)\right)}{2\left(\mu\left(\left(1 + e^{\frac{h\sigma_T}{\mu}}\right)h\sigma_T - 2\left(-1 + e^{\frac{h\sigma_T}{\mu}}\right)\mu\right)^2\right)}\right]c$$
$$+ O\left(c^2\right), \quad \text{(5.13b)}$$

$$\gamma = -\frac{h\sigma_T c}{\mu} + O\left(c^2\right). \quad \text{(5.13c)}$$

The expressions given above are $O(c^2)$, however by merely changing the number of terms retained in the Taylor expansion in *Mathematica* we should be able to determine α, β, and γ to any order we desire, assuming that *Mathematica* can handle the simplification procedure. Again the heavy dependence of this procedure on *Mathematica* points out why it would be beneficial to develop a more mathematically rigorous method to determine α, β, and γ.

The discretization described by Eqs. (5.12) and (5.13) has been implemented in the same iterative code as the $c = 1$ discretization with success. To evaluate the accuracy of the discretization we again consider the magnitude of the relative error in the cell average scalar flux for a sample problem. In this instance we are more interested in how the error varies with c than how it varies spatially so we will plot the relative error in the boundary cell and at the center-most cell versus c, where again we include S_2 DD results for the sake of comparison. The problem

considered in this case is given by

$$\mu_n \frac{d\psi_n}{dx} + \psi_n = c \sum_{m=1}^{M} \psi_m w_m + 1.0, \quad 0 < x < 10$$

$$\psi_n(0) = 0, \quad \mu_n > 0$$

$$\psi_n(20) = 0, \quad \mu_n < 0$$

$$h = 1.0.$$

The reference solution used to determine the relative errors is the exact S_2 solution, found and then averaged into the appropriate cell structure using *Mathematica* . The results of this numerical experiment are given in Figure 5.3.
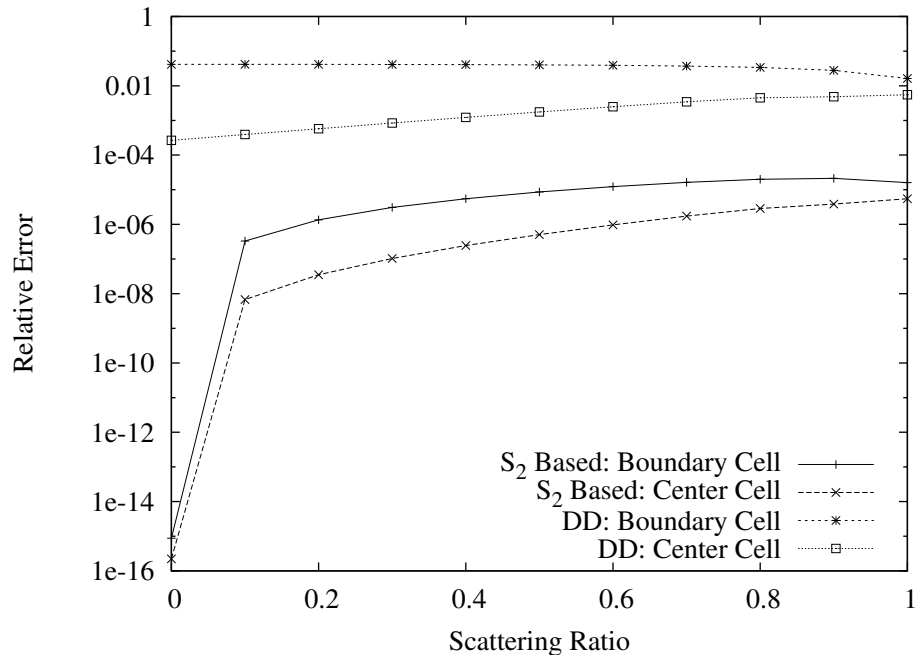
Figure 5.3. S_2 Discretization $(c < 1)$ Relative Error

The behavior shown by the new S_2 based is exactly as we would expect and confirms that α, β, and γ have been determined correctly. For the $c = 0$ case the relative error of the new method is practically zero and then increases with c, which makes sense since the deviation from the "true" values of the parameters α, β, and γ is $O(c^2)$. We see that even for large c values the new S_2 method has a relative error that is many orders of magnitude smaller than the DD error. By

considering the $O(c^2)$ terms the difference between the error in the DD results and the new S$_2$ based results would increase further.

This chapter presented some very preliminary results which should be studied more thoroughly and we recognize a great deal of work still exists in generalizing and expanding these results, with specific recommendations for ways to approach this given in 6.2. Still, the results generated to this point are encouraging. We have successfully created a one-dimensional transport discretization which can reproduce the exact S$_2$ solution in a purely scattering medium and described another for the case where $c < 1$ which is a good approximation to the S$_2$ solution. In theory the $c < 1$ discretization could generate solutions that are arbitrarily close to the exact solution by increasing the number of terms retained in the Taylor series expansion.

CHAPTER

SIX

Conclusions

6.1   Summary of Work

The objective of this work was to investigate the thick diffusion limit of various spatial discretizations of the one-dimensional, steady-state, monoenergetic, discrete-ordinates neutron transport equation. Though this area has been studied extensively in the literature this work was meant to specifically address the two lowest order nodal methods, AHOT-N0 and AHOT-N1, as well as reanalyze the DD method with the intent of focusing on cell average and not cell quantities.

In Chapter 1 the basic premise of this work was described followed by a review of the relative literature which covered the general realm of neutron transport theory, spatially continuous asymptotic analyses of the one-dimensional discrete-ordinates equations, spatially discretized asymptotic analyses of the one-dimensional discrete-ordinates equations, and the development of nodal transport methods.

Chapter 2 presented the mathematics and physical theory necessary to follow the works described in the literature review and the new work done in this thesis. The foundations of neutron transport theory were covered and the one-dimensional transport equation was subsequently discretized in both space and angle. Diffusion theory was also explained and spatially discretized for the one dimensional case. The asymptotic diffusion limit was then presented for the spatially continuous transport equation and then the analyses of spatially discretized transport equation

using the Step and DD methods were given along with some numerical results.

In Chapter 3 the asymptotic analyses of the AHOT-N0 and AHOT-N1 nodal methods were presented along with numerical results, confirming the analyses. It was seen that the AHOT-N0 method limits to the Step method in the optically thick, diffusive media and does not generally possess the thick diffusion limit for cell edge or cell average fluxes, although it can under certain restrictive conditions. It was also shown that the AHOT-N1 method limits to a legitimate diffusion discretization in the system interior and its boundary conditions limit to the appropriate diffusion boundary conditions, giving the AHOT-N1 method the thick diffusion limit for both the cell average and cell edge fluxes. The numerical tests presented in this section confirm the conclusions drawn regarding each method.

We then reexamined the DD method in Chapter 4 with the intention of deriving the limit using cell average and not cell edge scalar fluxes. The asymptotic limit derived was a tridiagonal linear system based solely on cell average scalar fluxes and the known incident fluxes. Although the resulting system may be a legitimate discretization of the diffusion equation, it is certainly not desirable. It was shown that the only when σ_t, h, and Q are constant and $\sigma_a = 0$ is the asymptotic limit of the DD method close to the diffusion discretization derived in Chapter 2, although there is still disparity between the systems at the boundary. In this chapter the asymptotic DD limit was considered for a homogeneous region and it was shown that in the precision of absorption the diffusion coefficient in the problem was not the physical D, but rather an effective diffusion coefficient, which was capable of becoming negative and thus introducing numeric error into the DD solution. Numerical errors introduced by the boundary conditions and material interfaces were also explored in a section dealing with the asymptotic DD cell average limit in a two-region problem.

A discrete diffusion solution which exactly solves the one-dimensional diffusion equation in a homogeneous region with constant cross sections and a uniform external source was also developed in Chapter 4. We saw that for the case where $c = 1$ the exact solution in the interior is the same as the finite-differenced diffusion discretization developed in Chapterchapt:background although the exact boundary conditions differed from the finite-differenced boundary conditions by a factor of $2/3$ applied to the external source. We also showed that for $c < 1$ the exact discrete

diffusion solution is based on hyperbolic functions, which limit to the exact solution for the $c = 1$ as $c \rightarrow 1$.

Finally, in Chapter 5 we outline the develop of a discrete-ordinates spatial discretization which is exact for the S_2 quadrature set in a purely scattering homogeneous region with vacuum boundaries. We also show preliminary work done in generalizing the discretization to be compatible with problems where $c < 1$.

6.2   Recommendations for Future Work

There are many avenues along which future research could proceed from this work. One particular area of interest is the failure mechanism of the AHOT-N0 method in the thick diffusion limit. We know that the AHOT-N0 solution is exact aside from the representation of the scattering source as a constant and still the method fails in the thick diffusion limit while the DD method succeeds in certain cases. It would be beneficial to construct the exact scattering source and experiment further with the AHOT-N0 and DD methods. With the exact scattering source used in conjunction with AHOT-N0 we should expect an exact solution, is this the case? By examining the exact scattering source can we pinpoint why AHOT-N0 fails and DD does not?

While the low order nodal methods, AHOT-N0 and AHOT-N1, were analyzed in the thick diffusion limit it may be worthwhile to examine these methods in the intermediate diffusion limit, which has received considerably less attention in the literature. While the Step method was analyzed in the intermediate diffusion limit it is not immediately clear that the results will be directly applicable to the AHOT-N0 method. The intermediate diffusion limit analysis of the AHOT-N1 method would also be interesting since Larsen, Morel, and Miller [10] only examined methods based on constant representations of the cell flux in their 1987 work. The thick limit results imply nothing about the results in the intermediate limit so it is very possible that AHOT-N0 may possess the intermediate diffusion limit while the AHOT-N1 method does not.

Aside from the diffusion limit research the exact S_N based discretization described in Chapter 5 is only in the very preliminary stages, leaving much work to be done. A mathematically rigorous approach to deriving the α, β, and γ param-

eters should be implemented both for $c = 1$ and for the case where $c < 1$. The discretization should also be extended so that it can be applied to problems containing heterogeneities and non-vacuum boundary conditions. Finally and maybe most importantly, the method should be extended so the exact calculated solution is exact quadrature sets of orders higher than S_2.

C=1 Mathematica Notebook

S_2 *Solution (c=1)*

$\text{bounds2} = \{\psi_1[-A] == 0, \psi_2[A] == 0\};$

General Solution

$\text{gensol2} = \text{Simplify}\left[\text{DSolve}\left[\left\{\mu\partial_x\left(\psi_1[x]\right) + \sigma_T\psi_1[x] - (\sigma_T)\left(\frac{\psi_1[x]+\psi_2[x]}{2}\right) - Q == 0,\right.\right.\right.$
$\left.\left.-\mu\partial_x\left(\psi_2[x]\right) + \sigma_T\psi_2[x] - (\sigma_T)\left(\frac{\psi_1[x]+\psi_2[x]}{2}\right) - Q == 0, \text{bounds2}\right\},\right.$
$\left.\{\psi_1[x], \psi_2[x]\}, x\right]\right];$
$\psi_1[\text{x\_}] = \psi_1[x]/.\text{gensol2};$
$\psi_2[\text{x\_}] = \psi_1[x]/.\text{gensol2};$

Cell average fluxes

$\text{c1}_1 = \text{Simplify}\left[\frac{1}{h}\text{Integrate}\left[\psi_1[z], \left\{z, x_i - 3\frac{h}{2}, x_i - \frac{h}{2}\right\}\right], Q > 0\&\&\sigma_T > 0\&\&\mu > 0\right];$
$\text{c1}_2 = \text{Simplify}\left[\frac{1}{h}\text{Integrate}\left[\psi_2[z], \left\{z, x_i - 3\frac{h}{2}, x_i - \frac{h}{2}\right\}\right], Q > 0\&\&\sigma_T > 0\&\&\mu > 0\right];$
$\text{c2}_1 = \text{Simplify}\left[\frac{1}{h}\text{Integrate}\left[\psi_1[z], \left\{z, x_i - \frac{h}{2}, x_i + \frac{h}{2}\right\}\right], Q > 0\&\&\sigma_T > 0\&\&\mu > 0\right];$
$\text{c2}_2 = \text{Simplify}\left[\frac{1}{h}\text{Integrate}\left[\psi_2[z], \left\{z, x_i - \frac{h}{2}, x_i + \frac{h}{2}\right\}\right], Q > 0\&\&\sigma_T > 0\&\&\mu > 0\right];$
$\text{c3}_1 = \text{Simplify}\left[\frac{1}{h}\text{Integrate}\left[\psi_1[z], \left\{z, x_i + \frac{h}{2}, x_i + 3\frac{h}{2}\right\}\right], Q > 0\&\&\sigma_T > 0\&\&\mu > 0\right];$
$\text{c3}_2 = \text{Simplify}\left[\frac{1}{h}\text{Integrate}\left[\psi_2[z], \left\{z, x_i + \frac{h}{2}, x_i + 3\frac{h}{2}\right\}\right], Q > 0\&\&\sigma_T > 0\&\&\mu > 0\right];$

Finding coefficients

$\text{Solve}\left[\left\{\text{Simplify}\left[\alpha c1_1 - \gamma\left(\frac{c1_1 + c1_2}{2}\right) - \left(\psi_1\left[x_i - \frac{h}{2}\right] - \psi_1\left[x_i - 3\frac{h}{2}\right]\right)\right.\right.\right.$
$\left.-\beta\left(\psi_1\left[x_i - \frac{h}{2}\right] + \psi_1\left[x_i - 3\frac{h}{2}\right]\right)\right] == 0, \text{Simplify}\left[\alpha c2_1 - \gamma\left(\frac{c2_1 + c2_2}{2}\right)\right.$
$\left.- \left(\psi_1\left[x_i + \frac{h}{2}\right] - \psi_1\left[x_i - \frac{h}{2}\right]\right) - \beta\left(\psi_1\left[x_i + \frac{h}{2}\right] + \psi_1\left[x_i - \frac{h}{2}\right]\right)\right] == 0,$
$\text{Simplify}\left[\alpha c3_1 - \gamma\left(\frac{c3_1 + c3_2}{2}\right) - \left(\psi_1\left[x_i + 3\frac{h}{2}\right] - \psi_1\left[x_i + \frac{h}{2}\right]\right)\right.$
$\left.\left.\left.-\beta\left(\psi_1\left[x_i + 3\frac{h}{2}\right] + \psi_1\left[x_i + \frac{h}{2}\right]\right)\right] == 0\right\}, \{\alpha, \beta, \gamma\}\right]$

C < 1 Mathematica Notebook

S_2 *Solution (c<1)*

bounds2 $= \{\psi_1[-A] == 0, \psi_2[A] == 0\}$;

General Solution

gensol2 $=$ Simplify $[$DSolve $[\{\mu \partial_x (\psi_1[x]) + \sigma_T \psi_1[x]$
$- (\sigma_T * c) \left(\frac{\psi_1[x] + \psi_2[x]}{2}\right) - Q == 0, -\mu \partial_x (\psi_2[x]) + \sigma_T \psi_2[x]$
$- (\sigma_T * c) \left(\frac{\psi_1[x] + \psi_2[x]}{2}\right) - Q == 0, \text{bounds2}\}$,
$\{\psi_1[x], \psi_2[x]\}, x], c < 1]$;
$\psi_1[\text{x\_}] := \psi_1 /.\text{gensol2}$;
$\psi_2[\text{x\_}] := \psi_2 /.\text{gensol2}$;

Cell average fluxes

$\text{cl}_1 =$ Simplify $\left[\frac{1}{h}\text{Integrate}[\psi_1[z], \{z, -A, -A + h\}]\right]$,
$c < 1 \&\& Q > 0 \&\& \sigma_T > 0 \&\& \mu > 0]$;
$\text{cl}_2 =$ Simplify $\left[\frac{1}{h}\text{Integrate}[\psi_2[z], \{z, -A, -A + h\}]\right]$,
$c < 1 \&\& Q > 0 \&\& \sigma_T > 0 \&\& \mu > 0]$;

$c2_1 = \text{Simplify}\left[\frac{1}{h}\text{Integrate}\left[\psi_1[z], \{z, -A+h, -A+2h\}\right],\right.$
$\left. c < 1 \&\& Q > 0 \&\& \sigma_T > 0 \&\& \mu > 0\right];$
$c2_2 = \text{Simplify}\left[\frac{1}{h}\text{Integrate}\left[\psi_2[z], \{z, -A+h, -A+2h\}\right],\right.$
$\left. c < 1 \&\& Q > 0 \&\& \sigma_T > 0 \&\& \mu > 0\right];$
$c3_1 = \text{Simplify}\left[\frac{1}{h}\text{Integrate}\left[\psi_1[z], \{z, -A+2h, -A+3h\}\right],\right.$
$\left. c < 1 \&\& Q > 0 \&\& \sigma_T > 0 \&\& \mu > 0\right];$
$c3_2 = \text{Simplify}\left[\frac{1}{h}\text{Integrate}\left[\psi_2[z], \{z, -A+2h, -A+3h\}\right],\right.$
$\left. c < 1 \&\& Q > 0 \&\& \sigma_T > 0 \&\& \mu > 0\right];$

Finding Coefficients

$\text{eq1} = \text{Simplify}\left[\alpha c1_1 - \gamma\left(\frac{c1_1+c1_2}{2}\right) - (\psi_1[-A+h] - \psi_1[-A])\right.$
$\left. -\beta\left(\psi_1[-A+h] + \psi_1[-A]\right)\right];$
$\text{eq2} = \text{Simplify}\left[\alpha c2_1 - \gamma\left(\frac{c2_1+c2_2}{2}\right) - (\psi_1[-A+2h] - \psi_1[-A+h])\right.$
$\left. -\beta\left(\psi_1[-A+2h] + \psi_1[-A+h]\right)\right];$
$\text{eq3} = \text{Simplify}\left[\alpha c3_1 - \gamma\left(\frac{c3_1+c3_2}{2}\right) - (\psi_1[-A+3h] - \psi_1[-A+2h])\right.$
$\left. -\beta\left(\psi_1[-A+3h] + \psi_1[-A+2h]\right)\right];$

Gamma

$\text{alpha1} = \text{Simplify}[\text{Solve}[\text{eq1} == 0, \alpha]];$
$\text{beta1} = \text{Simplify}[\text{Solve}[\text{eq2} == 0 /.\text{alpha1}, \beta][[1]]];$
$\text{gamma1} = \text{Solve}[\text{eq3} == 0 /.\text{alpha1} /.\text{beta1}, \gamma][[1]];$
$\text{Simplify}[\text{Series}[\gamma /.\text{gamma1}, \{c, 0, 1\}]]$

Beta

$\text{alpha2} = \text{Simplify}[\text{Solve}[\text{eq1} == 0, \alpha][[1]]];$
$\text{gamma2} = \text{Simplify}[\text{Solve}[\text{eq2} == 0 /.\text{alpha2}, \gamma][[1]]];$
$\text{beta2} = \text{Solve}[\text{eq3} == 0 /.\text{alpha2} /.\text{gamma2}, \beta][[1]];$
$\text{Simplify}[\text{Series}[\beta /.\text{beta2}, \{c, 0, 1\}], \text{TimeConstraint} \rightarrow 3000]$

Alpha

$\text{gamma3} = \text{Simplify}[\text{Solve}[\text{eq1} == 0, \gamma][[1]]];$
$\text{beta3} = \text{Simplify}[\text{Solve}[\text{eq2} == 0 /.\text{gamma3}, \beta][[1]]];$

```
alpha3 = Solve[eq3 == 0/.gamma3/.beta3, α][[1]];
Simplify[Series[α/.alpha3, {c, 0, 1}], TimeConstraint → 3000]
```

BIBLIOGRAPHY

[1] B. Davison and J. B. Sykes. *Neutron Transport Theory*. Oxford University Press, 1957.

[2] Kenneth M. Case and Paul F. Zweifel. *Linear Transport Theory*. Addison-Wesley Publishing Company, 1967.

[3] George I. Bell and Samuel Glasstone. *Nuclear Reactor Theory*. Van Nostrand Reinhold Company, 1970.

[4] E. E. Lewis and W. F. Miller, Jr. *Computational Methods of Neutron Transport*. American Nuclear Society, 1993.

[5] Edward W. Larsen and Joseph B. Keller. Asymptotic solution of neutron transport problems for small mean free paths. *Journal of Mathematical Physics*, 15(1):75–81, 1974.

[6] G.J. Habetler and B. J. Matkowsky. Uniform asymptotic expansions in transport theory with small mean free paths, and the diffusion approximation. *Journal of Mathematical Physics*, 16(4):846–854, April 1975.

[7] S. Chandrasekhar. *Radiative Transfer*. Dover, New York, 1960.

[8] Edward W. Larsen. Diffusion theory as an asymptotic limit of transport theory for nearly critical systems with small mean free paths. *Annals of Nuclear Energy*, 7:249–255, 1980.

[9] Edward W. Larsen. On numerical solutions of transport problems in the diffusion limit. *Nuclear Science and Engineering*, 83:90–99, 1983.

[10] Edward W. Larsen, J. E. Morel, and W. F. Miller, Jr. Asymptotic solutions of numerical transport problems in optically thick, diffusive regimes. *Journal of Computational Physics*, 69:283–324, 1987.

[11] Edward W. Larsen and J. E. Morel. Asymptotic solutions of numerical transport problems in optically thick, diffusive regimes II. *Journal of Computational Physics*, 83:212–236, 1989.

[12] J. E. Morel and Edward W. Larsen. A multiple balance approach for differencing the s$_n$ equations. *Nuclear Science and Engineering*, 105:1–15, 1990.

[13] Marvin L. Adams. Discontinuous finite element transport solutions in thick diffusive problems. *Nuclear Science and Engineering*, 137:298–333, 2001.

[14] M. L. Adams. Discontinuous finite element transport solutions in the thick diffusion limit in cartesian geometry. In *Int. Topl. Mtg. Advances in Mathematics, Computations, and Reactor Physics*, volume 5, pages 3–1, Pittsburgh, Pennsylvania, April 29 – May 2 1991. American Nuclear Society. Sec. 21.1.

[15] T. A. Wareing, E. W. Larsen, and M. L. Adams. Diffusion accelerated discontinuous finite element schemes for the s$_n$ equations in slab and x, y geometries. In *Int. Topl. Mtg. Advances in Mathematics, Computations, and Reactor Physics*, volume 3, pages 2–1, Pittsburgh, Pennsylvania, April 29 – May 2 1991. American Nuclear Society. Sec. 11.1.

[16] M. L. Adams, T. A. Wareing, and W. F. Walters. Characteristic methods in thick diffusion problems. *Nuclear Science and Engineering*, 130:18–36, 1998.

[17] W. F. Miller, Jr. An analysis of the finite-differenced, even-parity discrete ordinates equations in slab geometry. *Nuclear Science and Engineering*, 108:247, 1991.

[18] M. L. Adams. Even-parity finite element transport methods in the diffusion limit. *Prog. Nucl. Energy*, 25:159, 1991.

[19] T. S. Palmer and M. L. Adams. Analysis of spherical gemoetry finite element transport solutions in the thick diffusion limit. In *Int. Topl. Mtg. Advances in Mathematics, Computations, and Reactor Physics*, volume 5, pages 4–1, Pittsburgh, Pennsylvania, April 29 – May 2 1991. American Nuclear Society. Sec. 21.1.

[20] Edward W. Larsen. The asymptotic diffusion limit of discretized transport problems. *Nuclear Science and Engineering*, 112:336–346, 1992.

[21] R.D. Lawrence and J. J. Dorning. New coarse-mesh diffusion and transport theory methods for the efficient numerical calculation of multi-dimensional reactor power distributions. In *Proc. Spec. Meeting on the Calculation of Three-Dimensional Rating Distributions in Operating Reactors*, page 383, Paris, November 26–28 1979. NEACRP/OECD.

[22] J. J. Dorning, R. D. Lawrence, and A. M. Ougouag. Application of a new coarse-mesh computational method to the determination of power distributions in a heterogeneous-core large fast reactor. In *Proc. IAEA Symposium Fast Reactor Physics*, page 383, Vienna, September 24–28 1979. IAEA.

[23] R.D. Lawrence and J. J. Dorning. A discrete nodal integral transport theory method for multidimensional reactor physics and shielding calculations. In *Proc. Conf. 1980 Advances in Reactor Physics and Shielding*, page 840, Sun Valley, ID, September 14–19 1980. American Nuclear Society.

[24] W. F. Walters and R. D. O'Dell. Nodal methods for discrete-ordinates transport problems in (x-y) geometry. In *Proc. Conf. Advances in Mathematical Methods for the Solution of Nuclear Engineering Problems*, volume I, page 115, Munich, April 27–29 1980. American Nuclear Society.

[25] W. F. Walters and R. D. O'Dell. A comparison of linear nodal, linear discontinuous, and diamond schemes for solving the transport equation in (x,y) geometry. *Trans. Am. Nucl. Soc.*, 39:465, 1981.

[26] W. F. Walters. Recent developments in nodal and characteristics methods in transport theory. *Trans. Am. Nucl. Soc.*, 43:611, 1982.

[27] W. F. Walters. Augmented weighted diamond form of the linear nodal scheme for cartesian coordinate systems. In *Proc. International Meeting on Advances in Nuclear Engineering Computational Methods*, volume II, page 452, Knoxville, TN, April 9–11 1985. American Nuclear Society.

[28] R. E. Pevey and H. L. Dodds. A two-dimensional exponential expansion discrete-ordinates nodal method. *Trans. Am. Nucl. Soc.*, 39:751, 1981.

[29] R. E. Pevey. Development of a new two-dimensional cartesian geometry nodal multigroup discrete ordinates method. Technical report, Oak Ridge National Laboratory, 1982. ORNL/CSD/TM-182.

[30] R. D. Lawrence. Progress in nodal methods for the solution of the neutron diffusion and transport equations. *Progress in Nuclear Energy*, 17(3):271–301, 1986.

[31] Y. Y. Azmy. The weighted diamond-difference form of nodal transport methods. *Nuclear Science and Engineering*, 98:29–40, 1988.

[32] Y. Y. Azmy. Arbitrarily high order characteristic methods for solving the neutron transport equation. *Annals of Nuclear Energy*, 19(10–12):593–606, 1992.

[33] Y. Y. Azmy. Comparison of three approximations to the linear-linear nodal transport method in weighted diamond-difference form. *Nuclear Science and Engineering*, 100:190–200, 1988.

[34] François Golse, Shi Jin, and C. David Levermore. The convergence of numerical transfer schemes in diffusive regimes I: Discrete-ordinate method. *SIAM Journal of Numerical Analysis*, 36(5):1333–1369, 1999.

[35] Heath L. Hanshaw and Edward W. Larsen. The explicit slope s_N discretization. In *Nuclear, Mathematical, and Computational Sciences: A Century in Review, A Century Anew*, Gatlinburg, Tennessee, April 2003. American Nuclear Society.

[36] Y. Y. Azmy and J. J. Dorning. A nodal integral approach to the numerical solution of partial differential equations. In *Advances in Reactor Computation*, volume 2, pages 893–809, Salt Lake City, Utah, March 1983. American Nuclear Society.

[37] Herbert B. Keller. Approximate solutions of transports problems II. convergence and applications of the discrete ordinate method. *J. Soc. Indust. Appl. Math*, 8(1):43–73, March 1960.

[38] James S. Warsa. Analytical s_n solutions in heterogeneous slabs using symbolic algebra computer programs. *Annals of Nuclear Energy*, 29:851–874, 2002.